Flight Dynamics Simulation and Stability Control of Wingsuits

A Dissertation
Presented to
The Academic Faculty

By

Xiaomo Zhang

In Partial Fulfillment
of the Requirements for the Degree
Master of Science in the
School of Aerospace Engineering

Georgia Institute of Technology
December 2016

Flight Dynamics Simulation and Stability Control of Wingsuits

Approved by:

Dr. Mark Costello
School of Aerospace Engineering
Georgia Institute of Technology

Dr. John Paul Clarke
School of Aerospace Engineering
Georgia Institute of Technology

Dr. Eric Johnson
School of Aerospace Engineering
Georgia Institute of Technology

Date Approved: October 7, 2016

ACKNOWLEDGEMENTS

TABLE OF CONTENTS

LIST OF TABLES

LIST OF FIGURES

SUMMARY

Since French tailor Franz Reichelt made the earliest attempt in February 1912, wingsuits have been developed and widely used not only in extreme sports, but also for military purposes. In the late 1990s, the modern wingsuit was developed. It is defined as a special wearable suit that adds surface area to the human body to enable a significant increase in lift during flight through the air. A wingsuit flight normally starts by a pilot jumping from a point that provides sufficient altitude for flight and ends by deploying a parachute. During the flight, the pilot can adjust his or her arms and legs to make different body configurations, in order to modify the flight speed and flight path.

Modern wingsuits are made of special fabrics. There are wings under each arm and between the legs (Figure 1). The wings are designed to be ram-air inflated so that they become more rigid and have airfoil properties, which provides better flight performance. Compared to conventional air vehicles, configurations and performance of wingsuits are affected more by human factors, such as the pilot's body size, arm strength, stamina, and flight experience. Therefore, the shape of wingsuits can change dramatically under different flight conditions. Due to these issues, it is hard to study wingsuits and simulate wingsuit flight dynamics. For instance, in the history of the development of modern wingsuits, no full-sized wingsuit has ever been tested in wind tunnel to obtain data on wingsuit behavior under different settings and conditions. It will be an extensive and expensive process to conduct the wind tunnel set up and relevant preparation.

In this thesis, a reduced scale wingsuit model was designed and fabricated to fit in the low speed wind tunnel at Georgia Tech. This model was used in wind tunnel tests to determine aerodynamic characteristics. Since the measured aerodynamic loads were converted into dimensionless coefficients, the measured data was applied on a human scale wingsuit air vehicle system, which consisted a pilot and a full size modern wingsuit. The wingsuit air vehicle was constructed and used for flight dynamics simulation and stability analysis.

CHAPTER 1   INTRODUCTION

A wingsuit can be defined as a wearable suit manufactured with special fabrics that enables the user to fly, after jumping off of a high cliff, a bridge, out of an airplane, or similar environment. The modern wingsuit, first developed in the late 1990s, adds surface area with fabric between the legs and under the arms of the pilot, which functions in a similar manner to aircraft wings, in order to increase the lift acting on the human body during flight (Figure 1). This configuration is often called the tri-wing wingsuit. The "wings" are designed to be ram-air inflated in order to achieve more rigid wing structures and airfoil shapes along cross-sections, leading to better aerodynamic performance. The material used in wingsuits are commonly nylon (100% polyamide), taslan (100% polyester), belga (65% polyester 35% cotton, and polycotton (60% polyester, 40% cotton). Different materials have different weights and strengths, as well as various drag resistances when flying through air. Therefore they are used according to flight conditions such as slow, normal and fast speeds. To help a pilot wear a wingsuit, modern wingsuits use either zippers, cables or a combination of both to attach the wingsuit to the pilot. Usually four zippers are used in a modern wingsuit. Two zippers are used to secure two arms. The other two are longer, which zip from each foot to the chest of the pilot.

The flight speed of a typical skydiver ranges from 180 to 225 km/h (110 to 140 mph). A wingsuit can reduce these speeds dramatically. A vertical instantaneous velocity of 40 km/h (25 mph) has been recorded. However, the speed at which the body advances forward through the air is still high, up to 100 km/h (62 mph). A regular wingsuit flight where a pilot jumps out of an airplane usually begins at 4,000 m (13,000 ft.) and the pilot spends one to two minutes in free fall before drifting gently to Earth. In this case, the horizontal gliding distance is around 10,000 m (32,500 ft.). This wingsuit flight allows the pilot to achieve glide ratios of approximately 2.5 (2,500 m of horizontal travel for every 1,000 m of vertical descent). The glide ratio is also the

ratio between the lift force and drag force; each of these three parameters is important to wingsuit pilots. In general, for long range flight a high glide ratio is desired, for increasing fall time, a higher lift force is desired, and increasing forward speed requires a reduction in drag force. Wingsuit pilots are interested in the wingsuit's glide radio, maneuverability, and stability. In comparison, hang gliders fly with a glide ratio of 15. Space shuttles approach to Earth with a glide ratio of 4.5. Northern flying squirrels achieve glide ratios of at most 2.0. For wingsuit flight, the record of largest glide ratio of 4 can be achieved by the highly skilled skydiver wearing high performance wingsuit.

Figure 1 Typical modern wingsuit, TonySuit i-Bird

The current methodology that most wingsuit companies are using to improve wingsuit design is often referred as a "re-saw, jump, and observe" methodology. There are sensors attached to the body of the pilots so that flight data can be recorded and stored. However, this testing method is limited by a lot of factors such as weather, choice of testing location and timing to run tests. Wingsuit flying is also one of the most dangerous extreme sports. According to the fatalities list report on sports parachuting [Mei Don, 2013], the ratio of wingsuit fatalities over total parachuting accidents has been increasing for the past 30 years. Only during the first 8 months of year 2013, there were 18 parachuting accidents, 17 of the accidents are directly related to wingsuit flights.

In this thesis, the purpose was to explore testing wingsuits using a low speed wind tunnel, as well as to analyze the stability of wingsuits. Therefore, two main goals were achieved by the end of this thesis.

(1) Obtain aerodynamic characteristics of the wingsuit model in different body configurations. The process included designing, 3D printing, and fabricating a human body model and a wearable wingsuit within a certain size to fit in the wind tunnel. In addition, the human body model was designed to be moveable at connecting joints so that different configurations can be tested in the wind tunnel.

(2) Create a flight dynamic simulation of a wingsuit air vehicle system, which included:

(2.1) Created a rigid body 6-DOF simulations for the system and predicted glide performance and maneuver.

(2.2) Analyze its stability matrix, often referred as "A matrix", by deriving the linearized equations of motion and calculating its modes of vibration.

CHAPTER 2   LIMITATIONS AND CONSTRAINS

Due to practical constraints there are several limitations of the thesis. As mentioned previously, modern tri-wing wingsuits have three individual ram-air wings attached under the arms and between the legs. The inlets use the dynamic air pressure created by the wingsuit motion during flight to inflate the wings. Therefore, the inflated wings will have thickness to form an airfoil shape at cross sections, which gives better aerodynamic performance. In addition, the air inside the wings prevents flapping of the trailing edge of the wings, so that the wingsuit behaves in a more stable manner. However, due to the limitation of fabricating and stitching skills, the inlet design of the wingsuit model is beyond the scope this research. Therefore, no airfoil shapes were achieved in the wings of the designed wingsuit model. In addition, the thickness of the wings of the wingsuit was not a factor that affecting its aerodynamic performance.

The second limitation is that the pitching angles of the wingsuit in wind tunnel tests are less than +/-30 degrees. This is due to the fact that the limitations of the balance inside the wind tunnel are between +/-30 degrees for pitch and +/-45 degrees for yaw.

The third limitation is that no parachute section was considered during the design and analysis of the wingsuit system. The landing phase of the flight of a wingsuit system was not covered in this research. The parachutes are commonly designed to be on the back of the pilot. The parachutes actually affect the aerodynamic coefficients due to the change of the shape; however, this was not taken into consideration while obtaining the aerodynamic data from wind tunnel tests.

CHAPTER 3   CAD MODELING AND WIND TUNNEL TESTING

To accomplish the first goal of the research as mentioned in Chapter 1, the following tasks were conducted in the series of designing and modeling, wind tunnel testing.
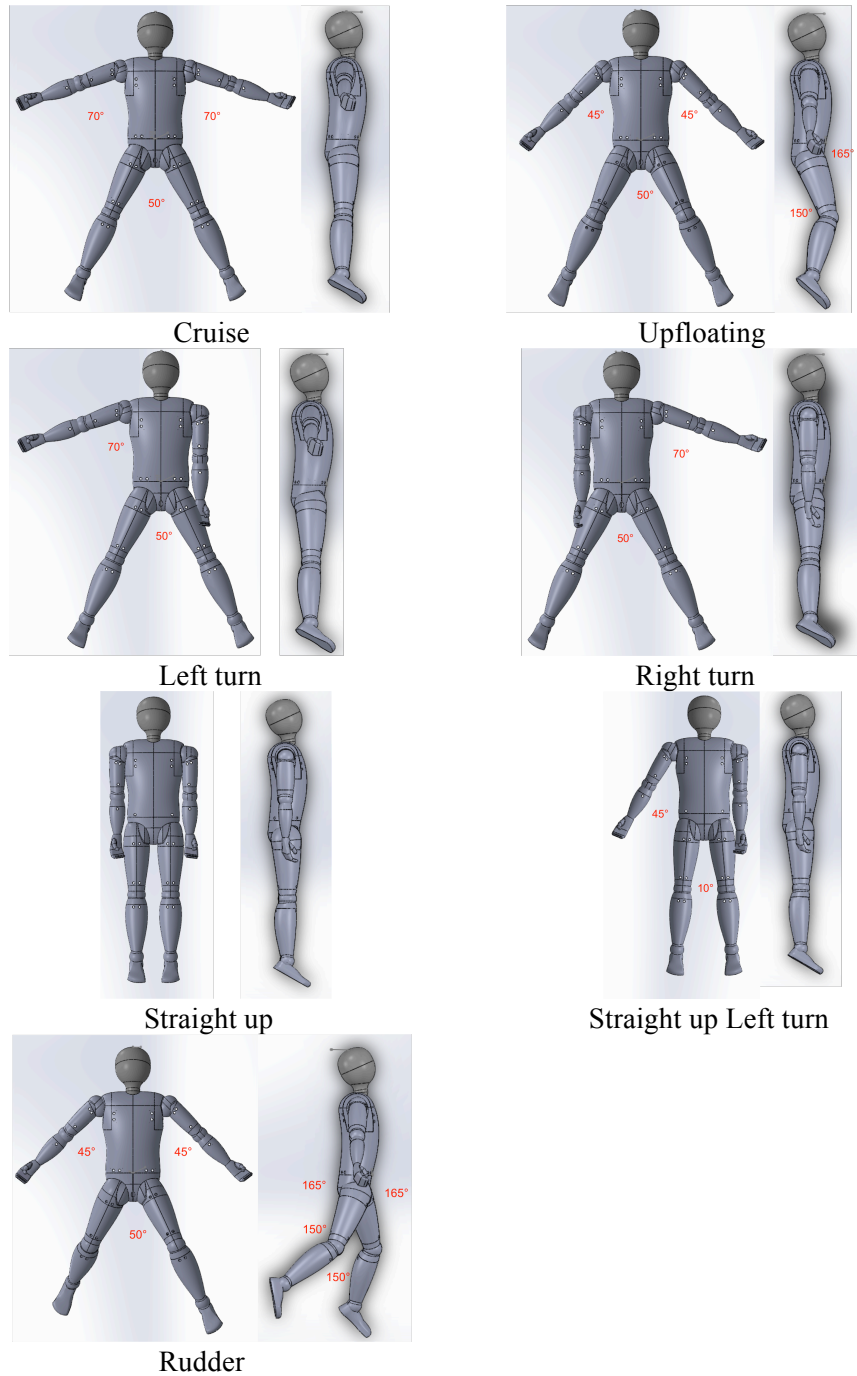
Cruise

Upfloating

Left turn

Right turn

Straight up

Straight up Left turn

Rudder

Figure 2 SolidWorks model and 7 configurations

3.1 Human Body Model in SolidWorks.

To achieve the most realistic aerodynamic data from wind tunnel tests, a reduced scaled human body model was designed, which has very similar ratios among different body parts compared to average size of real human bodies. The model has a size of approximately 11 inches in height, 12 inches in width (wingspan), and 1 inch in depth. In addition, for the purpose of ease of 3D printing, the model was designed with replaceable body joints including shoulders, elbows, thighs, and knees. As a result, the design saved a lot of time and material. The SolidWorks models are shown in Figure 2.

In a general wingsuit flight, a pilot adjusts his body to change flight path and control flight speed. Therefore, various configurations were used for testing in the wind tunnel. In this thesis, 7 different body configurations were tested in the wind tunnel, as shown in Figure 2. The analysis of these configurations can explain the majority of the movements including upfloating, barrel rolls and forward speed, which a pilot commonly experiences in a regular flight. The configurations were determined based on the knowledge and information provided both in flight manual videos [flylikebrick.com] and flight experiences of wingsuit pilots as mentioned in the literature review chapter of thesis proposal.

3.2 Rapid Prototyping of The Model

3D printing technology has been widely used in many engineering fields, especially in engineering research. In this case, Fortus 250mc 3D printer was used to print all the parts of the model with very high resolution and precision. There are two disadvantages of 3D printing the model. First, since the plastic extruded from the printer has a small thickness, which is not considered in SolidWorks, all parts did not perfectly match with each other while assembling them together. This caused looseness between connections among parts of the model. Many attempts were made to solve the problem until the combination of the use of wire and proper size in design was achieved. Second, due to the high resolution of the printer, it took around 15 hours

to complete all parts of the model by the printer. After printing, more time was needed to use the Soluble Concentrate P400SC solution mixed with heated water to dissolve the supporting materials in printed parts. That is why the model was designed with replaceable joints during the design phase as introduced in Chapter 3.1. See Figure 3 for detailed and overall look of the printed CAD model.
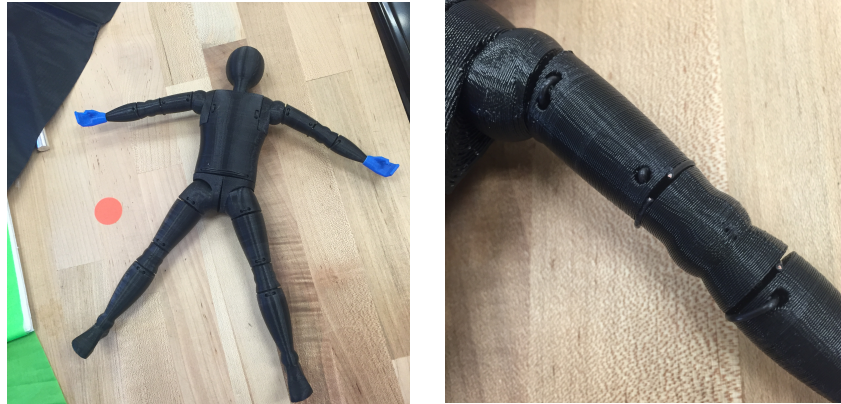

Figure 3 Rapid Prototyping model

Figure 4 Wingsuit model was mounted on the balance

3.3 Small Scaled Wingsuit Design and Fabrication.

The wingsuit model was designed to consist of three wings with two under the arms and one between the legs. The suit was fabricated with four zippers where one for each arm and each leg. Therefore, the suit is flexible and can be put on and taken off easily for different configurations. With this method, only one suit needed to be made throughout the research.

In this research, the wingsuit was designed to have two pieces: upper section for body and arms and lower section for thighs and legs, as shown in Figure 4. The wingsuit was fabricated by the combination of hand stitching and using the sewing machine. The applied fabric was 30-denier nylon ripstop. This material is widely used in the manufacture of parachutes because it is light, flexible, and windproof. It is able to handle high altitude winds and other environment elements. Figure 4 shows the preliminary prototype that being used for wind tunnel tests.

3.4 Aerodynamic Data Acquisition.

In order to conduct the simulation of the flight dynamics of the wingsuit model, aerodynamic coefficients must be calculated from the wind tunnel tests data, such as lift force, drag force, side force, as well as moments along each axis. First, an aluminum holder was designed. On one end of the holder, it was mounted tightly with set screws onto the strain gauge of the balance. And on the other end, it connected to an iron rod that was fixed in the human body model. Eventually, the wingsuit model was connected to the strain gauge for the purpose of data acquisition, as shown in Figure 4. There were six sets of data obtained from wind tunnel tests, which are axial force, side force, normal force, roll moment, pitch moment, and yaw moment along x, y, and z-axis respectively. Note that all the forces and moments were given in the body frame of the balance. After the data was exported from the wind tunnel data logger, all the forces and moments were transferred from the balance body frame to the wind frame. The center of gravity of each body configuration was calculated in SolidWorks. The distance between the wind tunnel balance measurement point and the center of gravity of the wingsuit model was measured and used in the calculation of pitching moment. Meaning that the pitching moment of the wingsuit model was calculated relative to its center of gravity.

Due to the weight of the model, the aluminum bar that holds the model in position is not always perfectly parallel with respect to the balance. The model experienced smaller angles of attack compared to the angles at which the balance was set up. The differences in angles vary

among different body configuration and wind speeds. Therefore 1 degree was chosen to shift the
y-axis to its left while plotting tests data.
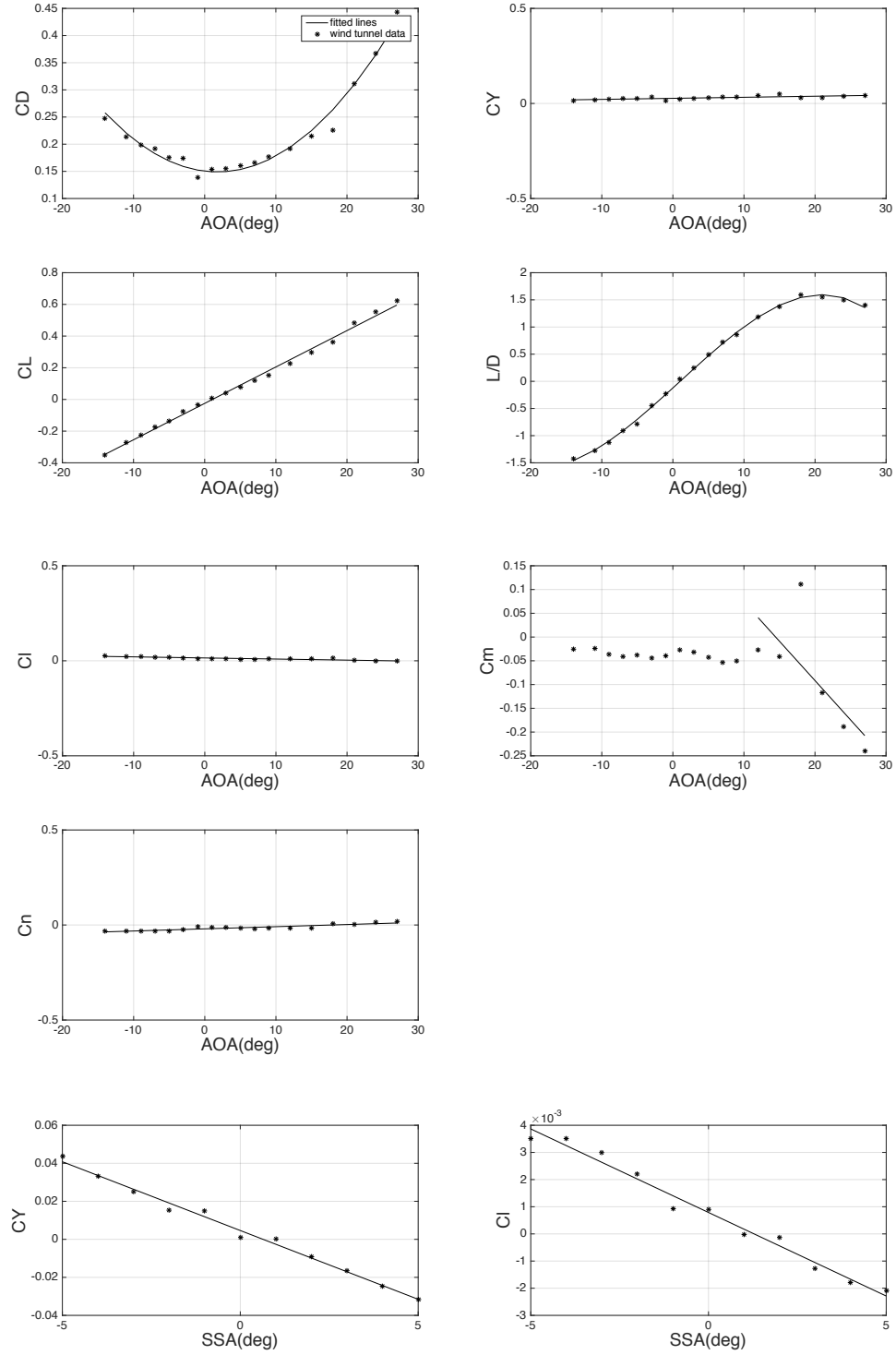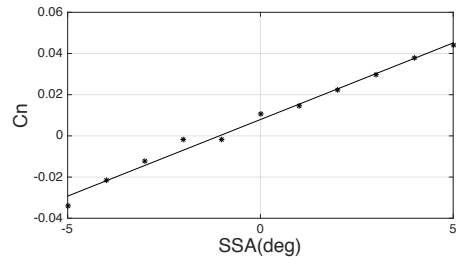
Figure 5 Fitted lines on wind tunnel tests data

The complete description of the 7 body configurations that were tested in wind tunnel tests are shown in Appendix A, which includes the plots of data, fitted functions, and tables of data points

CHAPTER 4   6-DOF SIMULATION AND STABILITY ANALYSIS

Using the measured aerodynamic forces and moments, the aerodynamic coefficients of the wingsuit model was calculated and a flight dynamic simulation model was developed. This mathematical model was used to apply the aerodynamic coefficients on the simulation of a wingsuit air vehicle system, which included an actual full size wingsuit and a pilot. The simulation included the analysis of stability and controllability of the system. In the end, the simulation was used to find out the flight dynamic modes of vibration of the wingsuit air vehicle system.

4.1 Moments of Inertial

Seven different body configurations were designed and tested in the wind tunnel testing. The next step was to take use of the aerodynamic coefficients obtained and to simulate the flight trajectories given certain circumstances. The basic geometries and moment of inertias of all body configurations are shown in the Table 1.

Table 1 moments of inertia and wingsuit geometries

	Cruise	Upfloating	Straight Up	SU turn	Rudder	Left turn	Right turn
$I_{xx}(kg*m^2)$	4.3	4.3	1.2	1.8	4.4	3.7	3.7
$I_{yy}(kg*m^2)$	12.6	11.5	13.4	13.6	12.4	12.4	12.4
$I_{zz}(kg*m^2)$	16.6	16.4	14.3	15.2	16.2	15.7	15.7
$I_{xz}(kg*m^2)$	0.1	0.3	0.1	0.1	0.8	0.1	0.1
$I_{xy}(kg*m^2)$	0.001	0.2	0.001	0.4	0.2	0.4	0.4
$I_{yz}(kg*m^2)$	0.002	0.3	0.001	0	0.4	0	0
Wing Area (S) (m^2)	1.393	1.346	0.879	1.056	1.302	1.319	1.319
Wing Span (b) (m)	1.857	1.857	0.598	0.598	1.857	1.228	1.228
Wing Chord (c_bar) (m)	0.75	0.718	1.47	1.74	0.701	1.07	1.07

Figure 6 shows the moments of inertia about a somersaulting axis (medial-lateral) and a twisting axis (longitudinal) for a human body. When the body parts are moved closer to the axis the moment of inertia is reduced and it increases when the body parts are moved further away from the axis. This information was used as references when doing comparison, the moment of

inertia of all body configurations of the wingsuit air vehicle system were calculated from SolidWorks. As Shown in Figure 6, an example of the cruise body configuration, the Mass Property function in SolidWorks can calculate the mass, volume, and moments of inertia of the model. In this case, the mass is equal to $304.48\ g$; the volume is equal to $304480\ mm^3$; and its corresponding moments of inertia. Comparing these values with the properties of the wingsuit air vehicle system used in the following simulations, the geometry scale ratio from the wingsuit model to the wingsuit system is 6.26. Therefore the volume scale ratio is equal to 6.26^3. By finding these ratios, the moments of inertia of the wingsuit system can be calculated for all kinds of body configurations.
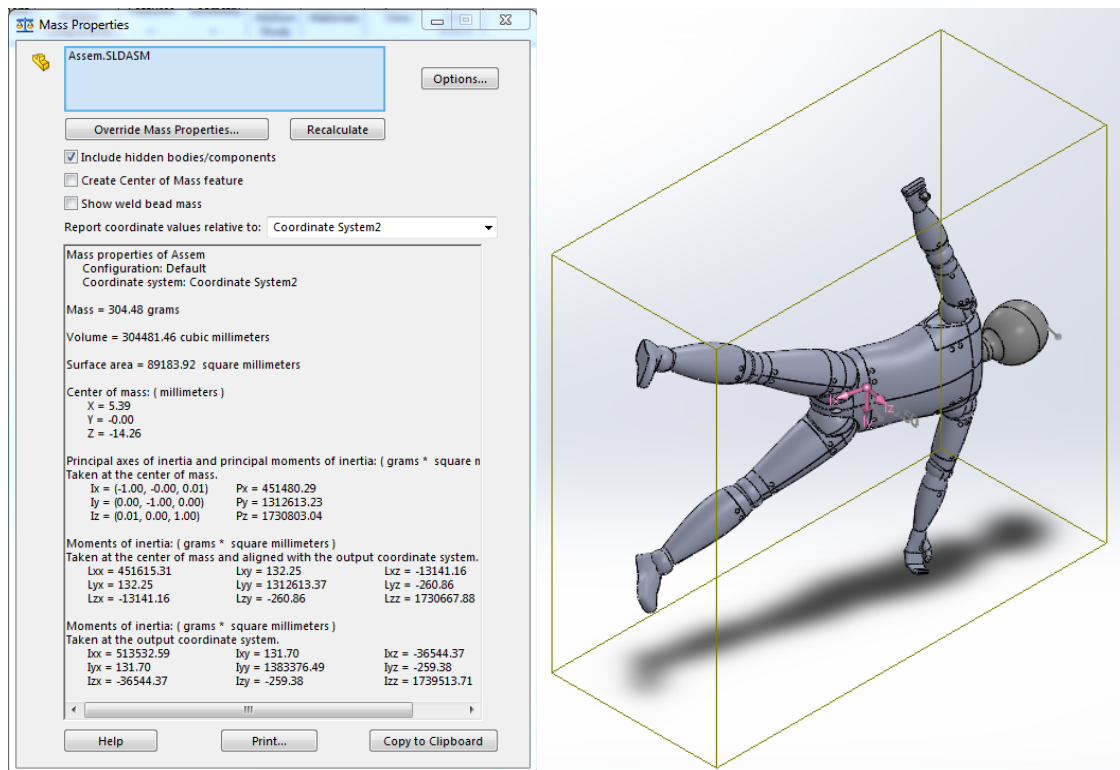
Figure 6 Mass Property Function in SolidWorks

The moments of inertia are only affected by the distribution of mass, regardless the forces acting on the human body. Therefore, the amount of moments of inertia contributed by the wingsuit could be neglected as well due to the relative low weight of fabric when comparing with the mass of the human body.

12

The wing areas, wingspans, and wing chords shown in the Table 1 were the estimated area and length values of an actual wingsuit air vehicle. In this thesis, the TonySuit i-Bird was chosen as the wingsuit in the wingsuit air vehicle system, as shown in Figure 1. The i-Bird series are the perfect introduction to wingsuit flying. The suit has been designed to make the pilot's transition into the discipline safer and easier. The suit is easy to attach, wear and fly in most conditions. Take the i-Bird as reference, the wing area of the wingsuit model is $0.0316\ m^2$ and the wing area of the TonySuit i-Bird wingsuit is $1.39\ m^2$. The average cord lengths were calculated with equations $\frac{S}{b}$.
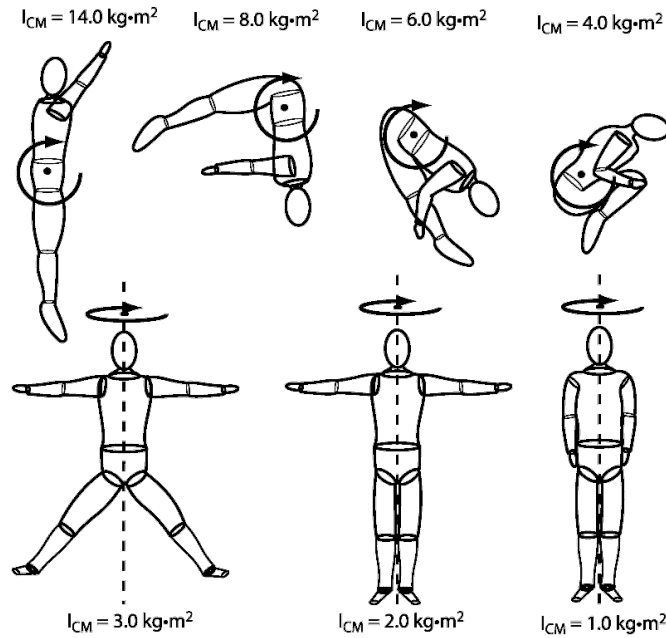
Figure 7 Moments of inertia of human body in different body configurations

4.2 State Variables in Flight Simulation

Since the simulation was 6 degree of freedom (6-DOF), there were 12 variables of each state at any given time in the flight simulation, along with the initial state of the wingsuit flight, as shown in Table 2.

The initial values of state variables were determined based on the assumption that the wingsuit started the flight with an altitude of $4000\ m$, a vertical velocity of $3\ m/s$, and a forward speed of $10\ m/s$ in body reference frame respectively. The wingsuit began to free-fall with $0m/s$

sideslip speed. The wingsuit air vehicle system had the cruise body configuration throughout the simulation.

Table 2 State Variables

Elements of a state x	Units	Initial values x0 (time = 0)
u	m/s	10
v	m/s	0
w	m/s	3
X_e	m	0
Y_e	m	0
Z_e	m	-4000
p	rad/s	0
q	rad/s	0
r	rad/s	0
ϕ	$degree$	0
θ	$degree$	30
ψ	$degree$	0

4.3 Numerical Iteration Method

In this thesis, the fourth order Runge-Kutta method was applied as the numerical analysis tool to run the simulation. In this process, first, the initial value was specified as shown in following derivations,

$$\dot{x} = f(t, x)$$

$$x = x_0$$

then a time step is picked and the size is always a positive number,

$$\delta_t = 0.01$$

secondly, the unknown function of time, x, was defined which usually is approximated,

$$x_0 = x_0 + \frac{1}{6}(k_1 + 2k_2 + 2k_3 + k_4)$$

$$k_1 = \delta_t f(t, x_0)$$

$$k_2 = \delta_t f\left(t, x_0 + \frac{k_1}{2}\right)$$

$$k_3 = \delta_t f\left(t, x_0 + \frac{k_2}{2}\right)$$

$$k_4 = \delta_t f(t, x_0 + k_3)$$

here x_{n+1} is the RK4 approximation of $y\ (t_{n+1})$, and the next value x_{n+1} is determined by the present value x_n plus the weighted average of four increments, where each increment is the product of the size of the interval, h, and an estimated slope specified by function f on the right-hand side of the differential equation,

k_1 is the increment based on the slope at the beginning of the interval, using x;

k_2 is the increment based on the slope at the midpoint of the interval, using $x + \frac{k_1}{2}$;

k_3 is again the increment based on the slope at the midpoint, but now using $x + \frac{k_2}{2}$;

k_4 is the increment based on the slope at the end of the interval, using $x + k_3$.

4.4 Equation of Motion

The flight dynamics of the wingsuit air vehicle system are described by its equations of motion (EOM). The set of equations contains the force, the moments, the translational kinematics, and the rotational kinematics equations.

4.4.1 Force

There are two important kinds of forces acting on the wingsuit, which are gravity and aerodynamic forces. Gravity forces are usually given in earth-fixed reference frame. However, the gravity forces need to be converted into the body-fixed reference frame through the transformation matrix $T_b E$. The aerodynamic forces are obtained from the following equations,

$$\bar{q} = \frac{1}{2}\rho V^2$$

$$D = \bar{q}SC_D$$

$$Y = \bar{q}SC_Y$$

$$L = \bar{q}SC_L$$

Where, C_D, C_Y and C_Y are results from the wind tunnel testing, $\bar{q}$ is the dynamic pressure, and D, Y, L denote the forces components in X, Y, and Z direction of inertial reference frame.

By combining the knowledge with the equation of motion for forces, there is,

$$X = X_T + X_G + X_A$$

$$Y = Y_T + Y_G + Y_A$$

$$Z = Z_T + Z_G + Z_A$$

$$\dot{u} = \frac{X}{m} + rv - qw$$

$$\dot{v} = \frac{Y}{m} - ru + pw$$

$$\dot{w} = \frac{Z}{m} + qu - pv$$

Where, similarly, X_A, Y_A, and Z_A denote the aerodynamic forces, X_G, Y_G, Z_G denote the gravity forces, X_T, Y_T, Z_T denote the thrust forces along body-fixed reference frame, respectively. In this case, since no thrust forces are involved, all thrust forces components were equal to zero.

4.4.2 Moments

It can also be distinguished that two types of moments are acting on the wingsuit. There are moments caused by gravity, and moments caused by aerodynamic forces. The moments caused by gravity are zero. (The resultant gravitational force acts at the CG.) Only the moments caused by aerodynamic forces need to be considered. Therefore, This turns the moment equation into,

$$L_A = \bar{q}SbC_l$$

$$M_A = \bar{q}S\bar{c}C_m$$

$$N_A = \bar{q}SbC_n$$

$$L = L_A + L_T$$

$$M = M_A + M_T$$

$$N = N_A + N_T$$

$$\det I = I_{xx}I_{yy}I_{zz} - I_{xx}I_{yz}^2 - I_{zz}I_{xy}^2 - I_{yy}I_{xz}^2 - 2I_{yz}I_{xz}I_{xy}$$

$$I_1 = I_{yy}I_{zz} - I_{yz}^2$$

$$I_2 = I_{xy}I_{zz} + I_{yz}I_{xz}$$

$$I_3 = I_{xy}I_{yz} + I_{yy}I_{xz}$$

$$I_4 = I_{xx}I_{zz} - I_{xz}^2$$

$$I_5 = I_{xx}I_{yz} + I_{xy}I_{xz}$$

$$I_6 = I_{xx}I_{yy} - I_{xy}^2$$

$$D_x = I_{zz} - I_{yy}$$

$$D_y = I_{xx} - I_{zz}$$

$$D_z = I_{yy} - I_{xx}$$

$$\dot{p} = \frac{1}{\det I}[LI_1 + MI_2 + NI_3 - p^2(I_{xz}I_2 - I_{xy}I_3) + pq(I_{xz}I_1 - I_{yz}I_2 - D_zI_3)$$

$$- pr(I_{xy}I_1 + D_yI_2 - I_{yz}I_3) + q^2(I_{yz}I_1 - I_{xy}I_3) - qr(D_xI_1 - I_{xy}I_2 + I_{xz}I_3)$$

$$- r^2(I_{yz}I_1 - I_{xz}I_2)]$$

$$\dot{q} = \frac{1}{\det I}[LI_2 + MI_4 + NI_5 - p^2(I_{xz}I_4 - I_{xy}I_5) + pq(I_{xz}I_2 - I_{yz}I_4 - D_zI_5)$$

$$- pr(I_{xy}I_2 + D_yI_4 - I_{yz}I_5) + q^2(I_{yz}I_2 - I_{xy}I_5) - qr(D_xI_2 - I_{xy}I_4 + I_{xz}I_5)$$

$$- r^2(I_{yz}I_2 - I_{xz}I_4)]$$

$$\dot{r} = \frac{1}{\det I}[LI_3 + MI_5 + NI_6 - p^2(I_{xz}I_5 - I_{xy}I_6) + pq(I_{xz}I_3 - I_{yz}I_5 - D_zI_6)$$

$$- pr(I_{xy}I_3 + D_yI_5 - I_{yz}I_6) + q^2(I_{yz}I_3 - I_{xy}I_6) - qr(D_xI_3 - I_{xy}I_5 + I_{xz}I_6)$$

$$- r^2(I_{yz}I_3 - I_{xz}I_5)]$$

4.4.3 Translational and Rotational Kinematics

By finding the force and the moment equations, the kinematic relations for the wingsuit air vehicle system could be denoted. When examining the translational kinematics, the velocity of the CG of the wingsuit system with respect to the ground should be concerned. Then the velocity components are different in earth-fixed reference frame and body-fixed reference frame. To relate those two vectors to each other, the transformation matrix T_bE is needed:

$$\dot{X}_e = (\cos\theta\cos\psi)u - (\cos\phi\sin\psi - \sin\phi\sin\theta\cos\psi)v + (\sin\phi\sin\psi + \cos\phi\sin\theta\cos\psi)w$$

$$\dot{Y}_e = (\cos\theta\sin\psi)u + (\cos\phi\cos\psi + \sin\phi\sin\theta\sin\psi)v - (\sin\phi\cos\psi - \cos\phi\sin\theta\sin\psi)w$$

$$\dot{Z}_e = (-\sin\phi)u + (\sin\phi + \cos\theta)v + (\cos\phi + \cos\theta)w$$

These are the translation kinematic equations, which can also be used to derive the change of the vehicle position by integrating the velocities with respect to time:

$$\dot{\phi} = p + q\sin\phi\tan\theta + r\cos\phi\tan\theta$$

$$\dot{\theta} = q\cos\phi + r\sin\phi$$

$$\dot{\psi} = q\frac{\sin\phi}{\cos\theta} + r\frac{\cos\phi}{\cos\theta}$$

These are the rotational kinematic equations. To solve the problem of singularity points in the equations of motion, the $\cos\theta$ terms in the third equation were checked to find whether or not its absolute values is smaller than a certain number. If the value was very close to 0, $\cos\theta$ was assigned 1e-5. This prevented the Matlab code result in "NAN" problem.

4.4.4 Dynamic Stability Derivatives

In the equations of motion used to run simulation, the dynamic damping derivatives C_{m_q}, C_{l_p}, C_{n_r} are calculated with the equations from Warren Phillips' textbook [Phillips, 2010]. The derivatives are then plugged into the moment equations to calculate the damping moments due to these coefficients,

$$C_{l_{\bar{p}}} = -\frac{C_{L_{w,\alpha}}}{12}\frac{(1+3\lambda)}{(1+\lambda)}$$

$$C_{m_{\bar{q}}} = -2\frac{l_w^2}{\bar{c}_w^2 C_{L_{w,\alpha}}}$$

$$C_{n_{\bar{r}}} = 0$$

$$L_{damping} = 0.25\rho VSb^2 C_{l_{\bar{p}}}\bar{p}$$

$$M_{damping} = 0.25\rho VS\bar{c}^2 C_{m_{\bar{q}}}\bar{q}$$

$$N_{damping} = 0.25\rho VSb^2 C_{n_{\bar{r}}}\bar{r}$$

18

4.5 Derivation of The Linearized Equations of Motion

The modes of vibration can be found from the stability matrix, also known as "A matrix", when the equations of motion of the wingsuit system are available. The analysis on vibration modes tells how the wingsuit would behave when given a small disturbance at its equilibrium state. The method used to calculate the stability matrix is by developing linear equations to describe small perturbation motions and apply them to aircraft dynamic equations.

First, define the set of nonlinear function $f(x)$. Here, x is the state of the wingsuit system as mention in previous content. When applied linearization, the higher order terms are neglected,

$$f(x) \approx f(x_0) + f_{x_1}(x_0)\Delta x_1$$

Here, x_0 is the equilibrium state point about which the linearization of the wingsuit system occurred. The linearization is only valid close to this point. The term Δx_i indicates the deviation of variable x_i from the equilibrium point x_0.

After applying linearization to the force and moment equations, the 12 equations of motion are rearranged in order as shown in the following equations,

$$\dot{x}_{longitudinal} = f[x_{longitudinal}(t)]$$

$$\dot{u} = \frac{X}{m} + rv - qw$$

$$\dot{w} = \frac{Z}{m} + qu - pv$$

$$\dot{X}_e = (\cos\theta\cos\psi)u - (\cos\phi\sin\psi - \sin\phi\sin\theta\cos\psi)v + (\sin\phi\sin\psi + \cos\phi\sin\theta\cos\psi)w$$

$$\dot{Z}_e = (-\sin\phi)u + (\sin\phi + \cos\theta)v + (\cos\phi + \cos\theta)w$$

$$\dot{p} = \frac{1}{\det I}[LI_1 + MI_2 + NI_3 - p^2(I_{xz}I_2 - I_{xy}I_3) + pq(I_{xz}I_1 - I_{yz}I_2 - D_zI_3)$$

$$- pr(I_{xy}I_1 + D_yI_2 - I_{yz}I_3) + q^2(I_{yz}I_1 - I_{xy}I_3) - qr(D_xI_1 - I_{xy}I_2 + I_{xz}I_3)$$

$$- r^2(I_{yz}I_1 - I_{xz}I_2)]$$

$$\dot{\theta} = q\cos\phi + r\sin\phi$$

$$\dot{x}_{lateral} = f[x_{lateral}(t)]$$

$$\dot{v} = \frac{Y}{m} - ru + pw$$

$$\dot{Y}_e = (\cos\theta\sin\psi)u + (\cos\phi\cos\psi + \sin\phi\sin\theta\sin\psi)v - (\sin\phi\cos\psi - \cos\phi\sin\theta\sin\psi)w$$

$$\dot{q} = \frac{1}{\det I}[LI_2 + MI_4 + NI_5 - p^2(I_{xz}I_4 - I_{xy}I_5) + pq(I_{xz}I_2 - I_{yz}I_4 - D_zI_5)$$

$$- pr(I_{xy}I_2 + D_yI_4 - I_{yz}I_5) + q^2(I_{yz}I_2 - I_{xy}I_5) - qr(D_xI_2 - I_{xy}I_4 + I_{xz}I_5)$$

$$- r^2(I_{yz}I_2 - I_{xz}I_4)]$$

$$\dot{r} = \frac{1}{\det I}[LI_3 + MI_5 + NI_6 - p^2(I_{xz}I_5 - I_{xy}I_6) + pq(I_{xz}I_3 - I_{yz}I_5 - D_zI_6)$$

$$- pr(I_{xy}I_3 + D_yI_5 - I_{yz}I_6) + q^2(I_{yz}I_3 - I_{xy}I_6) - qr(D_xI_3 - I_{xy}I_5 + I_{xz}I_6)$$

$$- r^2(I_{yz}I_3 - I_{xz}I_5)]$$

$$\dot{\phi} = p + q\sin\phi\tan\theta + r\cos\phi\tan\theta$$

$$\dot{\psi} = q\frac{\sin\phi}{\cos\theta} + r\frac{\cos\phi}{\cos\theta}$$

There is a distinction between symmetric and asymmetric forces and deviations. The symmetric deviations are u, w, and q. The symmetric forces and moments are X, Z, and M. Similarly, the asymmetric deviations are v, p, and r. The asymmetric forces and moments are Y, L, and N. It is shown that there is minimal coupling between the symmetric and the asymmetric properties as long as the deviations are small. Meaning that X is unaffected by v, p, and r. Thus, $X_v = X_p = X_r = 0$. The same properties work for the other forces and moments as well. This simplifies the equations used in linearization steps.

With the set of equations available, the system matrix can be written down in the following 12 by 12 matrix form:

$$F(t) = \begin{bmatrix} \dfrac{\partial f_1}{\partial u} & \dfrac{\partial f_1}{\partial w} & \cdots & \dfrac{\partial f_1}{\partial \psi} \\ \dfrac{\partial f_2}{\partial u} & \dfrac{\partial f_2}{\partial w} & \cdots & \dfrac{\partial f_2}{\partial \psi} \\ \vdots & \vdots & \ddots & \vdots \\ \dfrac{\partial f_{12}}{\partial u} & \dfrac{\partial f_{12}}{\partial w} & \cdots & \dfrac{\partial f_{12}}{\partial \psi} \end{bmatrix}$$

The matrix can be distinguished with four 6 by 6 blocks in terms of longitudinal and lateral directional effects, as shown below:

$$F = \begin{bmatrix} F_{Lon} & F_{Lat}^{Lon} \\ F_{Lon}^{Lat} & F_{Lat} \end{bmatrix}$$

F_{Lon} is the effects of longitudinal perturbations on longitudinal motion;

F_{Lat} is the effects of lateral directional perturbations on lateral directional motion;

F_{Lat}^{Lon} is the effects of lateral directional perturbations on longitudinal motion;

F_{Lon}^{Lat} is the effects of longitudinal perturbations on lateral directional motion;

4.6 Flight Dynamics Modes

The vibration modes of an air vehicle can be analyzed by examining the eigenvalues and eigenvectors of its stability matrix. Each eigenvalues can be either real or complex. If one of the eigenvalues is complex, then its complex conjugate is also an eigenvalue. Complex eigenvalues therefore always come in pairs. A mode of vibration is a characteristic way in which the air vehicle can vibrate. The number of modes depends on the eigenvalues. It is equal to the number of different eigenvalues. The eigenvalues λ are important for the stability of a system. To examine stability, it is to look at the limit:

$$\lim_{S_c \to \infty} c_1 A_1 e^{\lambda_{c_1} S_c} + c_2 A_2 e^{\lambda_{c_2} S_c} + c_3 A_3 e^{\lambda_{c_3} S_c} + \cdots$$

If only one of the eigenvalues has a positive real part, then the limit will diverge. This means that the system is unstable. If, however, all eigenvalues have negative real parts, then the system is stable. The symmetric and asymmetric modes of vibration both existed in the wingsuit

air vehicle system. The cruise configuration was analyzed and the results are discussed in Chapter

5 Wingsuit Flight Dynamic Characteristics.

CHAPTER 5   WINGSUIT FLIGHT DYNAMIC CHARACTERISTICS

5.1 Static Margin

As mentioned in previous text, the location of the center of gravity of the wingsuit model can be found in SolidWorks. Therefore, the neutral point can be found by adjusting its center of gravity so that pitching moment about the model is not a function of angle of attack. Figure 8 shows the example of calculating the static margin of the model. The flat black and white line ($Lcg = 0.1455m$) indicates that the pitching moment remains constant regardless the angle of attack. In this case,

$$L_{neutral} = 0.1455 \; m$$

Where L is the distance measured from the top of the head of the wingsuit model.

Since $L = 0.1205 \; m$, the static margin is equal to $0.025 \; m$, where the neutral point is located behind the center of gravity on this wingsuit model. This is as expected that the aerodynamic forces on the wingsuit cause a decrease/increase in angle of attack so that the disturbance does not cause a continuous increase/decrease in angle of attack.
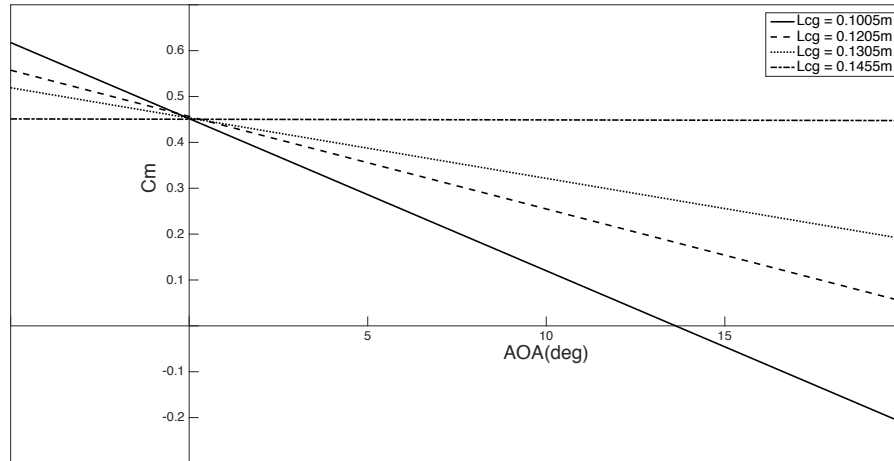
Figure 8 Static Margin of Cruise Configuration

5.2 Longitudinal Simulations of Symmetric Body Configurations

  The results of longitudinal trajectory simulation of each symmetric body configuration (cruise, upfloating, and straight up) are shown in the following Figures 9 - 11. The initial states of each simulation are the same, as mentioned in Table 2. Since no sideslip force and velocity are considered in these simulations, all trajectories are within the XZ symmetric plane of the wingsuit. Thus, the values of side distance (y), sideslip velocity (v), roll angle (ϕ), yaw angle (ψ), roll rate (p), and yaw rate (r) are all zero and remain zero.

  Take the cruise configuration as an example, as shown in Figure 8, the wingsuit starts to glide down as the forward velocity (u) increases. After released from $4000\ m$ above the ground, the wingsuit air vehicle system vibrates in the XZ plane with respect to its rotation center. The angle of attack (AOA) and pitch angle (θ) come to equilibrium states gradually. The AOA takes 8 seconds to reach its steady state while the velocities and angular rates take 25 seconds to reach their steady states. When the wingsuit system reaches its steady state the AOA is 13.62 degrees, the glide ratio is 1.27, the pitch attitude is -24.51 degrees relative to the horizon, and the total velocity is $183\ km/h$.

  Since the upfloating body configuration is very close to the cruise configuration, the flight simulation results of both are almost identical to each other. The upfloating configuration provides a more cambered body shape than cruise configuration. This causes a higher lift capability, in return, higher drag. In result, the upfloating configuration has a lower glide ratio, slower total velocity, and more negative pitch attitude. The results of the straight up configuration are different from the other two body configurations. Since the straight up configuration has the least capability of providing lift, it can be viewed as a flying flat plate with very small aspect ratio. Therefore, the straight up configuration has the worst glide ratio, the most negative pitch attitude, and smallest AOA. It also has the lowest drag, which in return, provides the highest total velocity. The equilibrium states of the simulations of three body configurations are shown in Appendix B.
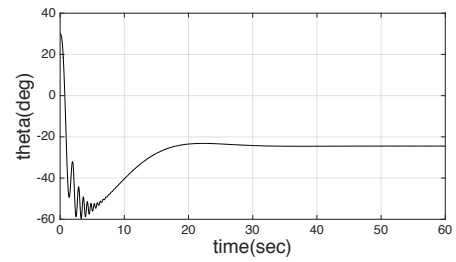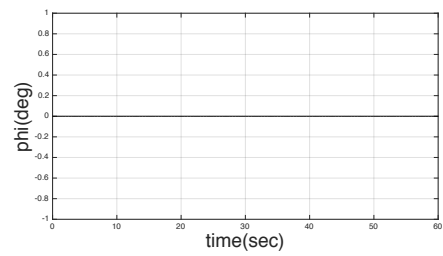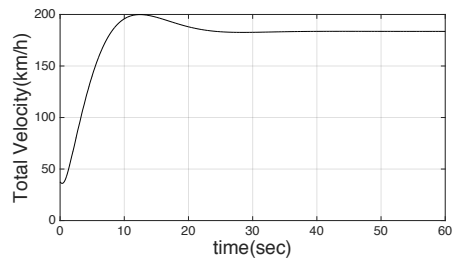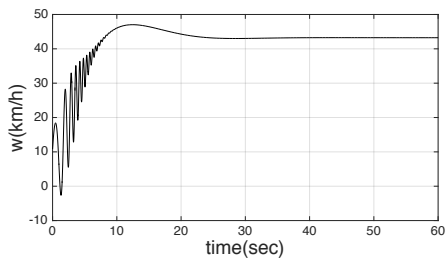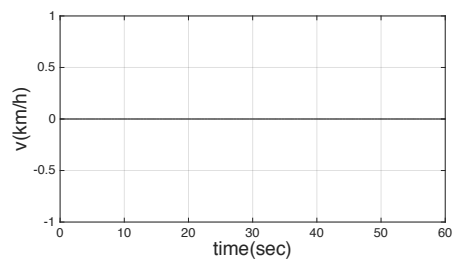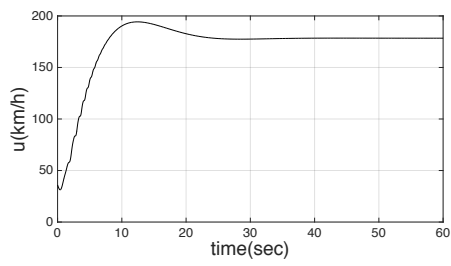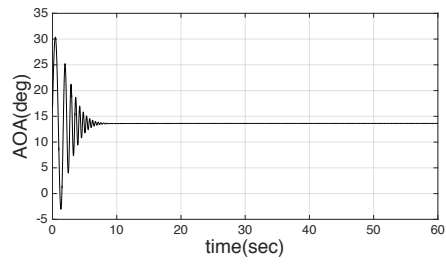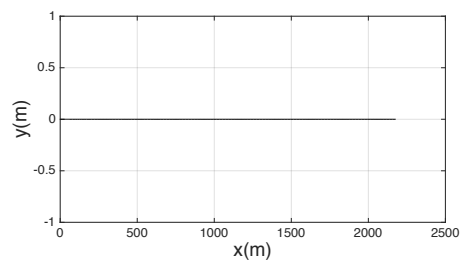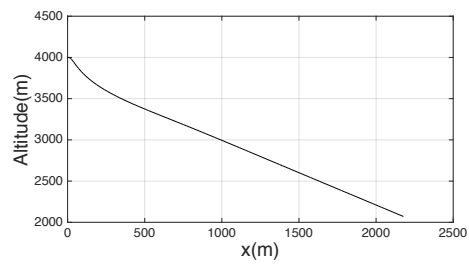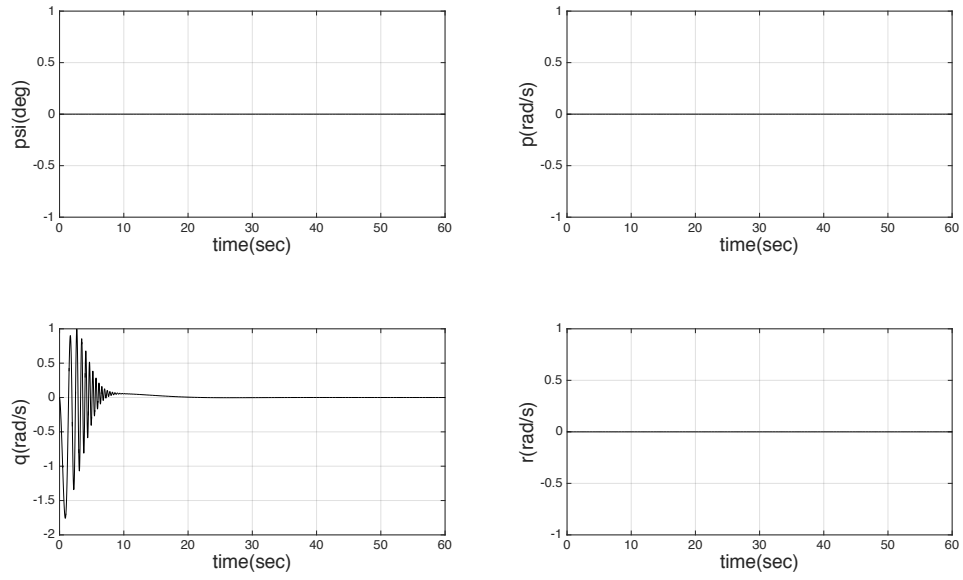
Figure 9 Flight Simulation of Body Configuration – Cruise
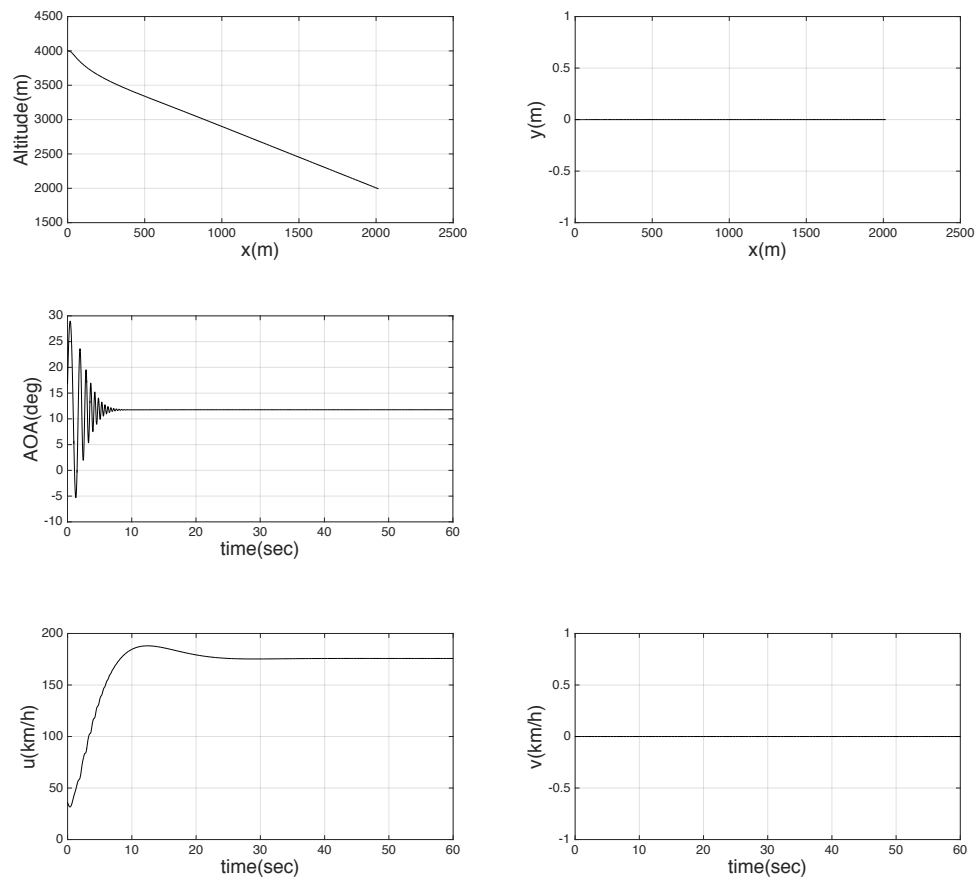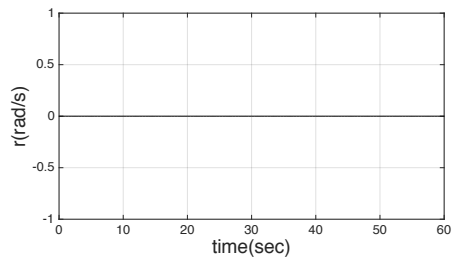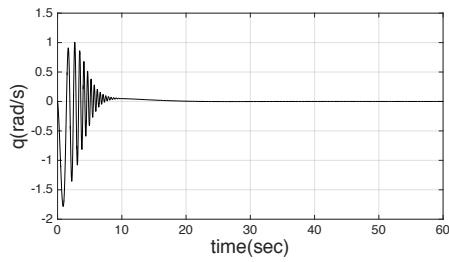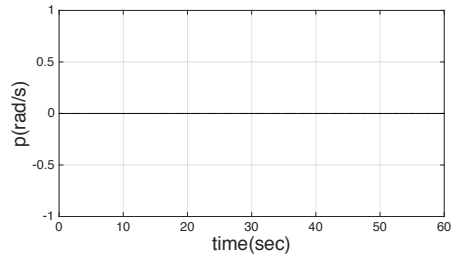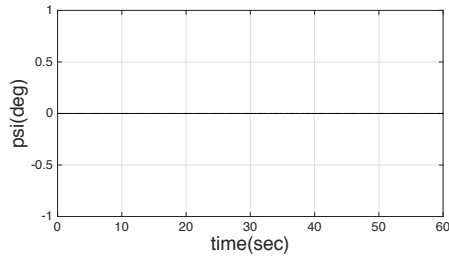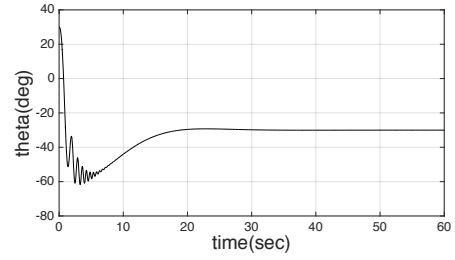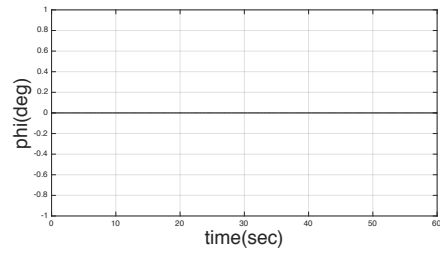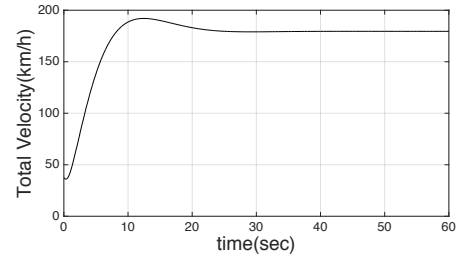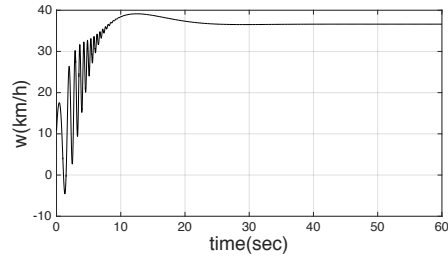
Figure 10 Flight Simulation of Body Configuration – Upfloating
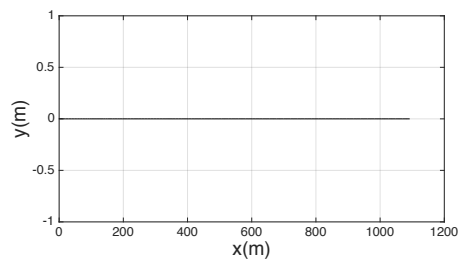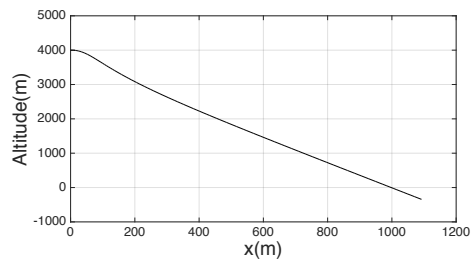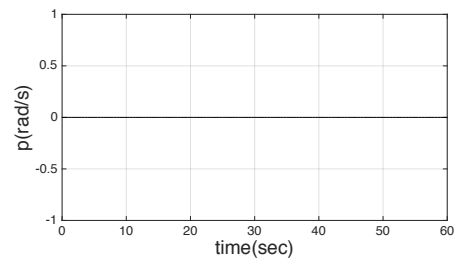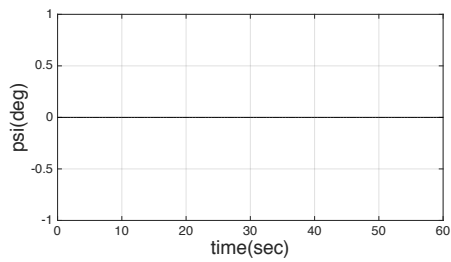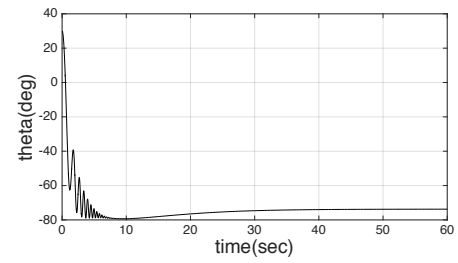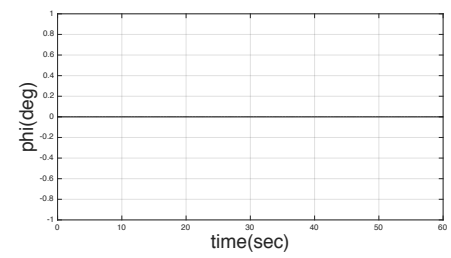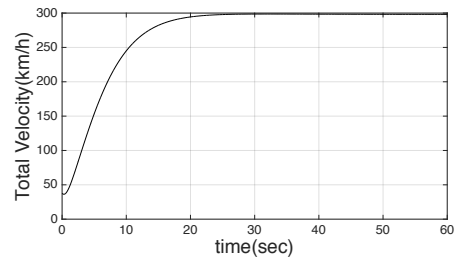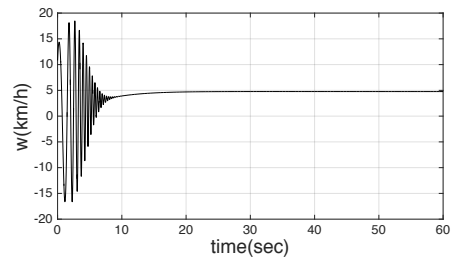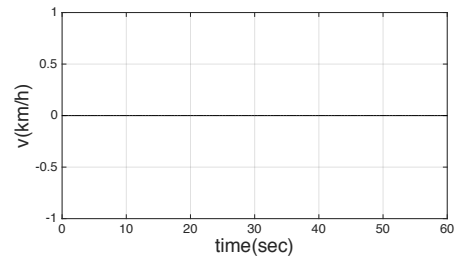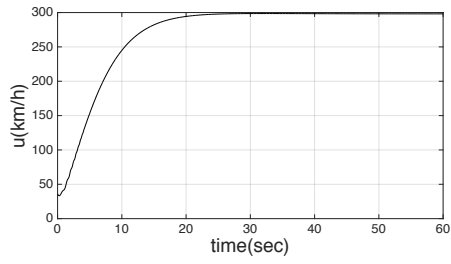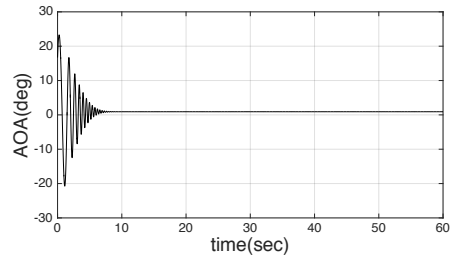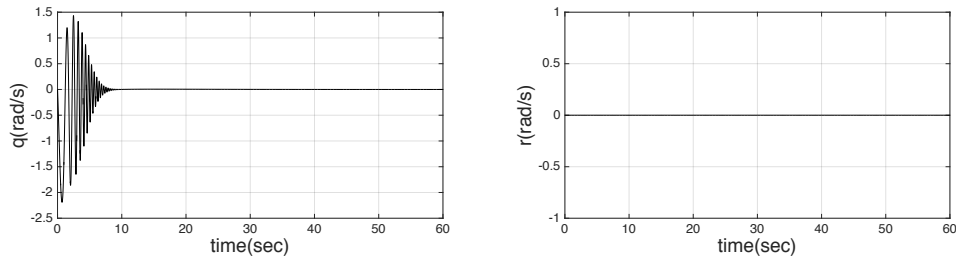
Figure 11 Flight Simulation of Body Configuration – Straight Up

5.3 Recorded Flight Data of Professional Wingsuit Flying

According to the data obtained from Paralog Performance Competition (PPC), the wingsuit air vehicle in this thesis behaves very closely to the existing commercial flying wingsuits. The PPC collects the flight data of wingsuit flying around the world and categorizes the data into groups such as "time challenge", "distance challenge", and "speed challenge" (Figure 12).

To compare the data with the results from Matlab simulation, digitalization of the plots was applied so that the information in Figure 13 could be imported into Matlab for further use. Figure 13 shows an example set of flight data recorded in a specific wingsuit flight. An wingsuit pilot, Udit Thapar completed this flight, on September 12th, 2015. The flight location was Netheravon, England. The wingsuit used in this flight is called Scorpion 2, an experience wingsuit designed and manufactured by TonySuits. This suit is designed for high speed. The arm and leg wing profile thickness has been adjusted to increase forward airspeed. The design has very similar feature as the wingsuit system in this thesis. As a result, the Scorpion 2 has an average flight velocity around 280 km/h and glide ratio around 1.5, which are close to the flight performance of the cruise configuration of the wingsuit air vehicle system, as shown in Figure 9.

Paralog Performance Competition

GPS Based Wingsuit Performance Flying

Tracks for the Speed Challenge

Show 25 entries   Search:

	Name	IOC	Place	Suit	Date	Time [s]	Distance [km]	H. Speed [km/h]	Details	
	Travis Mickle		Zephyrhills	Jedei 2	2016-01-10	17.0	1.649	349.5		
	Spike Harper		Netheravon	Jedei	2015-07-19	18.3	1.648	324.4		
	Alexey Galda		Rochelle	CR+	2016-06-27	29.7	2.637	319.5		
	Richard Lidström		Gotö	R-Bird Pro	2016-08-26	24.0	2.134	319.4		
	Frits Jensen		Sundbylille	CR+	2015-12-20	26.6	2.334	316.0		
	Chris Geiler		Elsinore	C-Race	2015-11-18	21.4	1.893	313.9		
	Joseph Likierman		Zephyrhills	Jedei 2	2016-02-08	33.7	2.919	311.9		
	Joe Ridler		Rochelle	C-Race	2015-10-17	20.4	1.769	311.8		
	Gilaad Elstein		Rosharon	Jedei 2	2014-10-14	24.3	2.074	307.1		
	Espen Fadnes		Netheravon	Jedei 2	2015-05-28	21.1	1.773	302.5		
	Boris Esin		Puschino	Jedei	2014-06-29	21.9	1.830	301.0		
	Tony Uragallo		Netheravon	Jedei 2	2015-05-28	25.9	2.162	300.7		
	Steven Holden		Netheravon	Jedei	2015-05-28	22.7	1.897	300.5		
	Jason Bresson		Netheravon	Jedei 2	2015-05-28	20.7	1.724	300.3		
	Ulf Munkedal		Rødby	CR+	2016-08-06	18.5	1.533	298.1		
	Noah Bahnson		Rochelle	C-Race	2015-10-02	22.7	1.868	296.8		
	Kyle Lobpries		Netheravon	Jedei 2	2015-05-28	21.6	1.776	296.4		
	Florian Kaschuba		Netheravon	Apache	2015-05-28	24.9	2.048	295.6		
	Per Björn Poulsen		Rødby	CR+	2016-08-06	24.6	2.015	295.1		
	Nicolas Alie-Charland		Victoriaville	Jedei 2	2016-07-03	19.4	1.590	294.9		

Figure 12 Screenshot of PPC website

30
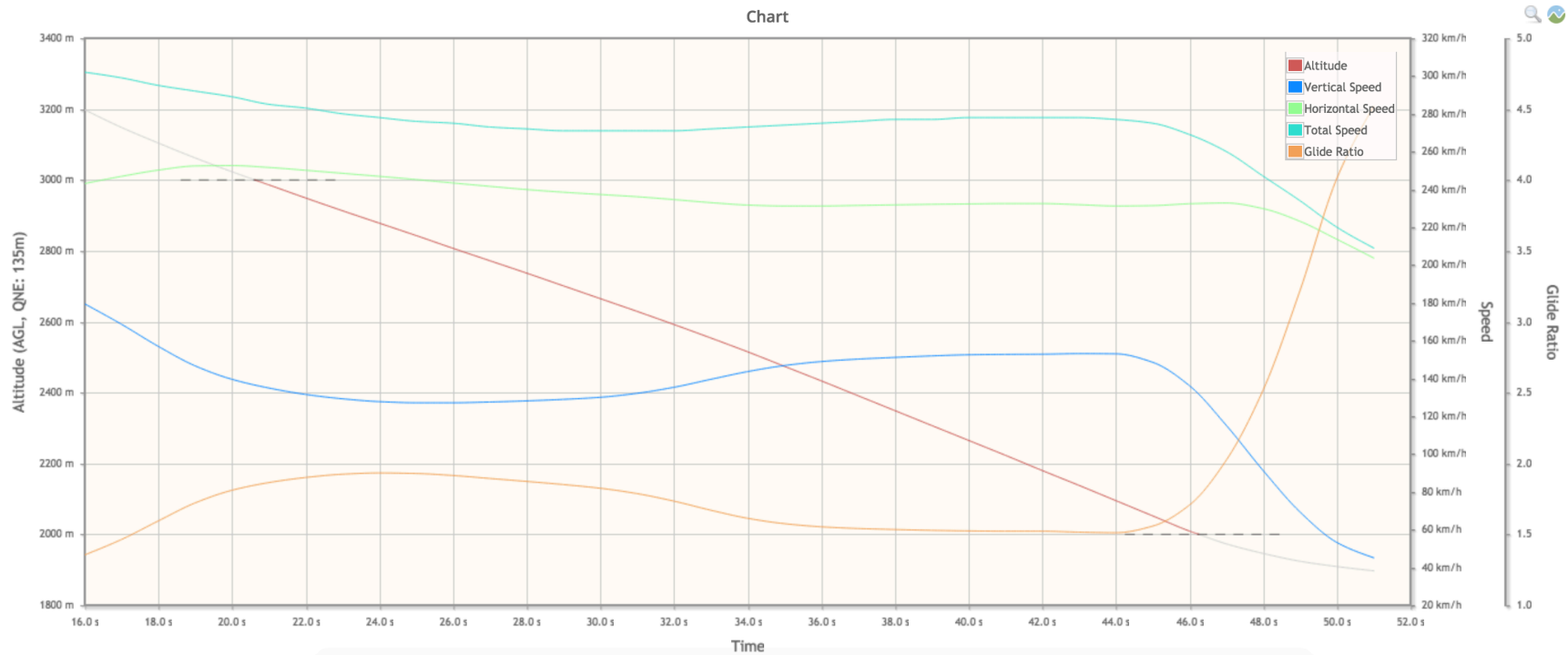
Figure 13 Example flight data from PPC website

5.4 Flight Simulation Involves Cruise, Upfloating, and Straight up Configurations
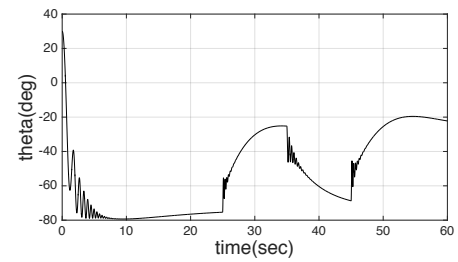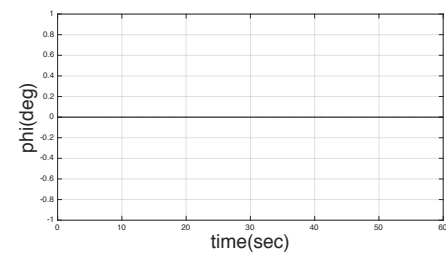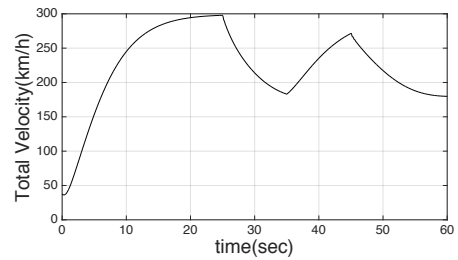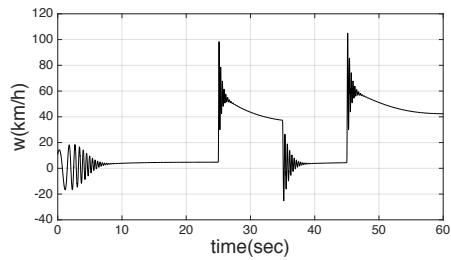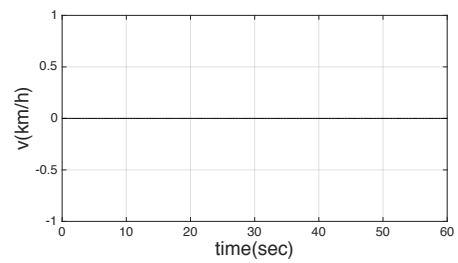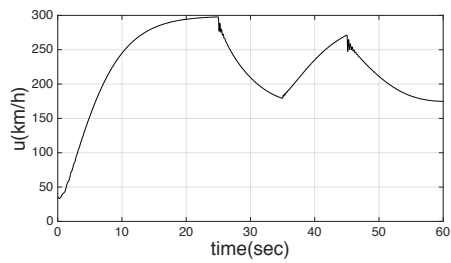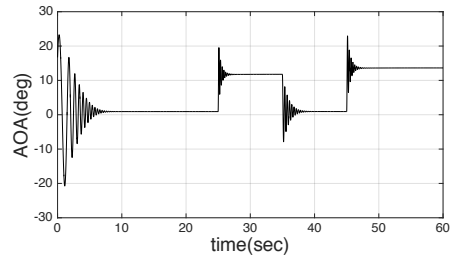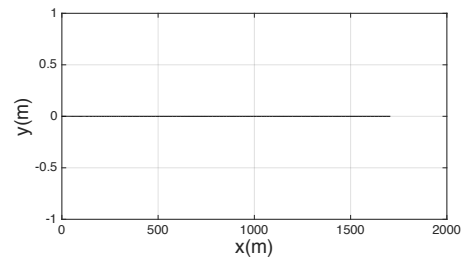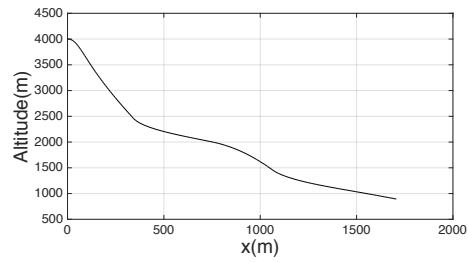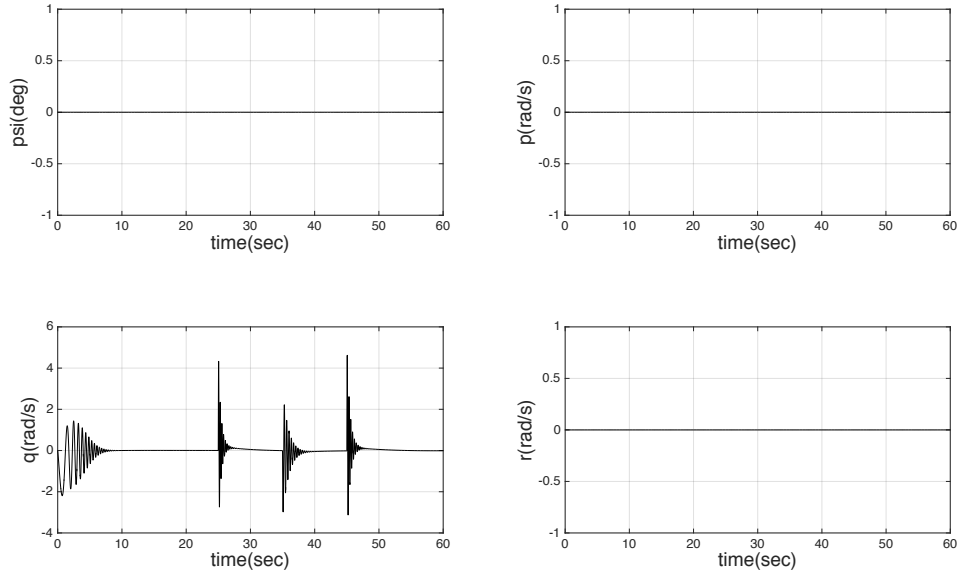
Figure 14 Simulation involves 3 body configurations

Figure 14 shows the simulation of a specific flight that involved 3 different body configurations. The flight starts at 0 second with cruise configuration and finishes at 60 seconds; the process can be described as following:

- When $t = 25\ s$, the pilot switches from cruise configuration to upfloating configuration.

- When $t = 35\ s$, the pilot switches to straight up configuration.

- When $t = 45\ s$, the pilot finally switches back to cruise configuration and remains this configuration till the end of this flight.

In the "Altitude vs. X" plot, it shows that the flight trajectory can be divided into four sections. The first and the last sections correspond to the cruise configuration. Therefore, the slopes of the curve are the same when the flight comes to equilibrium state. From previous results, different configurations have different steady states. This makes the wingsuit system to find its new equilibrium state whenever there is a switch between different configurations. One assumption is that the transaction between configurations happens instantaneously. This can be interpreted that the simulation assumes the pilot chose to maneuver fast during transactions. In reality, a sudden change on control surfaces of an air vehicle will inevitably result in vibrations.

33

So it can be seen from the plots that there are clearly four vibrations throughout the flight simulation. In the "Total Velocity vs. Time" plot, it shows that wingsuit system tries to come to steady state after the flight starts, however, the total velocity dramatically increases after switching to straight up configuration. Then the total velocity drops down again after switching back to cruise configuration when the flight comes to the end. These results match the conclusions of the previous analysis on flight simulation of each individual body configuration.

5.5 Simulations of Turning Configurations

Figure 15 - 16 show the flight simulation of the left turn and right turn configurations. In both simulations, the flight starts with the same initial condition as the one used in previous simulations. When t=25, the wingsuit system switches from cruise configuration to right turn (Figure 15) and left turn (Figure 16) configurations respectively. In the "Y vs. X" plots, positive y indicates east and negative y indicates west. The wingsuit system turns to east in Figure 15 and turns to west in Figure 16. Longitudinal aerodynamic coefficients such as C_L, C_D are barely affected when the configurations are changed. Therefore the glide ratio and total velocity remain relatively constant.
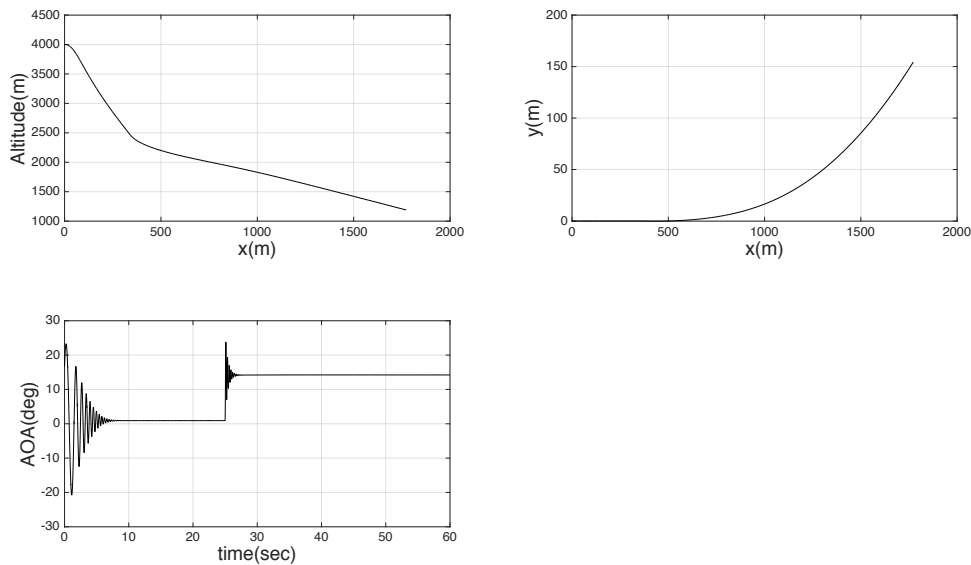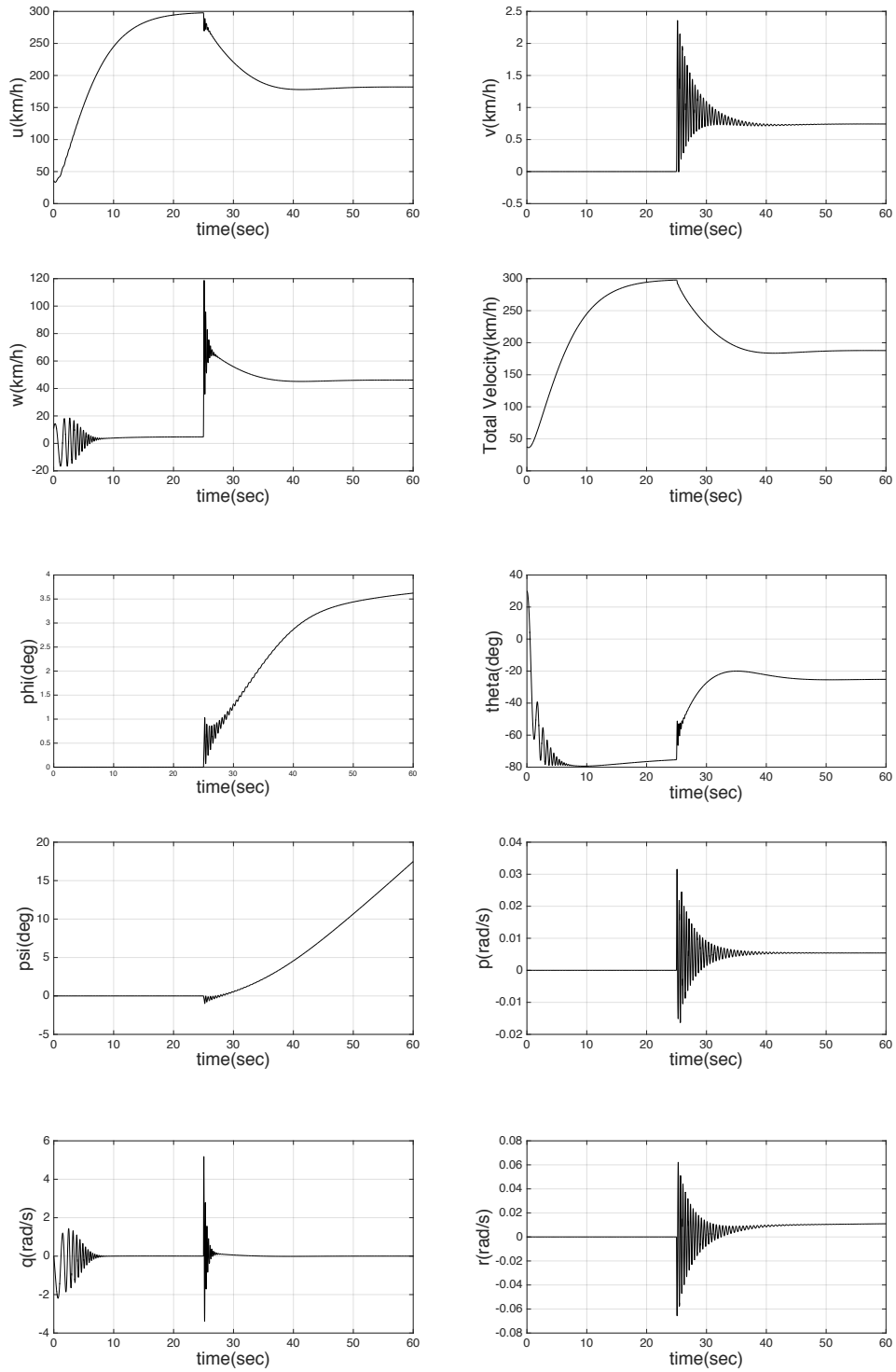
Figure 15 Simulation of turning right
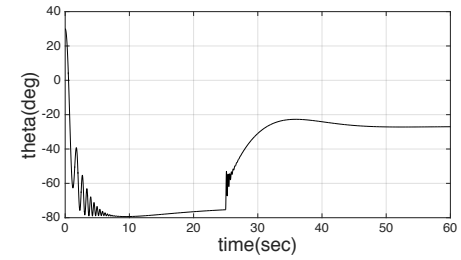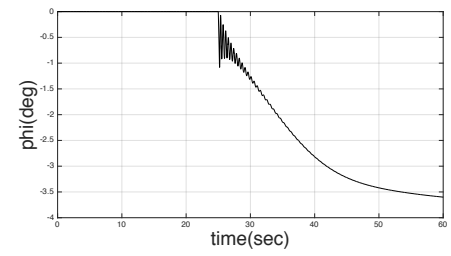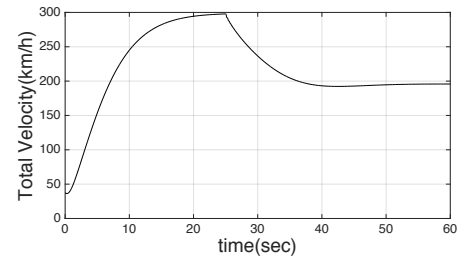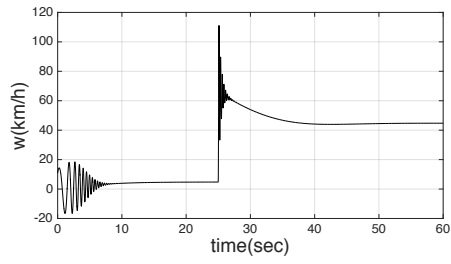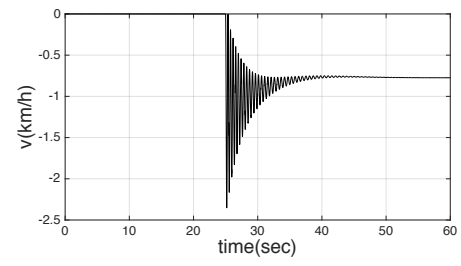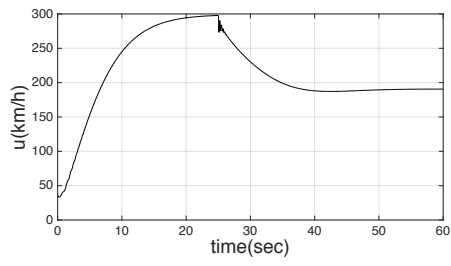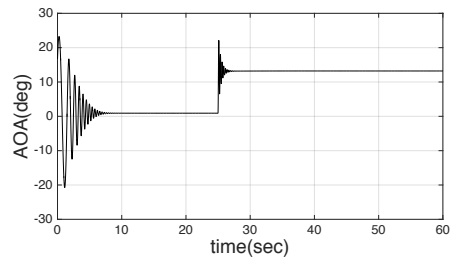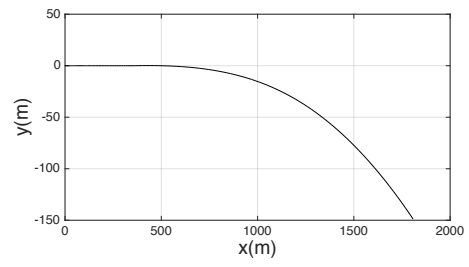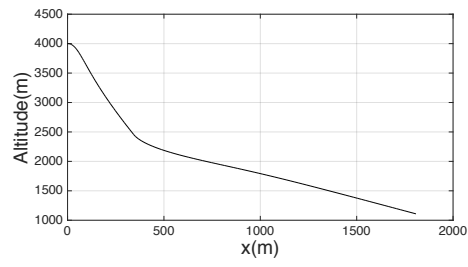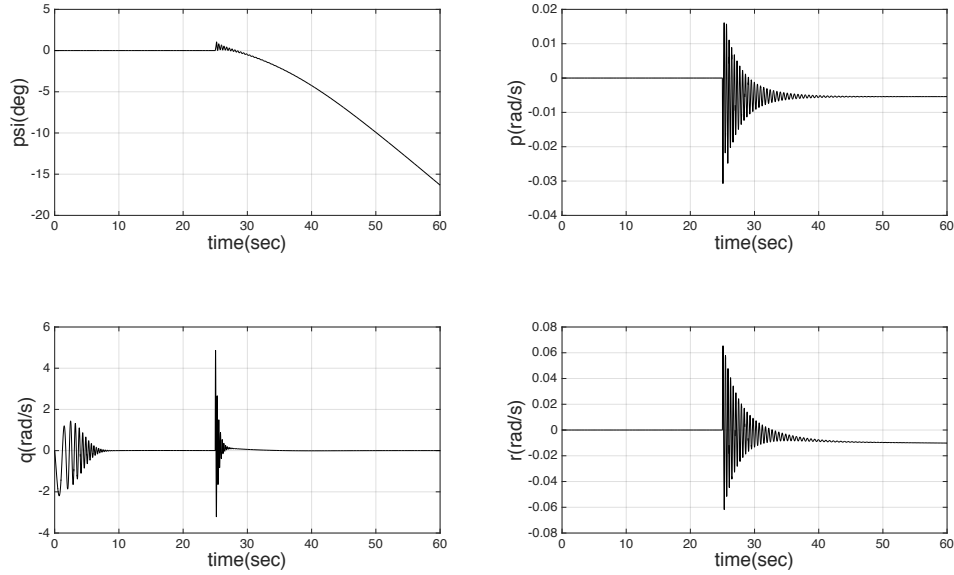
Figure 16 Simulation of turning left

5.6 Linearization Between Turning Configurations
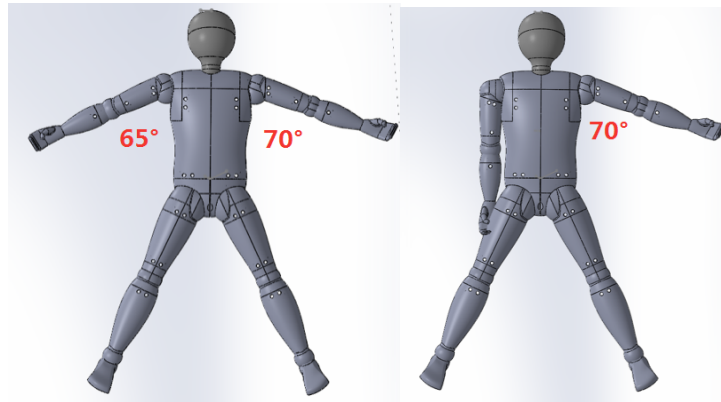
Figure 17 Right turn configurations in Matlab simulation (left) and in wind tunnel testing (right)

In these simulations, the turning configurations are not exactly the same as the ones introduced in previous content (Chapter 3). The turning configurations are defined that one arm remains 70 degrees relative to the chest and the other arm closes. However, in the flight simulation, the turning configurations are modified so that one arm still has 70 degrees while the other arm has 65 degrees relative to the chest, as shown in Figure 17. The aerodynamic coefficients of the turning configurations used in Matlab simulations are obtained from the interpolation of the wind tunnel testing data. The interpolation was between the aerodynamic

37

coefficients of the turning configurations and the cruise configuration. This is an effective way of estimating the aerodynamic coefficient of an arbitrary turning configuration that is slight asymmetric with a small arm angle or leg angle difference.

5.7 Symmetric and Asymmetric Modes of Vibration of The Cruise Configuration

As mention in previous introduction on modes of vibration, an example solution of calculating eigenvalues and eigenvectors of the wingsuit air vehicle system is shown in this chapter. The cruise configuration is chosen and its corresponding system matrix is derived. The solution of its eigenvalues is given by:

$$\lambda_{c_{1,2}} = -1.1321 \pm 15.8321i$$

$$\lambda_{c_{3,4}} = -0.1827 \pm 0.2226i$$

$$\lambda_{c_{5,6}} = -0.2299 \pm 10.3121i$$

$$\lambda_{c_7} = -0.08$$

$$\lambda_{c_8} = -2.5872$$

There are three pairs of complex conjugate eigenvalues. All pairs of eigenvalues have negative real parts. This means that the wingsuit air vehicle system is stable. Since there are another two real eigenvalues, there are in total five different modes of vibration.

5.7.1 Short Period oscillation

$$\lambda_{c_{1,2}} = -1.1321 \pm 15.8321i$$

This pair of eigenvalues has a relatively large real part. The damping is therefore large. The complex part is relatively large as well, making the frequency high. In conclusion, this is a highly damped high-frequency oscillation. This motion is known as the short period oscillation. This oscillation can be animated by simulating the system with its corresponding eigenvector as the derivation around the equilibrium point, as shown in Figure 18 The short period oscillation starts by applying a step input on pitch angular velocity to the steady state of the wingsuit system.

In this case, the small perturbation is equal to the real part of the corresponding eigenvector. The steady state and the short period eigenvector are shown here:

$$x_0 = \begin{bmatrix} u \\ w \\ q \\ \theta \\ v \\ Y_e \\ p \\ r \\ \phi \\ \psi \end{bmatrix} = \begin{bmatrix} 49.56\ m/s \\ 12.0099 m/s \\ 0 \\ -0.4272\ rad \\ 0 \\ 0 \\ 0 \\ 0 \\ 0 \\ 0 \end{bmatrix}$$
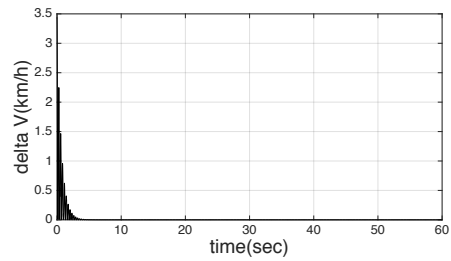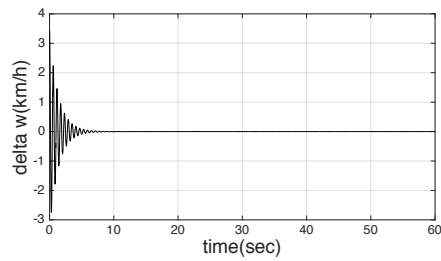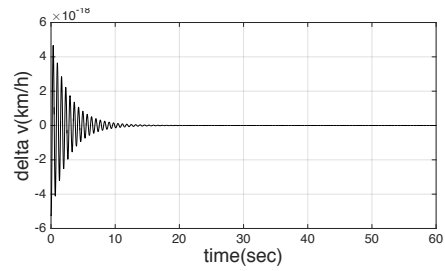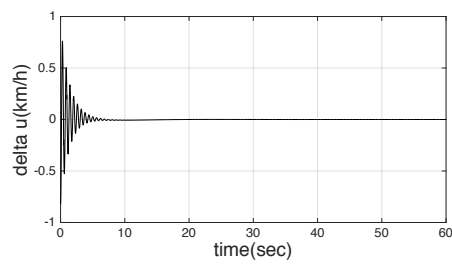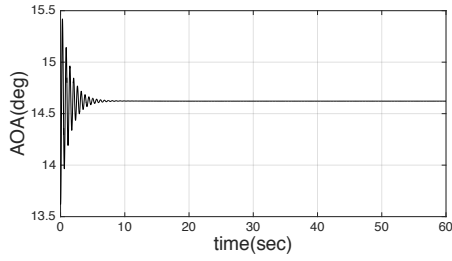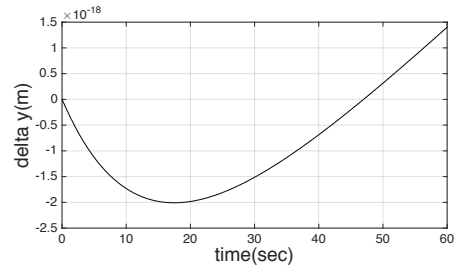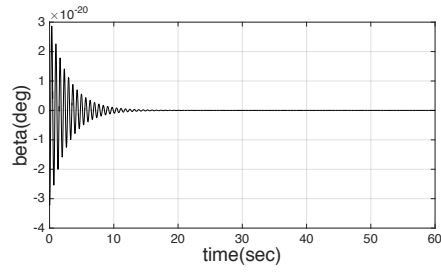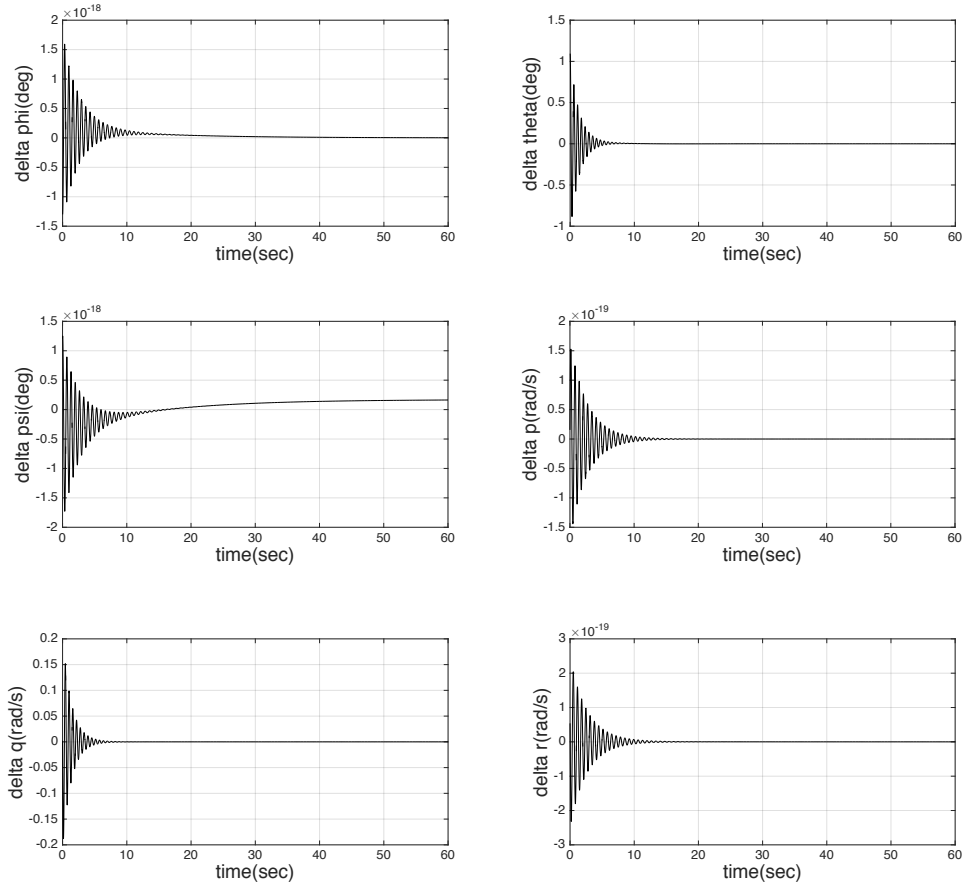
Figure 18 Short Period oscillation

5.7.2 Phugoid

$$\lambda_{c_{3,4}} = -0.1827 \pm 0.2226i$$

The second pair of eigenvalues has a smaller real part and a smaller complex part. Therefore this mode of vibration has a lower damping and frequency. This motion is known as the Phugoid mode. When applying an impulse input on pitch angular velocity to the wingsuit system, the pitch angle increases after the short period motion has more or less damped out. Therefore, the wingsuit system goes upward. This causes the velocity to decrease; because of this the lift is reduced. The pitch angle slowly decreases again and makes the vehicle go downward. In a similar way, this causes the velocity to increase, and in turn, increases the lift. In the Phugoid mode, the angle of attack is approximately constant, as shown in Figure 19. The Phugoid eigenvector is shown here:

40
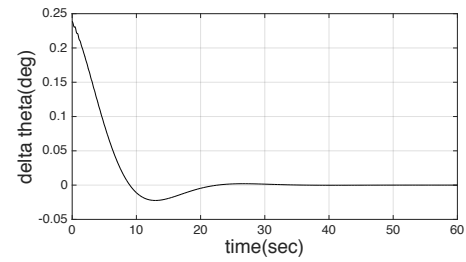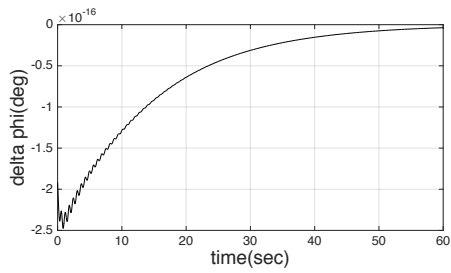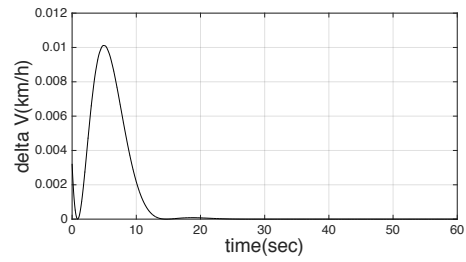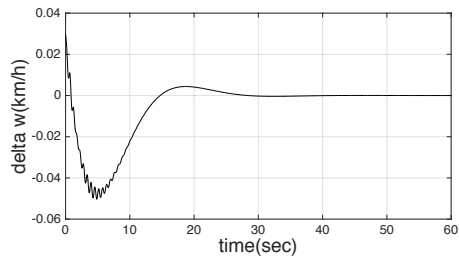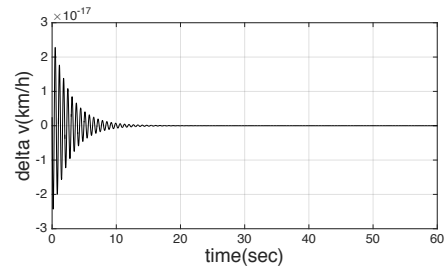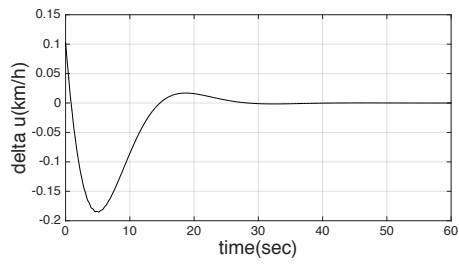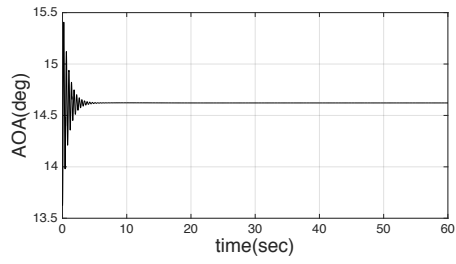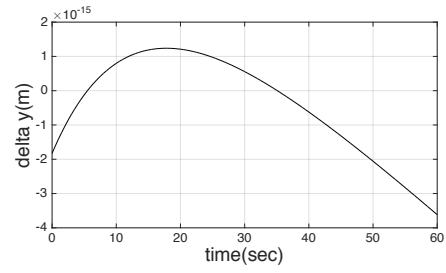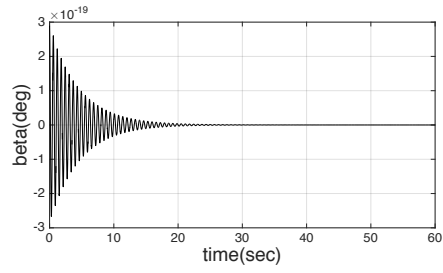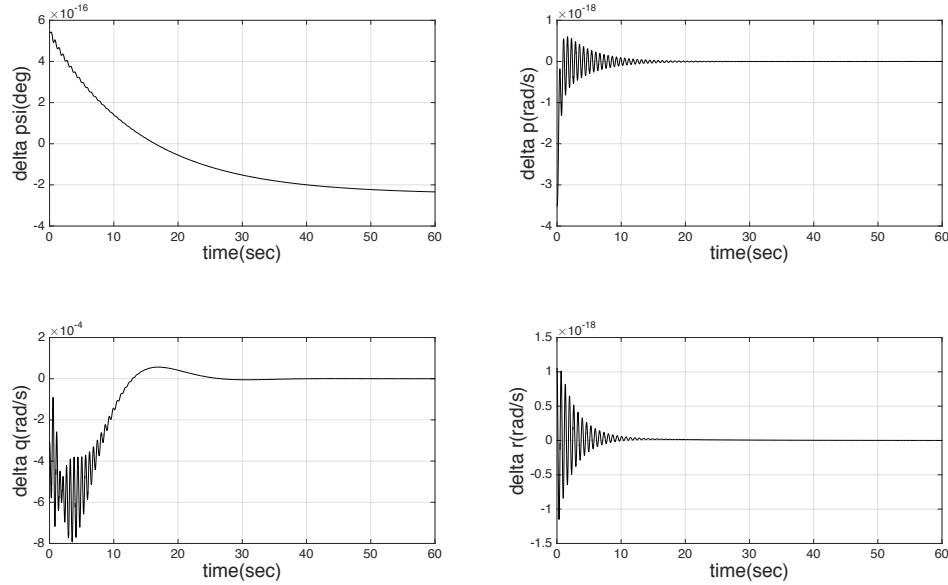
Figure 19 Phugoid mode

5.7.3 The Dutch Roll

$$\lambda_{c_{5,6}} = -0.2299 \pm 10.3121i$$

The pair of eigenvalues $\lambda_{c_{5,6}}$ has a slightly low damping and a slightly high frequency. In the mode of vibration corresponding to these eigenvalues, the wingsuit system alternately performs a yawing and a rolling motion. This mode of vibration is referred as the Dutch roll. To initiate the Dutch roll, an impulse input is applied to the wingsuit system to make the system has a yaw angular velocity. This causes the aircraft to yaw; in this case the wingsuit system yaws to the right. The lift on the left wing then increases, while the lift on the right wing decreases. This moment causes the wingsuit system to roll to the right even further. When the vehicle is rolling to the right, the lift vector of the right wing is tilted forward. Similarly, the left wing has a lift vector tilting backward, causing the vehicle to yaw to the left. This shows the alternation between roll motion and yaw motion. It is important to notice that roll and yaw are alternatively present. When the roll rate is at its maximum, the yaw rate is approximately 0, and vice versa. The Dutch roll is very uncomfortable not only for the wingsuit pilot, but also for passengers on regular commercial airlines. The Dutch roll eigenvector is shown here:

42
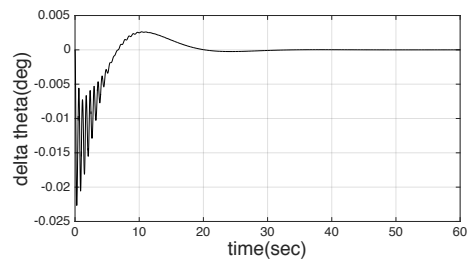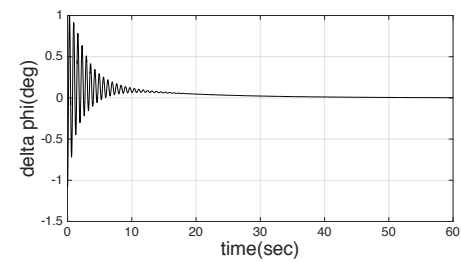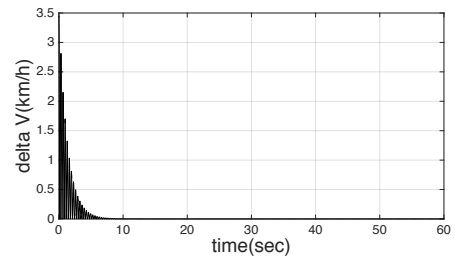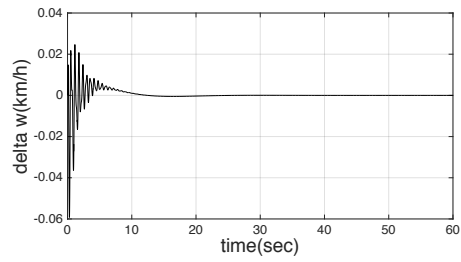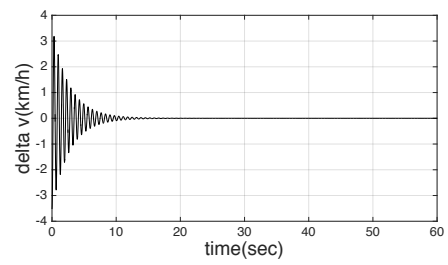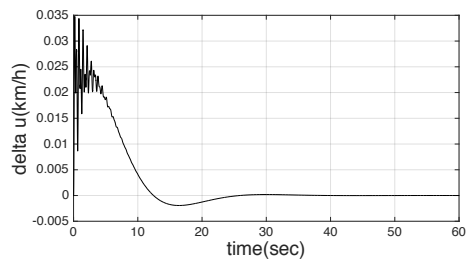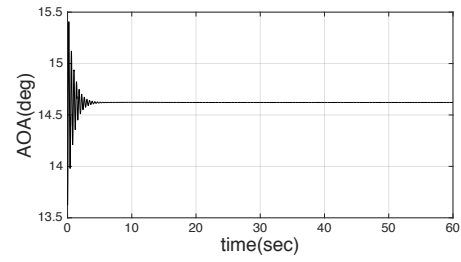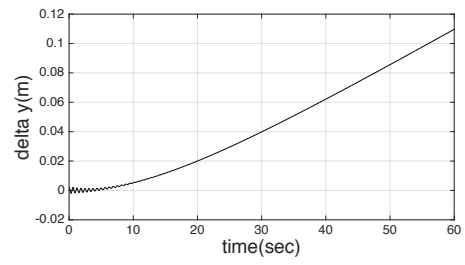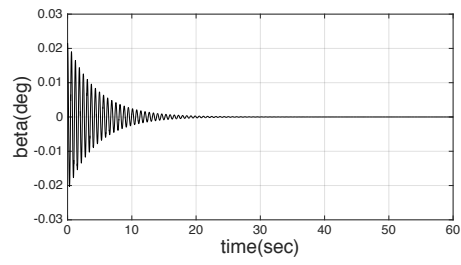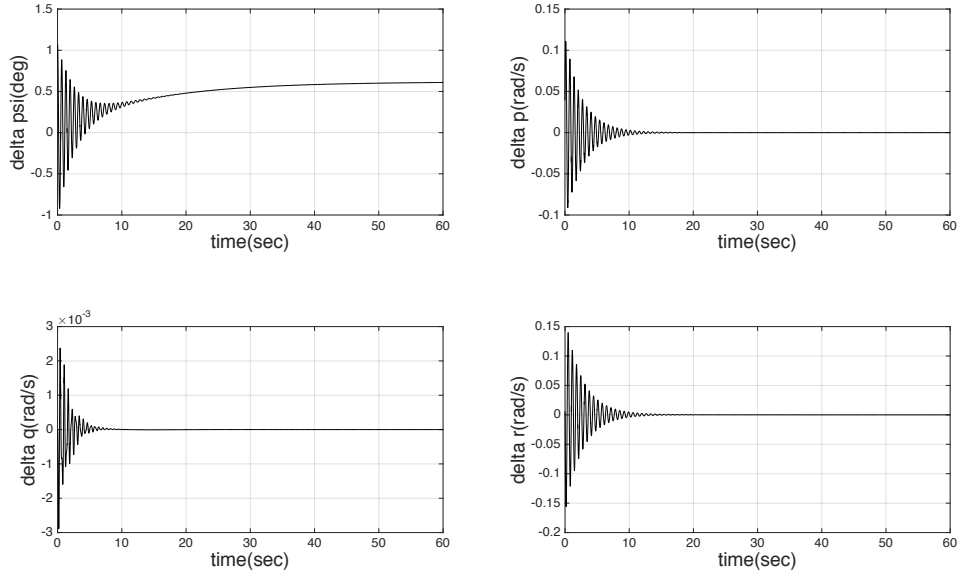
Figure 20 Dutch Roll

5.7.4 Spiral

$$\lambda_{c_7} = -0.08$$

The eigenvalue is very small. This means that divergence occurs only very slowly. In addition, the real part is still negative. Thus it is often called spiral motion and marginally stable. The spiral motion is induced by an initial roll angle. This causes the lift vector to be tilted. The horizontal component of the lift will cause the wingsuit system to make a turn. In the meanwhile, the vertical component of the lift vector has slightly decreased. This causes the wingsuit system to lose altitude. Combining these two facts will mean that the wingsuit system will perform a spiral motion. The spiral motion eigenvector is shown here:

44
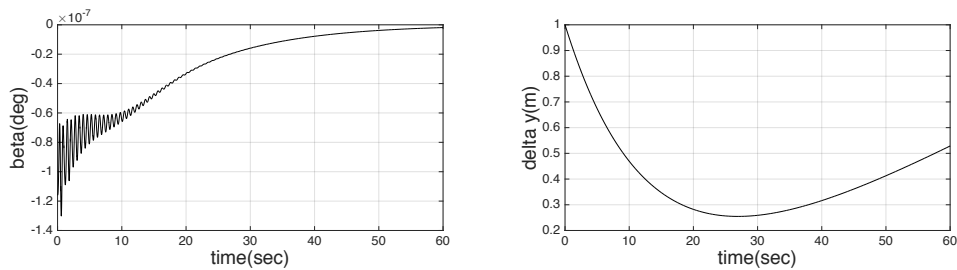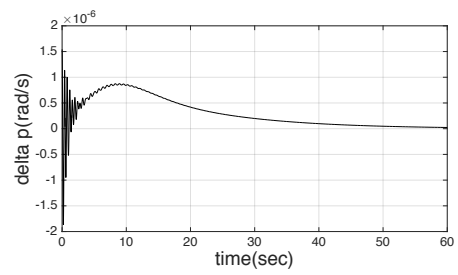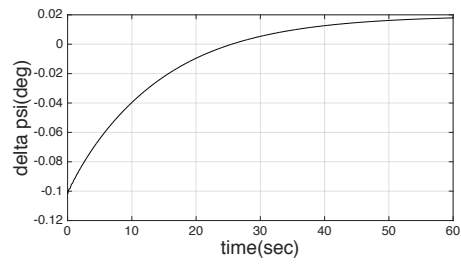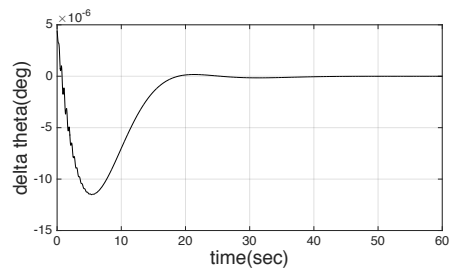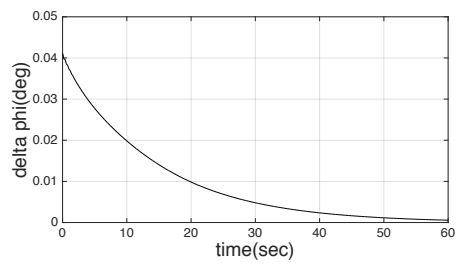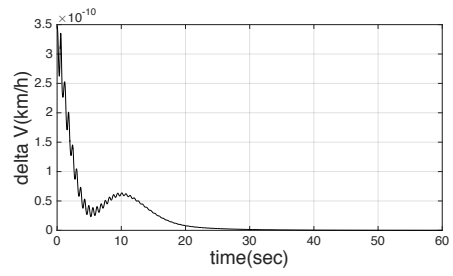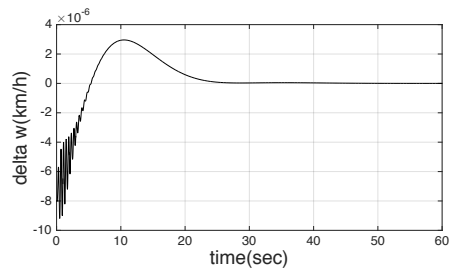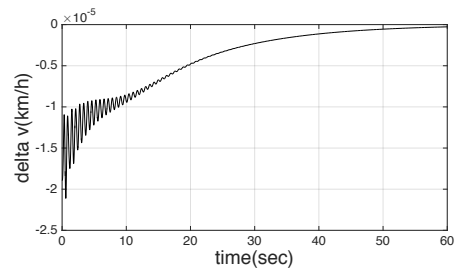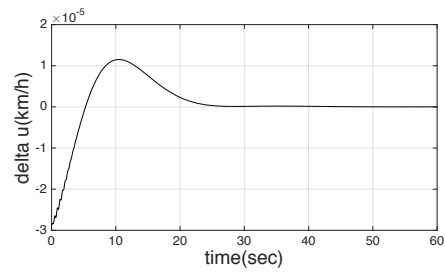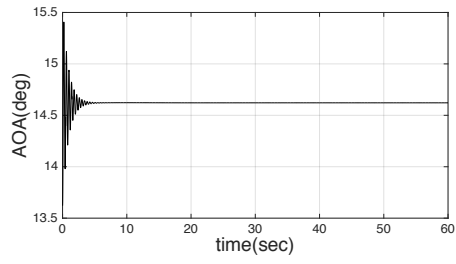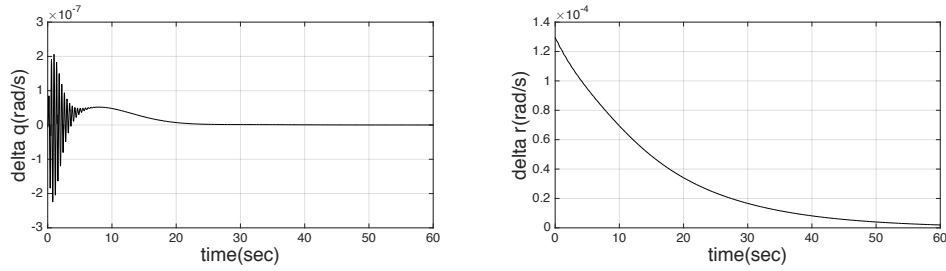
Figure 21 Spiral

5.7.4 Aperiodic Roll

$$\lambda_{c_8} = -2.5872$$

The real part of the eigenvalue is relatively more negative. This motion is therefore exponential first order damped. Its corresponding eigenvector has zero terms in longitudinal variables and nonzero terms in lateral directional variables. This is an asymmetric mode of vibration and is referred as the aperiodic roll. Applying a step input on roll angular velocity to the wingsuit system induces the aperiodic roll. When this happens, the wingsuit system starts to roll. In this case, the vehicle rolls to the right at the beginning. The right wing then goes down. This means that the right wing gets a higher angle of attack. The lift of the right wing thus increases. The opposite effect happens to the left wing. The lift on the left wing decreases. This lift difference causes a moment opposite to the rolling motion. Therefore, this motion is damped out. The roll rate will converge rather quickly to a constant value. The aperiodic roll is a very fast motion. There is no time for sideslips or yaw effects to appear. The aperiodic roll eigenvector is shown here:

46
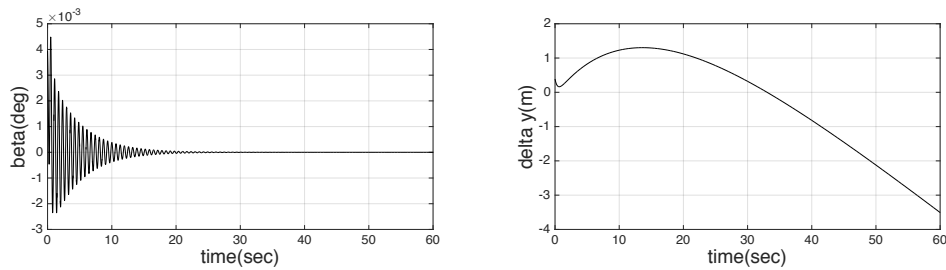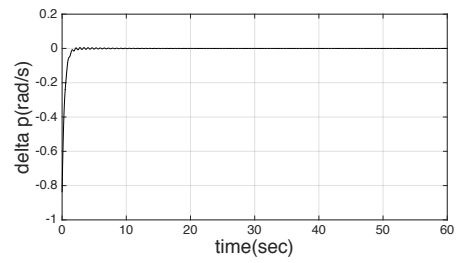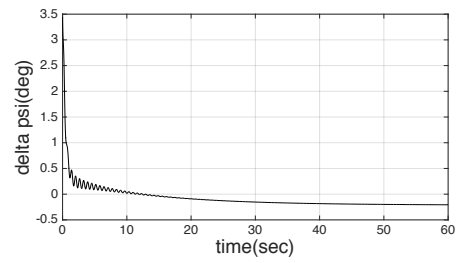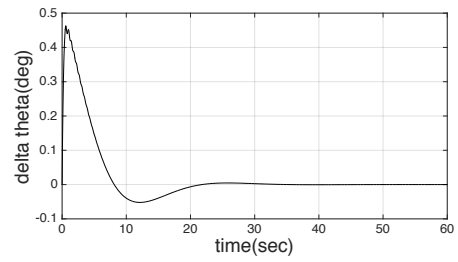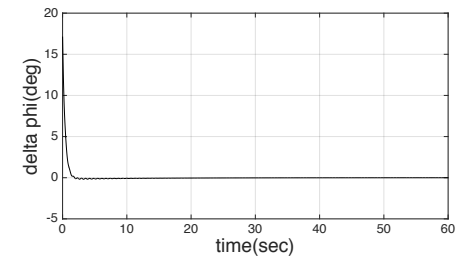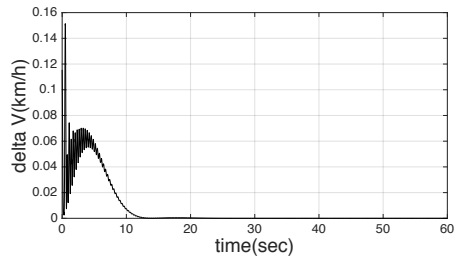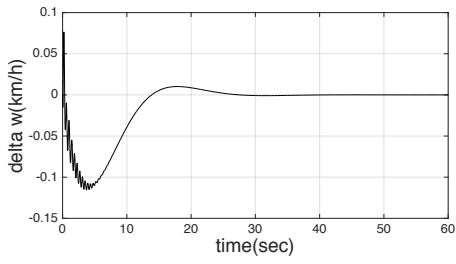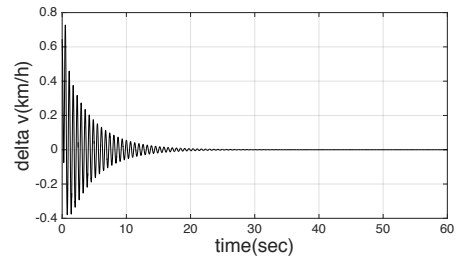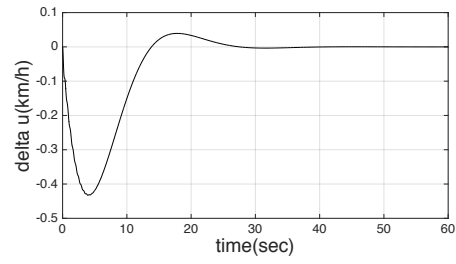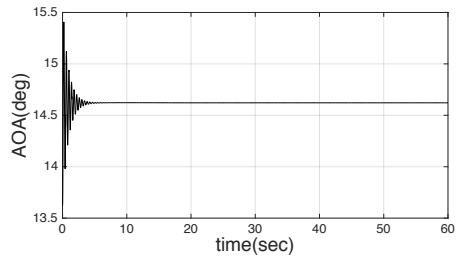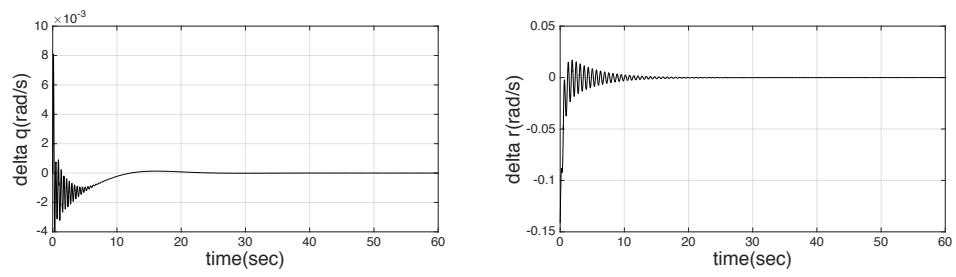
Figure 22 Aperiodic Roll

CHAPTER 6   CONCLUSION

This thesis focused on building a reduced scaled wingsuit air vehicle to acquire aerodynamic characteristics from wind tunnel tests. The whole procedure included the design, modification, and fabrication of the wingsuit model. The model was tested in wind tunnel at various angle of attack and sideslip angles. Seven different body configurations were designed to fulfill the basic flying techniques and aerobatic moves during regular wingsuit flights. Based on the data obtained from wind tunnel tests, the wingsuit air vehicle system was modeled a 6-DOF rigid body in order to simulate the flight trajectories for different flight conditions. This wingsuit air vehicle system applied the aerodynamic coefficients of the wingsuit model to a pilot with a full size commercial wingsuit. The simulations show that the wingsuit air vehicle system is a highly maneuverable flight vehicle. It can make transitions among different body configurations and turn smoothly via yaw and roll maneuvers.

Finally, the air vehicle system was simulated and analyzed about its modes of vibration. This explains the five different modes of the wingsuit air vehicle system when reacting to different disturbances during flights, including short period, the Phugoid, the Dutch roll, spiral motion, and the roll mode, damping of rolling motion. In addition, the results of simulations and vibrations analysis feed back into the design of wingsuits model and wind tunnel tests.

# APPENDIX A   AERODYNAMIC DATA OF ALL BODY

CONFIGURATIONS

A. 1 Cruise Configuration

A. 1-1 3D model
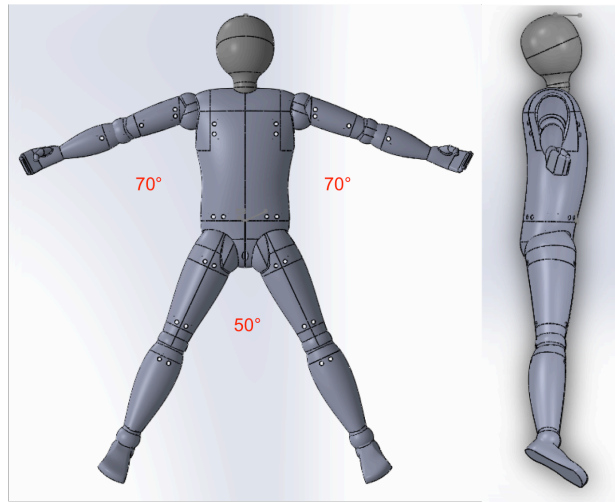
A. 1-2 Plots of Aerodynamic Data and Fit Functions
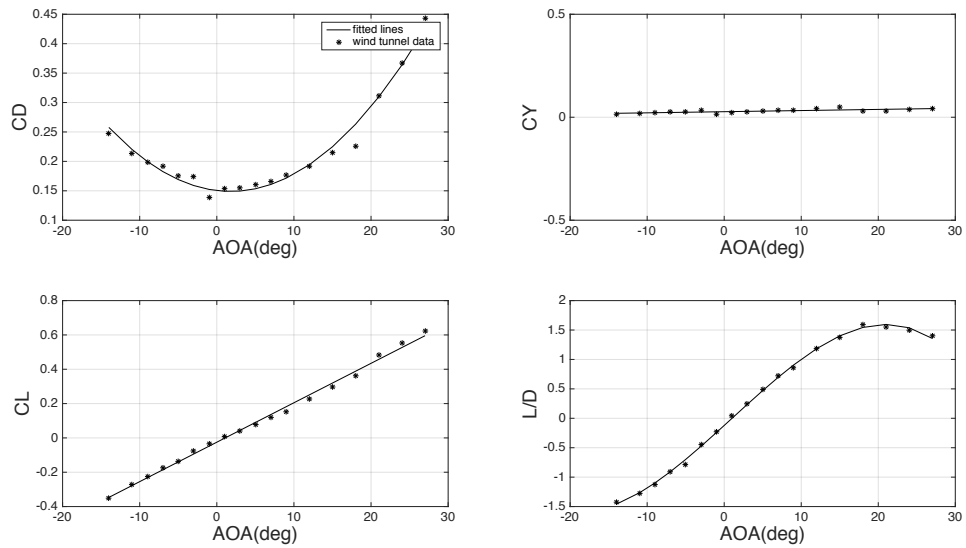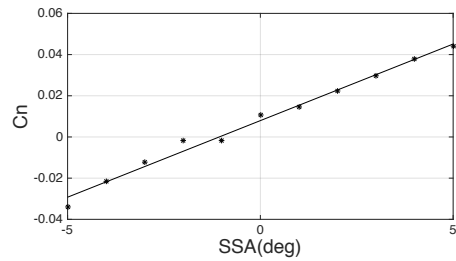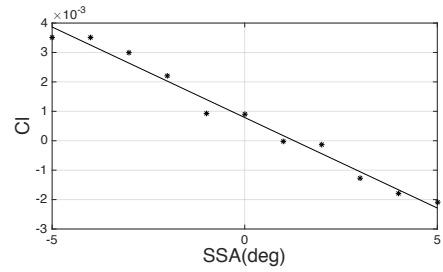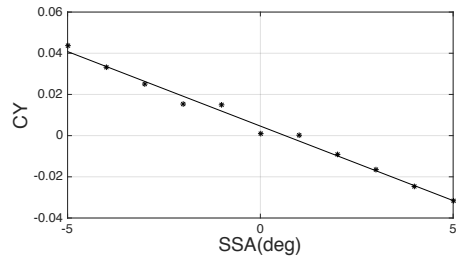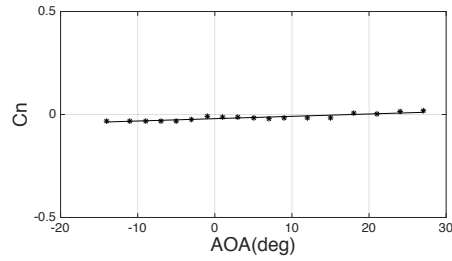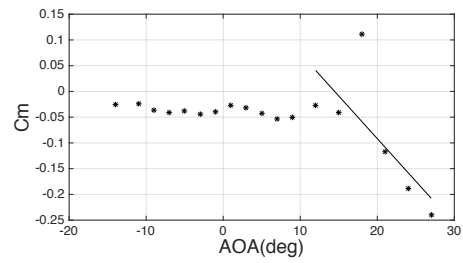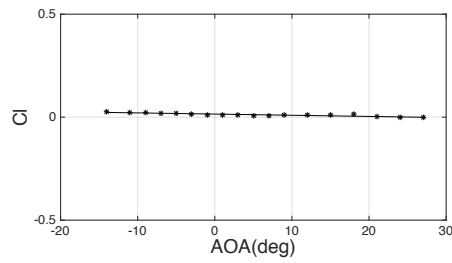
Fit Functions:

Drag Coefficient	CD = 0.00043675*alfad^2 - 0.0020578*alfad + 0.15138
Side Force Coefficient	CY = -0.0062614*betad
Lift Coefficient	CL = 0.022905*alfad - 0.028434
Roll Moment Coefficient	Cl = -0.00077*betad
Pitch Moment Coefficient	Cm = -0.033169*alfad + 0.48498
Yaw Moment Coefficient	Cn = 0.0070632*betad

Table of Data Points:

| Angle of Attack	CD	CL	Cm	SideSlip Angl	CY	Cl	Cn
-14	-0.2476488	0.3060654	-0.0260494	-5	0.0416	0.0007	0.0295
-11	-0.2138023	0.25573813	-0.0241475	-4	0.036	0.0011	0.0219
-9	-0.1984955	0.17951594	-0.0369055	-3	0.0315	0.0019	0.0155
-7	-0.1911946	0.13737253	-0.0403689	-2	0.0237	0.0025	0.0092
-5	-0.1759512	0.09500139	-0.0384551	-1	0.018	0.0025	0.0025
-3	-0.1737755	0.05519351	-0.0447916	0	0.012	0.0028	0
-1	-0.1389006	0.02033266	-0.0400477	1	0.0068	0.0033	-0.0131
1	-0.1532578	-0.0174463	-0.0275918	2	0.0009	0.0035	-0.0194
3	-0.1546897	-0.0582528	-0.0324891	3	-0.0075	0.0037	-0.0286
5	-0.1608427	-0.1069626	-0.0424685	4	-0.0142	0.004	-0.0341
7	-0.1656339	-0.1556095	-0.0537618	5	-0.0212	0.0048	-0.0401
9	-0.1774128	-0.20945	-0.0499375				
12	-0.1920593	-0.2923807	-0.0264598				
15	-0.2148817	-0.3744722	-0.0407152				
18	-0.2253208	-0.4451798	0.1119269				
21	-0.3116089	-0.5377618	-0.1171535				
24	-0.367408	-0.5993563	-0.1879258				
27	-0.4431932	-0.6462681	-0.2398142				

A. 2 Upfloating Configuration

A. 2-1 3D model
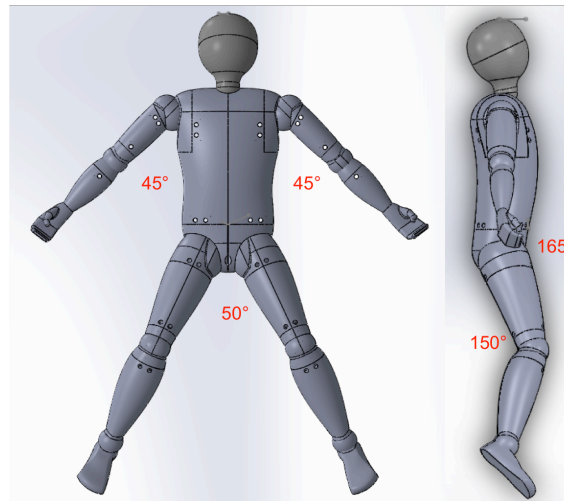
A. 2-2 Plots of Aerodynamic Data and Fit Functions
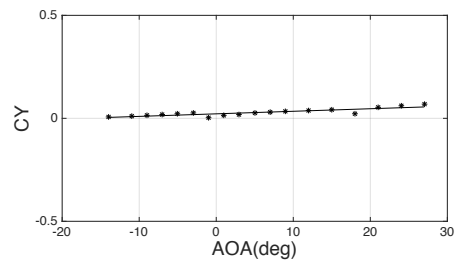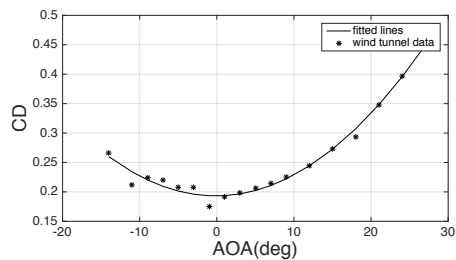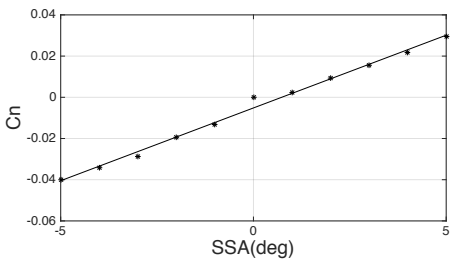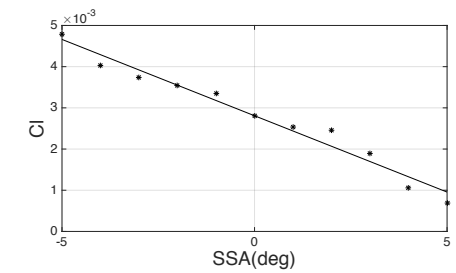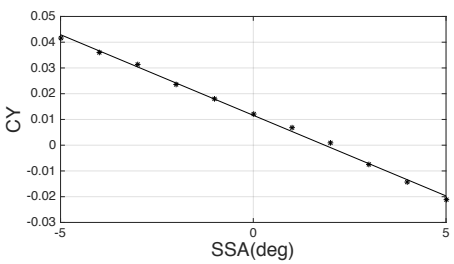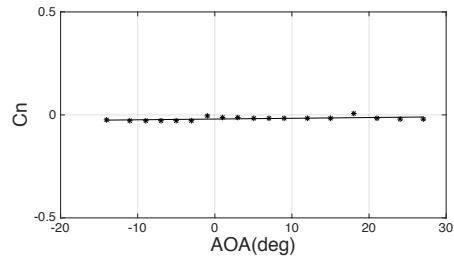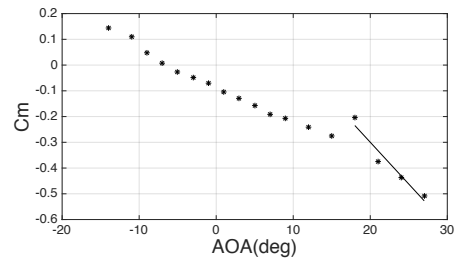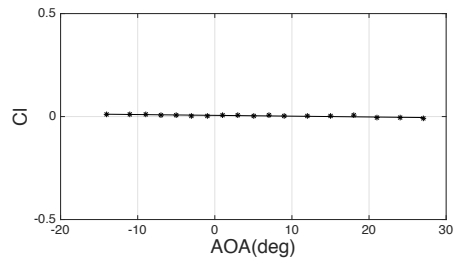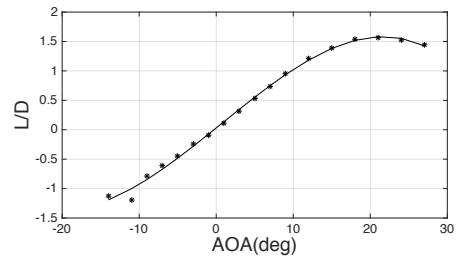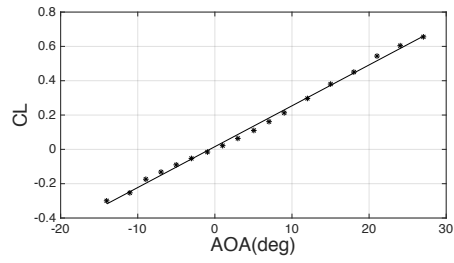
Fit Functions:

Drag Coefficient	CD = 0.00034811*alfad^2 - 0.00020835*alfad + 0.19316
Side Force Coefficient	CY = -0.0061514*betad
Lift Coefficient	CL = 0.023728*alfad + 0.01718

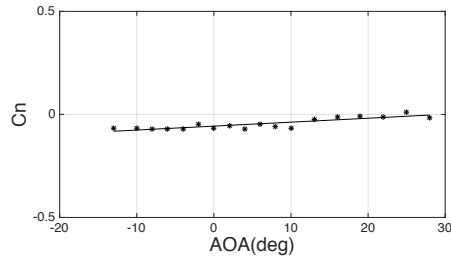| Roll Moment Coefficient | Cl = -0.00076*betad |
| Pitch Moment Coefficient | Cm = -0.032485*alfad + 0.35077 |
| Yaw Moment Coefficient | Cn = 0.0071234*betad |

Table of Data Points:

Angle of Attack	CD	CL	Cm	SideSlip Angle	CY	Cl	Cn
-14	-0.2667576	0.30145575	0.14397307	-5	0.0435	-0.0021	0.044
-11	-0.2116256	0.25208315	0.11126954	-4	0.0332	-0.0018	0.0377
-9	-0.2234542	0.17564288	0.04629578	-3	0.0251	-0.0013	0.0297
-7	-0.2203654	0.13354696	0.00790612	-2	0.0153	-0.0001	0.0224
-5	-0.2070972	0.09140096	-0.0271434	-1	0.0148	0	0.0145
-3	-0.2076354	0.05157763	-0.0480513	0	0.0009	0.0009	0.0105
-1	-0.174855	0.01728365	-0.0688794	1	0	0.0009	-0.0018
1	-0.1913764	-0.0207895	-0.1045784	2	-0.0091	0.0022	-0.0019
3	-0.1985773	-0.0617279	-0.1307726	3	-0.0164	0.003	-0.0122
5	-0.2059552	-0.1105738	-0.1568422	4	-0.0247	0.0035	-0.0215
7	-0.2151397	-0.1593885	-0.1904238	5	-0.0317	0.0035	-0.0341
9	-0.2248954	-0.2134075	-0.2058511				
12	-0.2449606	-0.296701	-0.2412237				
15	-0.2725477	-0.3792866	-0.274564				
18	-0.293364	-0.4503683	-0.2045395				
21	-0.3473792	-0.5439072	-0.3745948				
24	-0.3964599	-0.6063679	-0.436015				
27	-0.4535762	-0.6542837	-0.5089174				

A. 3 Straight Up Configuration

A. 3-1 3D model
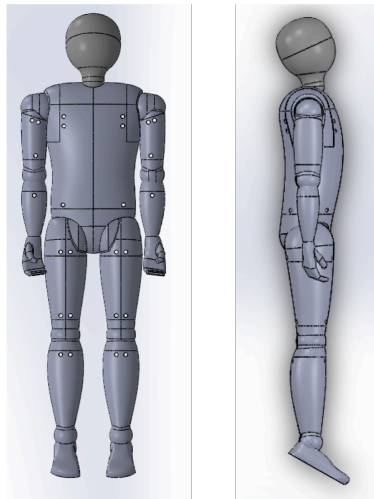
A. 3-2 Plots of Aerodynamic Data and Fit Functions
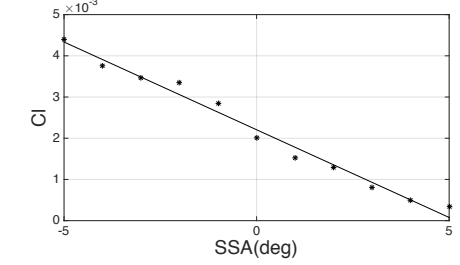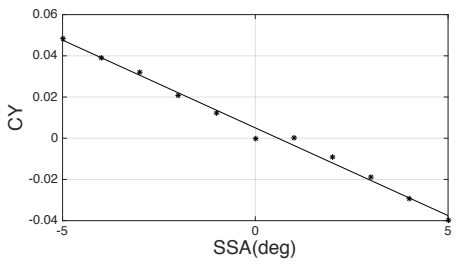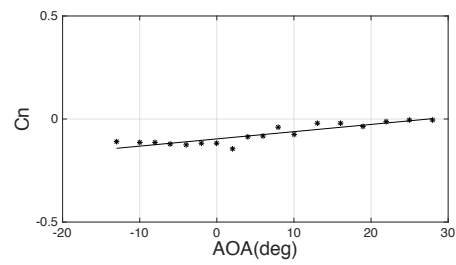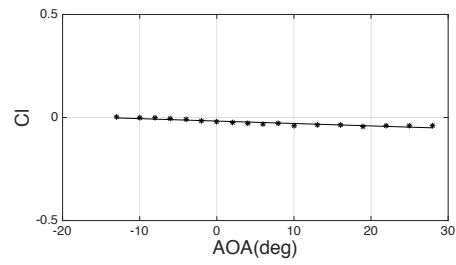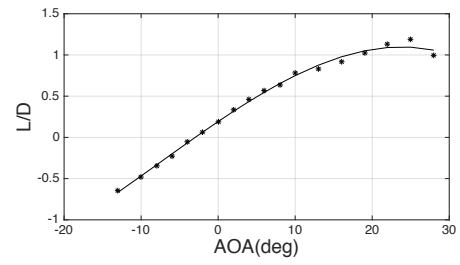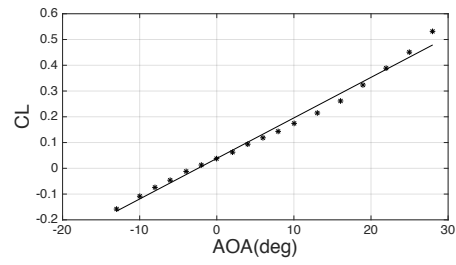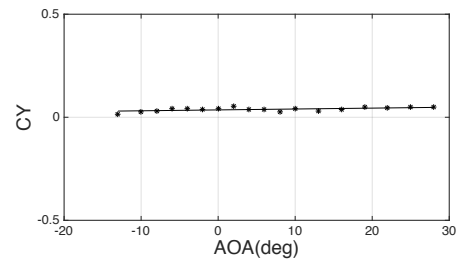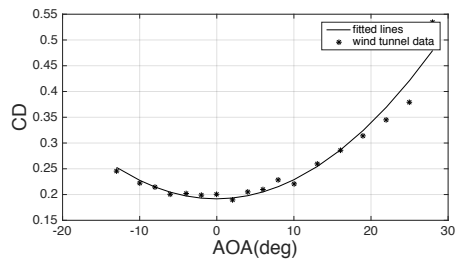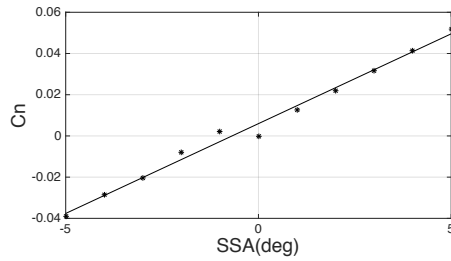
Fit Functions:

Drag Coefficient	CD = 0.00036527*alfad^2 + 0.000056419*alfad + 0.19164;
Side Force Coefficient	CY = -0.0060643*betad;
Lift Coefficient	CL = 0.015736*alfad + 0.038311;
Roll Moment Coefficient	Cl = -0.00077*betad;
Pitch Moment Coefficient	Cm = -0.031479*alfad + 0.028828;
Yaw Moment Coefficient	Cn = 0.0071321*betad;

Table of Data Points:

| Angle of Attack	CD	CL	Cm	SideSlip Angle	CY	Cl	Cn
-14	-0.2480292	0.1548801	-0.1443121	-5	0.0482	0.0003	0.0517
-11	-0.2246505	0.10372525	-0.2088679	-4	0.0389	0.0005	0.0415
-9	-0.2156648	0.069877	-0.2409977	-3	0.0319	0.0008	0.0315
-7	-0.2014415	0.04171824	-0.2744596	-2	0.0209	0.0013	0.0218
-5	-0.2024317	0.00812985	-0.304062	-1	0.0122	0.0015	0.0126
-3	-0.1989346	-0.0169787	-0.3184039	0	0	0.002	0
-1	-0.2000302	-0.0423878	-0.336175	1	0.0002	0.0028	0.0022
1	-0.1884274	-0.067153	-0.3561552	2	-0.009	0.0034	-0.0078
3	-0.2038943	-0.0980206	-0.3904802	3	-0.019	0.0035	-0.0204
5	-0.2071882	-0.1219361	-0.4112977	4	-0.0292	0.0038	-0.0285
7	-0.226659	-0.1486982	-0.4266045	5	-0.0398	0.0044	-0.039
9	-0.2176176	-0.177196	-0.4478401				
12	-0.2561859	-0.2191017	-0.4784902				
15	-0.2808441	-0.2674584	-0.5388904				
18	-0.3078436	-0.3277924	-0.6203763				
21	-0.3374294	-0.3949938	-0.6697655				
24	-0.3708202	-0.4586175	-0.7484117				
27	-0.5257257	-0.5394654	-0.9089521				

A. 4 Straight Up Left Turn Configuration

A. 4-1 3D model
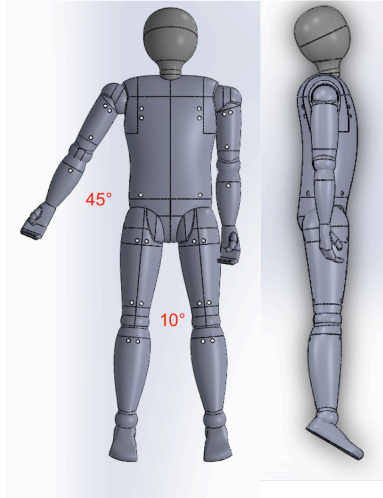
A. 4-2 Plots of Aerodynamic Data and Fit Functions
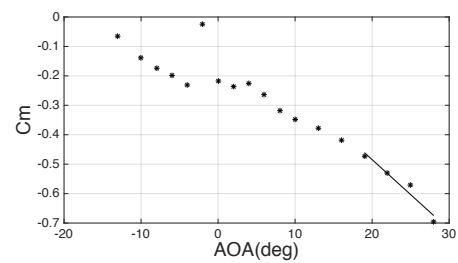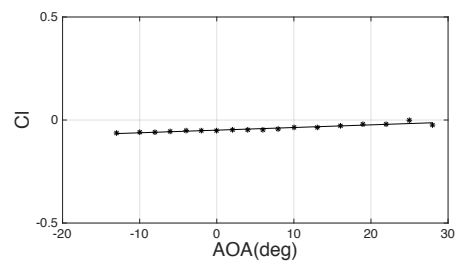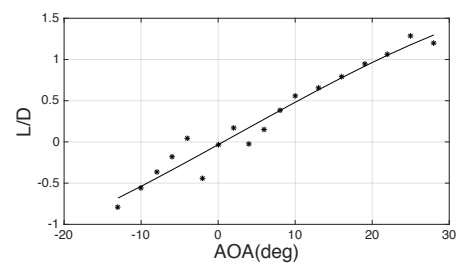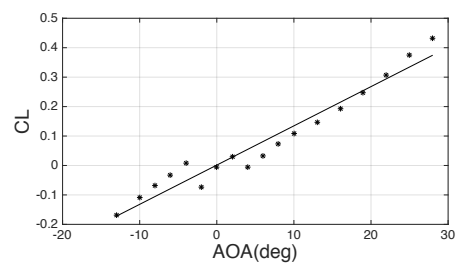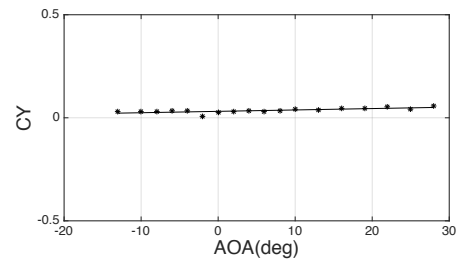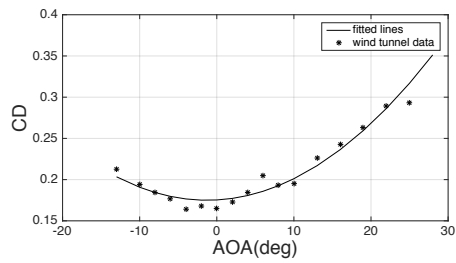
Fit Functions:

Drag Coefficient	CD = 0.00020593*alfad^2 + 0.000051759*alfad + 0.17532;
Side Force Coefficient	CY = 0;
Lift Coefficient	CL = 0.013328*alfad + 0.014626;
Roll Moment Coefficient	Cl = 0.0012826*alfad - 0.049175;
Pitch Moment Coefficient	Cm = -0.027468*alfad + 0.06227;
Yaw Moment Coefficient	Cn = 0;

Table of Data Points:

Angle of Attack	CD	CL	Cm	CY	Cl	Cn
-14	-0.21583891	0.165229468	-0.066425021	0.028418002	-0.062648839	-0.069486205
-11	-0.19572166	0.104385766	-0.138597516	0.029833214	-0.05953229	-0.067082574
-9	-0.186105614	0.064875119	-0.174568152	0.031487622	-0.056443046	-0.070434783
-7	-0.177532661	0.028713304	-0.197902116	0.033821233	-0.053395248	-0.07017126
-5	-0.163548286	-0.009678445	-0.229985282	0.032382548	-0.051065066	-0.071345748
-3	-0.168958602	0.071178415	-0.024047969	0.006083336	-0.04925795	-0.046638208
-1	-0.164861384	0.003445981	-0.216302384	0.028054419	-0.051398405	-0.067729842
1	-0.172224173	-0.031884606	-0.237790884	0.028464025	-0.046422414	-0.054369859
3	-0.184841394	0.001388799	-0.226413495	0.033386494	-0.046246627	-0.072585491
5	-0.203960729	-0.035098789	-0.264100516	0.029926023	-0.047145258	-0.048045224
7	-0.191894968	-0.077053806	-0.318545922	0.034291366	-0.041632639	-0.058263244
9	-0.193033858	-0.112188755	-0.346753952	0.040667151	-0.03604933	-0.067757938
12	-0.223405921	-0.151167811	-0.376906488	0.039728098	-0.034624564	-0.023475576
15	-0.239078204	-0.195733186	-0.418441307	0.043748452	-0.028755982	-0.013294219
18	-0.25894932	-0.252904339	-0.471913826	0.0462336	-0.021383257	-0.007720666
21	-0.283880768	-0.311967786	-0.531429564	0.051964977	-0.019552756	-0.011315263
24	-0.286224403	-0.381233737	-0.571322875	0.040035536	-0.000724908	0.011407902
27	-0.353115784	-0.437441134	-0.696237242	0.058160938	-0.023503878	-0.016181001

A. 5 Left Turn Configuration

A. 5-1 3D model

58
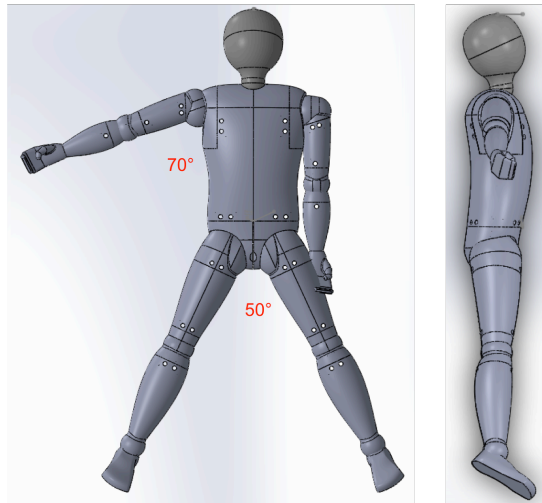
A. 5-2 Plots of Aerodynamic Data and Fit Functions
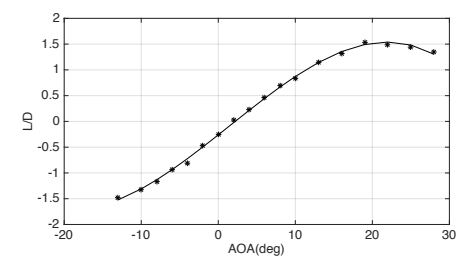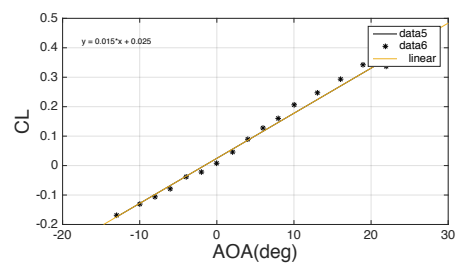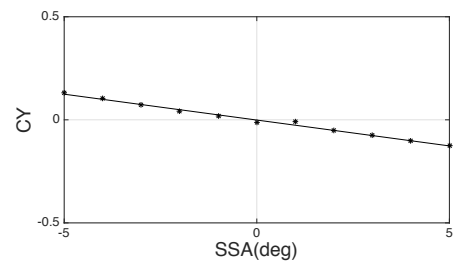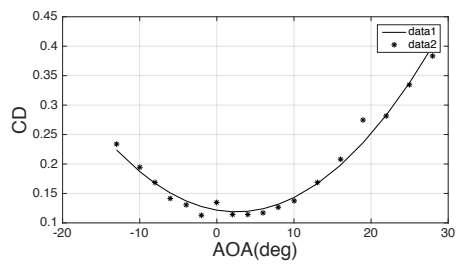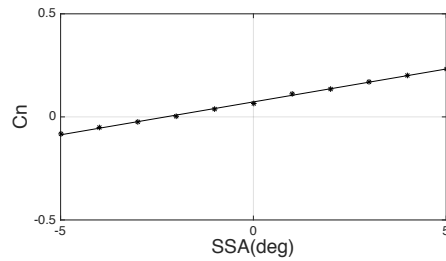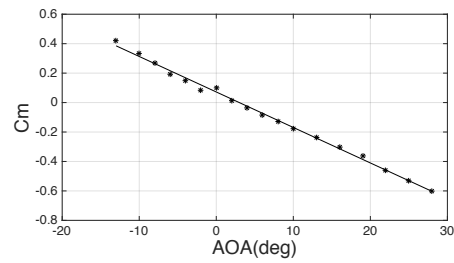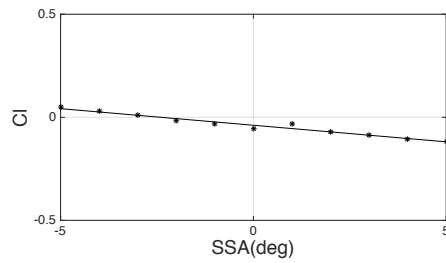
Fit Functions:

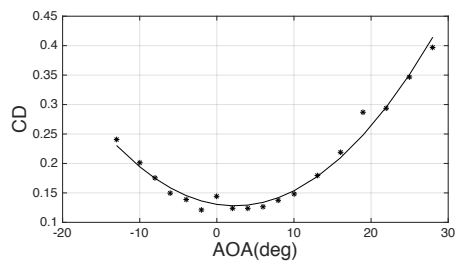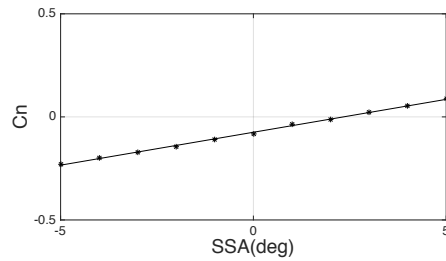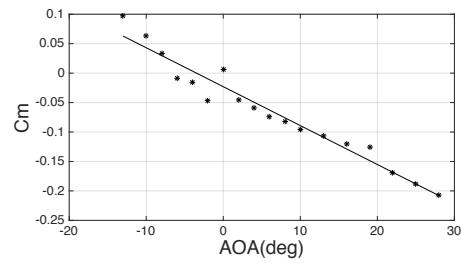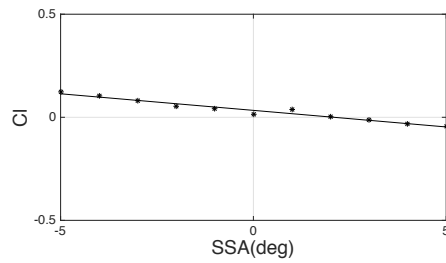| Drag Coefficient	CD = 0.00043*alfad^2 - 0.0022*alfad + 0.12
Side Force Coefficient	CY = -0.025*betad – 0.0011
Lift Coefficient	CL = 0.01567*alfad + 0.04110
Roll Moment Coefficient	Cl = -0.01*betad - 0.039
Pitch Moment Coefficient	Cm = -0.024*alfad + 0.048
Yaw Moment Coefficient	Cn = 0.032*betad + 0.073

Table of Data Points:

Angle of Attack	CD	CL	Cm	SideSlip Angle	CY	Cl	Cn
-14	-0.2559	0.2103	0.4704	-5	0.1388	0.0606	-0.0798
-11	-0.2116	0.1731	0.3784	-4	0.1097	0.0394	-0.0498
-9	-0.1835	0.1476	0.3088	-3	0.0795	0.0166	-0.0205
-7	-0.1544	0.1201	0.2291	-2	0.0447	-0.0121	0.0066
-5	-0.1401	0.0788	0.1834	-1	0.0214	-0.0258	0.0394
-3	-0.1198	0.063	0.1145	0	-0.0115	-0.0521	0.0675
-1	-0.1392	0.0329	0.1288	1	-0.0082	-0.0313	0.1136
1	-0.1163	-0.0042	0.0407	2	-0.0506	-0.0699	0.1368
3	-0.1133	-0.0493	-0.0104	3	-0.0767	-0.0872	0.1683
5	-0.1126	-0.0856	-0.0627	4	-0.1039	-0.1061	0.1991
7	-0.1202	-0.1202	-0.1068	5	-0.1263	-0.1187	0.2324
9	-0.1277	-0.1643	-0.1558				
12	-0.1552	-0.2043	-0.2195				
15	-0.1902	-0.2517	-0.2861				
18	-0.2533	-0.3009	-0.3431				
21	-0.2562	-0.2934	-0.438				
24	-0.3052	-0.339	-0.5086				
27	-0.35	-0.3844	-0.578				

A. 6 Right Turn Configuration

A. 6-1 3D model
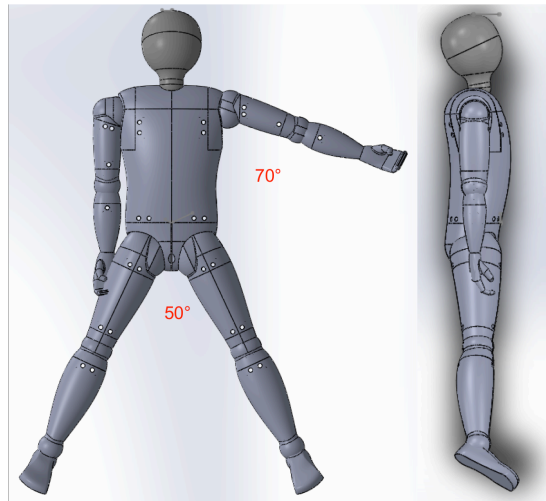
A. 6-2 Plots of Aerodynamic Data and Fit Functions
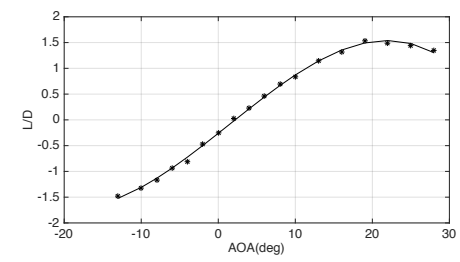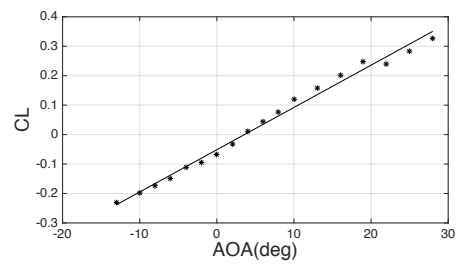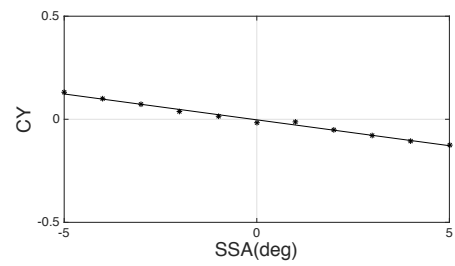
Fit Functions:

Drag Coefficient	CD = 0.00043*alfad^2 - 0.0023*alfad + 0.13
Side Force Coefficient	CY = -0.025*betad – 0.0027
Lift Coefficient	CL = 0.014*alfad - 0.0051
Roll Moment Coefficient	Cl = -0.016*betad - 0.034
Pitch Moment Coefficient	Cm = -0.0066*alfad – 0.025
Yaw Moment Coefficient	Cn = 0.032*betad – 0.075

Table of Data Points:

Angle of Attack	CD	CL	Cm	SideSlip Angle	CY	Cl	Cn
-14	-0.2624	0.273	0.1305	-5	0.1372	0.1328	-0.227
-11	-0.2186	0.2386	0.0909	-4	0.1081	0.1116	-0.197
-9	-0.1908	0.215	0.0563	-3	0.0779	0.0888	-0.1677
-7	-0.162	0.1895	0.0116	-2	0.0431	0.0601	-0.1406
-5	-0.1482	0.15	0.0009	-1	0.0198	0.0464	-0.1078
-3	-0.1282	0.1362	-0.033	0	-0.0131	0.0201	-0.0797
-1	-0.1479	0.1079	0.0163	1	-0.0098	0.0409	-0.0336
1	-0.1254	0.0728	-0.0368	2	-0.0522	0.0023	-0.0104
3	-0.1227	0.0296	-0.0529	3	-0.0782	-0.015	0.0211
5	-0.1223	-0.0048	-0.0702	4	-0.1055	-0.0339	0.0519
7	-0.1303	-0.0376	-0.0793	5	-0.1279	-0.0465	0.0852
9	-0.1382	-0.0797	-0.0933				
12	-0.1662	-0.1169	-0.1045				
15	-0.2016	-0.1614	-0.1186				
18	-0.2652	-0.2078	-0.1231				
21	-0.2686	-0.1974	-0.1655				
24	-0.3182	-0.2402	-0.1836				
27	-0.3635	-0.2827	-0.2006				

A. 7 Rudder Configuration

A. 7-1 3D model
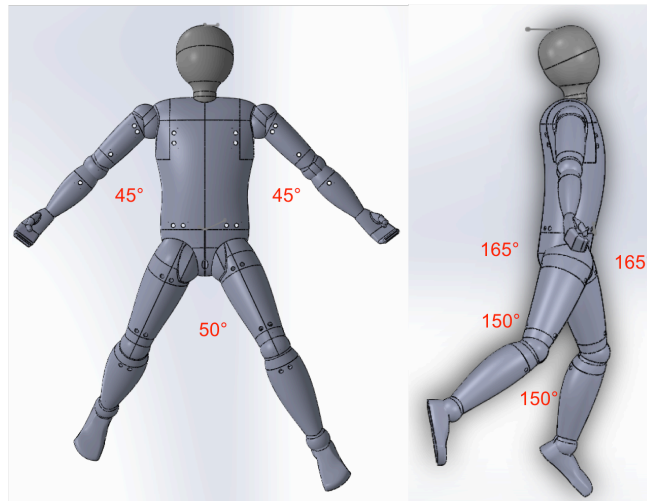
A. 7-2 Plots of Aerodynamic Data and Fit Functions
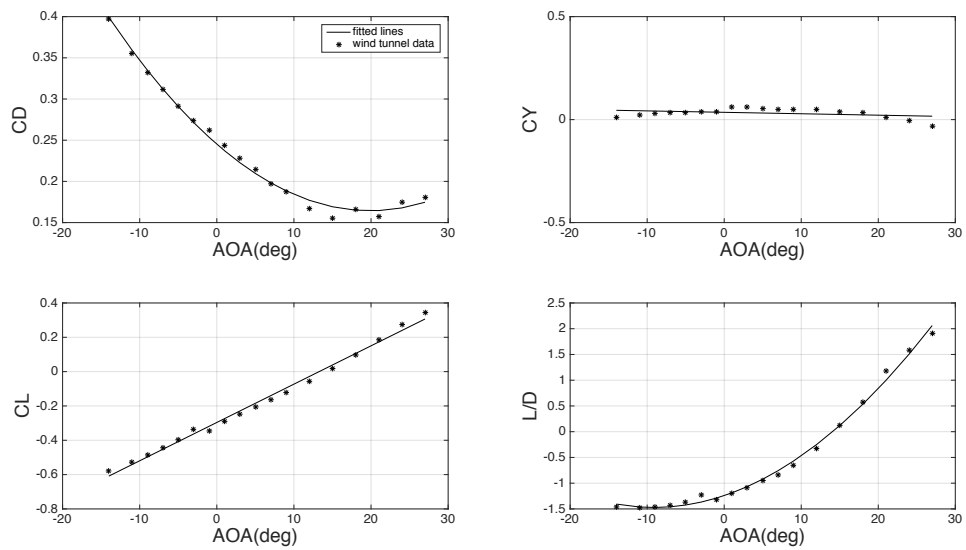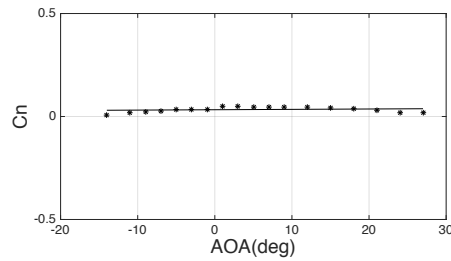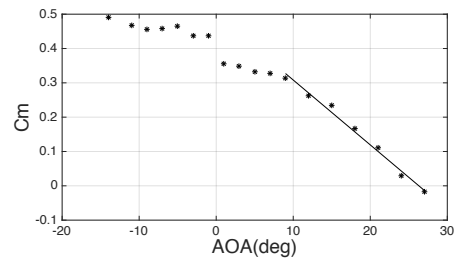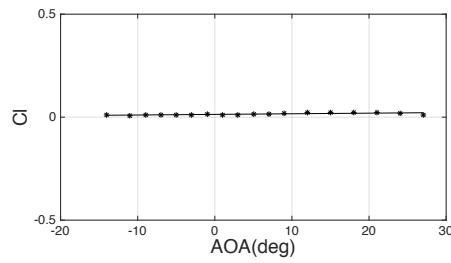
Fit Functions:

Drag Coefficient	CD = 0.00020706*alfad^2 - 0.00818911*alfad + 0.24771
Side Force Coefficient	CY = 0
Lift Coefficient	CL = 0.022417*alfad - 0.3007
Roll Moment Coefficient	Cl = 0.0019206*alfad
Pitch Moment Coefficient	Cm = -0.018897*alfad + 0.51472
Yaw Moment Coefficient	Cn = 0

Table of Data Points:

Angle of Attack	CD	CL	Cm	CY	Cl	Cn
-14	-0.396847245	0.579711639	0.490517595	0.01067976	0.008912589	0.008554039
-11	-0.35546028	0.525339697	0.46793697	0.023214414	0.008285591	0.018610736
-9	-0.331962262	0.485999348	0.45613541	0.028473681	0.00962577	0.022909043
-7	-0.311515293	0.445784649	0.457109749	0.032170001	0.011144171	0.02754297
-5	-0.290873486	0.397836073	0.464279927	0.035663304	0.012313286	0.03227004
-3	-0.274194734	0.335764939	0.436935517	0.036751354	0.012262388	0.034575178
-1	-0.262309674	0.345129658	0.436935517	0.036751354	0.013461574	0.034126165
1	-0.243640359	0.290698822	0.354726942	0.060180693	0.011391956	0.048973155
3	-0.228584909	0.247740692	0.348588865	0.0605006	0.012273867	0.050426449
5	-0.214746851	0.204354973	0.331878699	0.054159634	0.013293171	0.046886252
7	-0.197250358	0.165237329	0.327770884	0.048159448	0.01595496	0.044628529
9	-0.187451329	0.122074362	0.313488225	0.051069599	0.019694121	0.046237015
12	-0.167126572	0.05462255	0.262438833	0.048799338	0.022599104	0.045705343
15	-0.155259816	-0.018438047	0.235368167	0.03795584	0.023253623	0.042212423
18	-0.166394459	-0.096597161	0.166948026	0.035717278	0.023940236	0.036932764
21	-0.157525743	-0.185365473	0.110059856	0.012297957	0.021884224	0.028259372
24	-0.174315716	-0.276103791	0.02913861	-0.00609564	0.018710459	0.019823946
27	-0.180996399	-0.346118828	-0.01833745	-0.03308556	0.010503673	0.019229674

APPENDIX B   SIMULATIONS OF ALL BODY CONFIGURATIONS

B.1 Cruise Configuration

B.1-1 Initial Condition

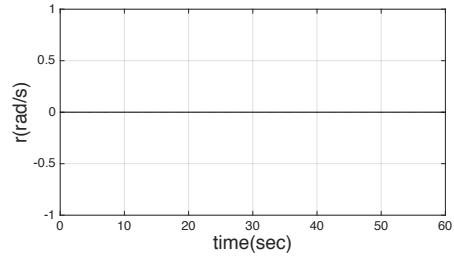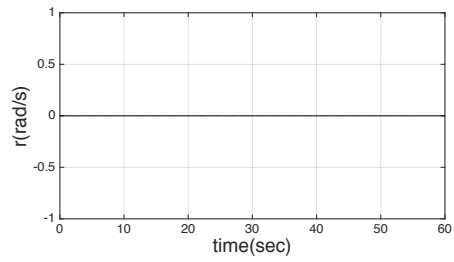| Elements of a state x	Units	Initial values x0 (time = 0 sec)	Steady State (time = 60 sec)
u	m/s	10	46.4
v	m/s	0	0
w	m/s	3	12
X_e	m	0	2172.2
Y_e	m	0	0
Z_e	m	-4000	-2295.4
p	rad/s	0	0
q	rad/s	0	0
r	rad/s	0	0
ϕ	$degree$	0	0
θ	$degree$	30	-20.54
ψ	$degree$	0	0

B.1-2 Geometric Data and Moments of Inertia

I_{xx}	$kg*m^2$	4.3
I_{yy}	$kg*m^2$	12.6
I_{zz}	$kg*m^2$	16.6
I_{xz}	$kg*m^2$	0.1
I_{xy}	$kg*m^2$	0.001
I_{yz}	$kg*m^2$	0.002
Wing Area *(S)*	m^2	1.393
Wing Span *(b)*	m	1.857
Wing Chord (c_bar)	m	0.75

B. 1-3 Flight Simulation
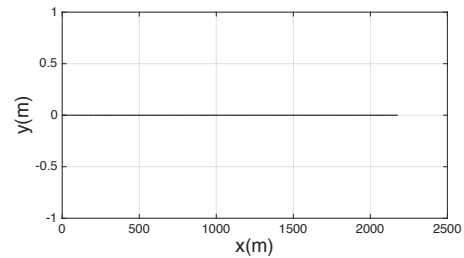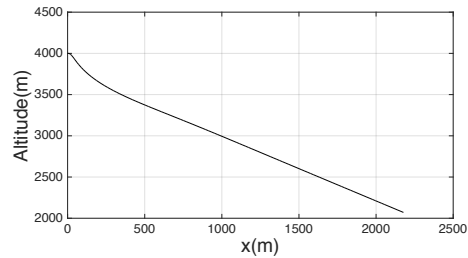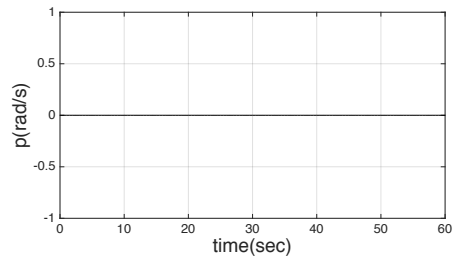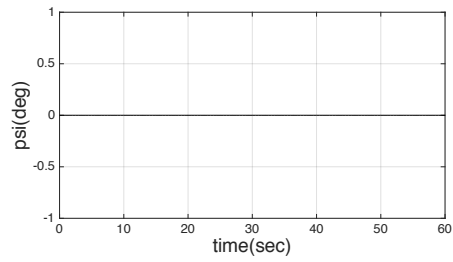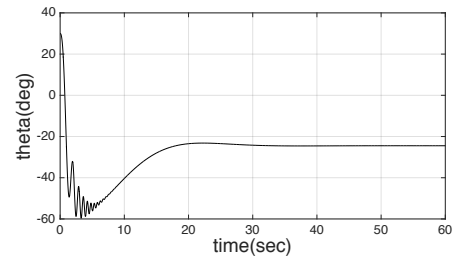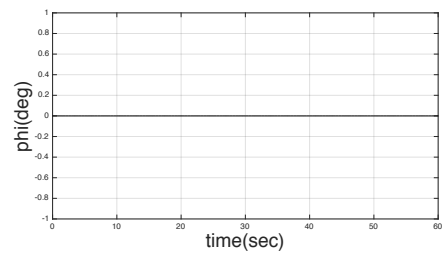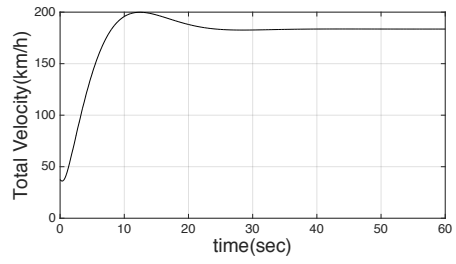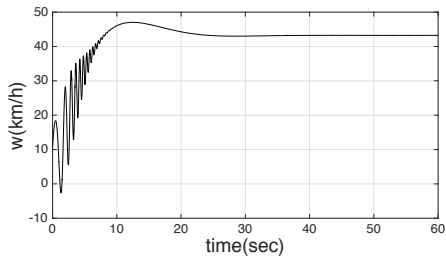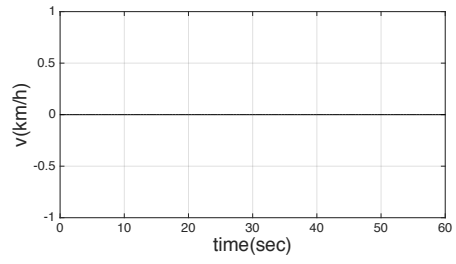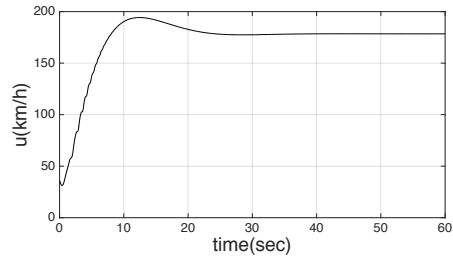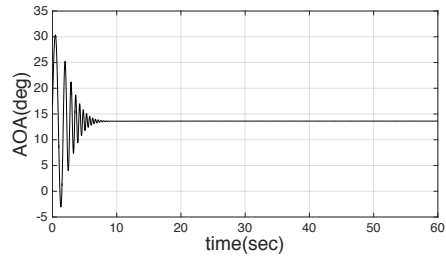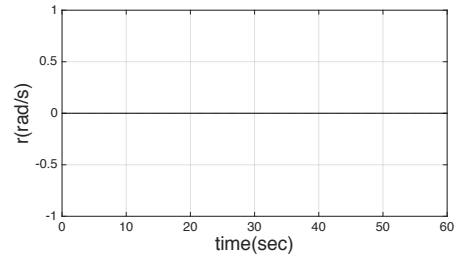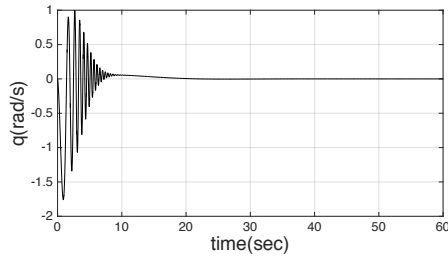
B.2 Upfloating Configuration

B.2-1 Initial Condition

Elements of a state x	Units	Initial values x0 (time = 0 sec)	Steady State (time = 60 sec)
u	m/s	10	48.8
v	m/s	0	0
w	m/s	3	10.2
X_e	m	0	2011
Y_e	m	0	0
Z_e	m	-4000	-1992.4
p	rad/s	0	0
q	rad/s	0	0
r	rad/s	0	0
ϕ	$degree$	0	0
θ	$degree$	30	-28.65
ψ	$degree$	0	0

B.2-2 Geometric Data and Moments of Inertia

| I_{xx}	$kg*m^2$	4.3
I_{yy}	$kg*m^2$	11.5
I_{zz}	$kg*m^2$	16.4
I_{xz}	$kg*m^2$	0.3
I_{xy}	$kg*m^2$	0.2
I_{yz}	$kg*m^2$	0.3
Wing Area (S)	m^2	1.346
Wing Span (b)	m	1.857
Wing Chord (c_bar)	m	0.718

B. 2-3 Flight Simulation
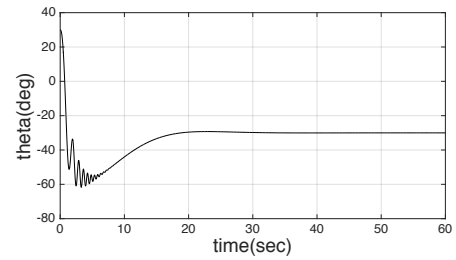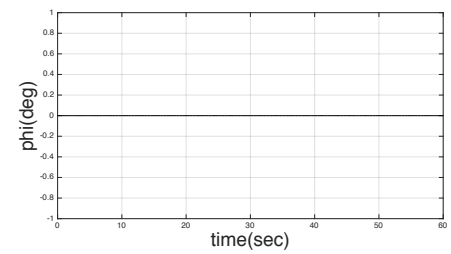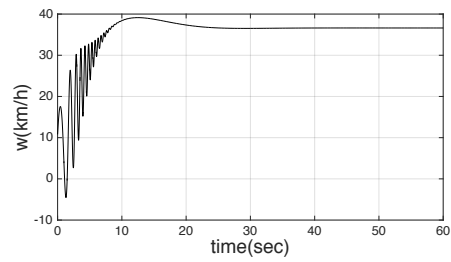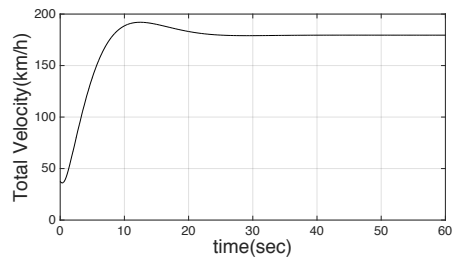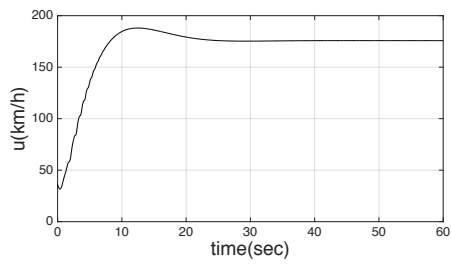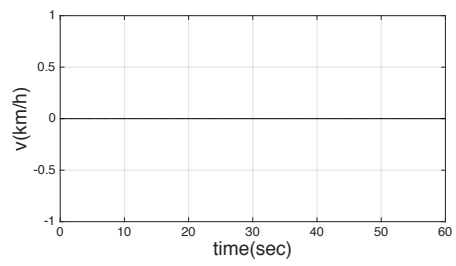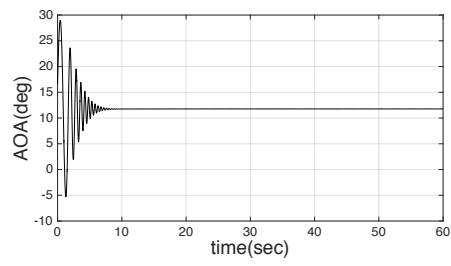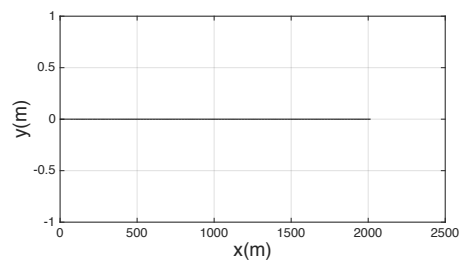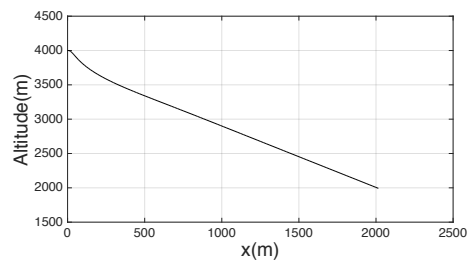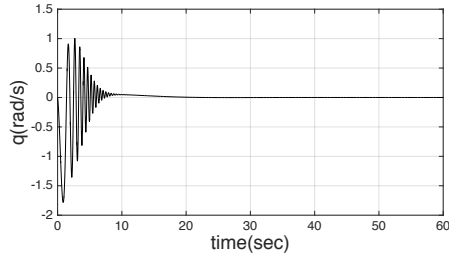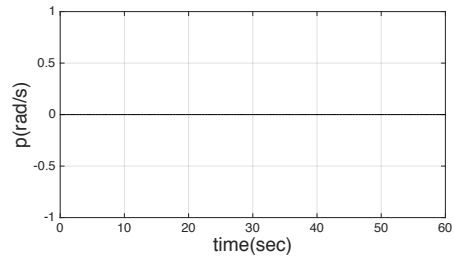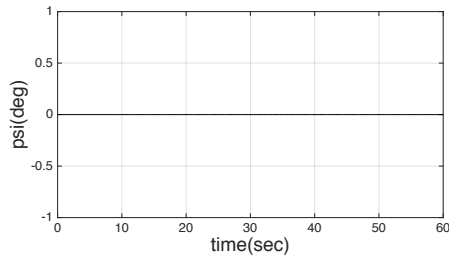
B.3 Straight Up Configuration

B.3-1 Initial Condition and Steady State

Elements of a state x	Units	Initial values x0 (time = 0 sec)	Steady State (time = 60 sec)
u	m/s	10	82.8
v	m/s	0	0
w	m/s	3	1.3
X_e	m	0	1080
Y_e	m	0	0
Z_e	m	-4000	334.7
p	rad/s	0	0
q	rad/s	0	0
r	rad/s	0	0
ϕ	$degree$	0	0
θ	$degree$	30	-74.5
ψ	$degree$	0	0

B.3-2 Geometric Data and Moments of Inertia

| I_{xx}	$kg * m^2$	1.2
I_{yy}	$kg * m^2$	13.4
I_{zz}	$kg * m^2$	14.3
I_{xz}	$kg * m^2$	0.1
I_{xy}	$kg * m^2$	0.001
I_{yz}	$kg * m^2$	0.001
Wing Area *(S)*	m^2	0.879
Wing Span *(b)*	m	0.598
Wing Chord (c_bar)	m	1.47

B. 3-3 Flight Simulation

psi(deg)   time(sec)

p(rad/s)   time(sec)

q(rad/s)   time(sec)

r(rad/s)   time(sec)
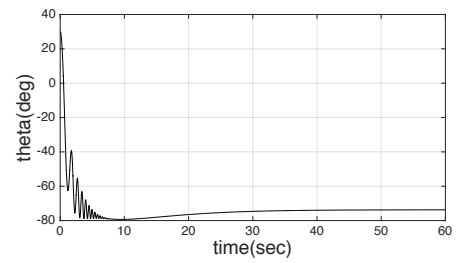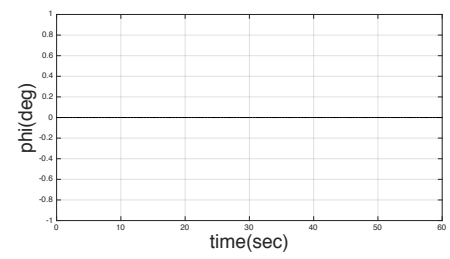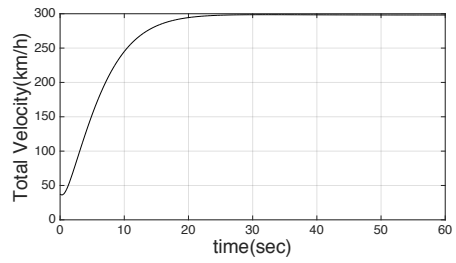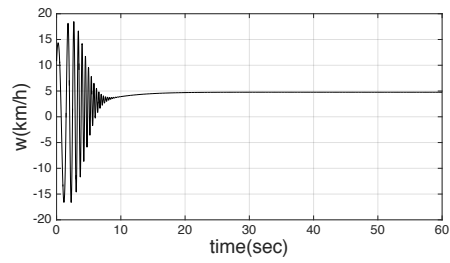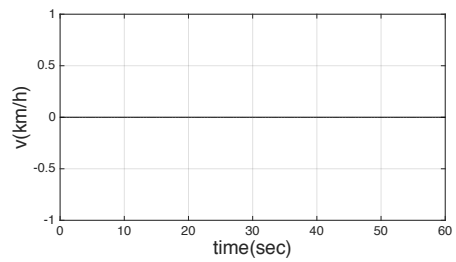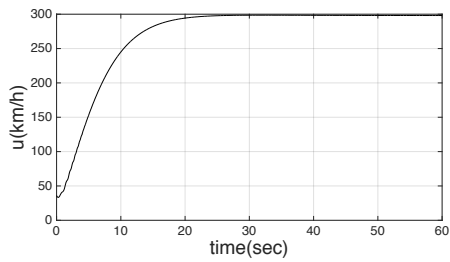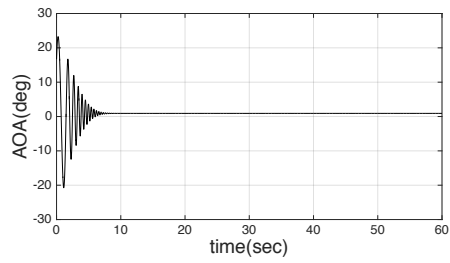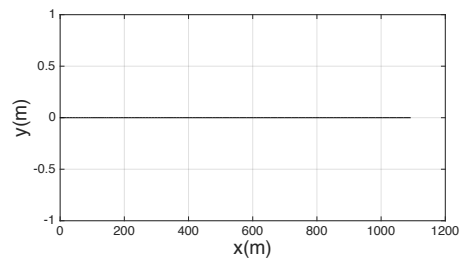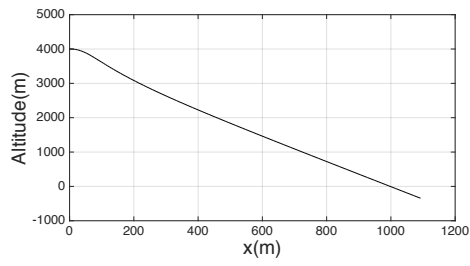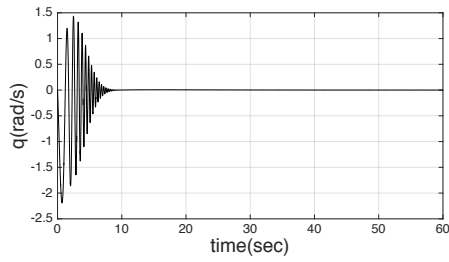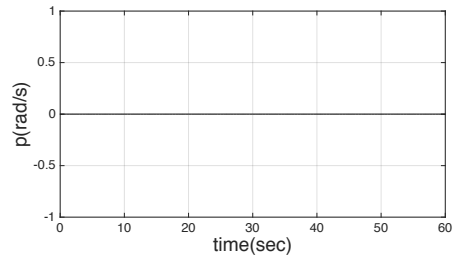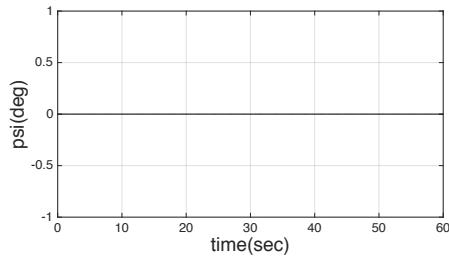
B.4 Straight Up Turn Configuration

B.4-1 Initial Condition

Elements of a state x	Units	Initial values x0 (time = 0)
u	m/s	10
v	m/s	0
w	m/s	3
X_e	m	0
Y_e	m	0
Z_e	m	-4000
p	rad/s	0
q	rad/s	0
r	rad/s	0
ϕ	$degree$	0
θ	$degree$	30
ψ	$degree$	0

B.4-2 Geometric Data and Moments of Inertia

I_{xx}	$kg * m^2$	1.8
I_{yy}	$kg * m^2$	13.6
I_{zz}	$kg * m^2$	15.2
I_{xz}	$kg * m^2$	0.1
I_{xy}	$kg * m^2$	0.4
I_{yz}	$kg * m^2$	0
Wing Area *(S)*	m^2	1.056
Wing Span *(b)*	m	0.598
Wing Chord (*c_bar)*	m	1.74

B. 4-3 Time History

Time interval	Configuration used in simulation
0 sec ~ 25 sec	Straight Up
25 sec ~ 60 sec	Straight Up Left Turn

B. 4-4 Flight Simulation
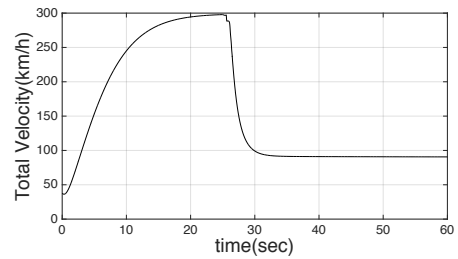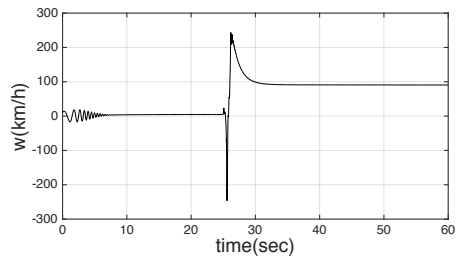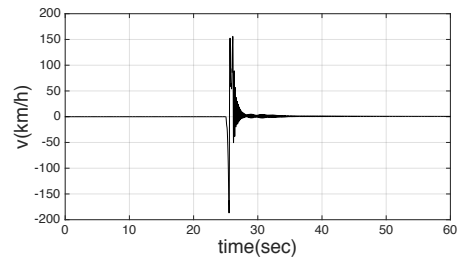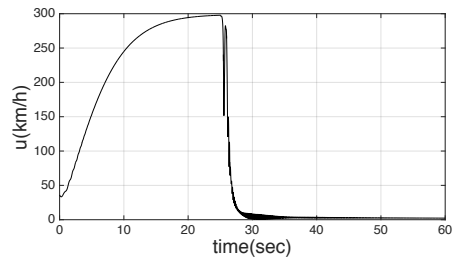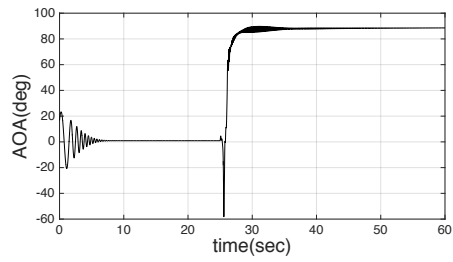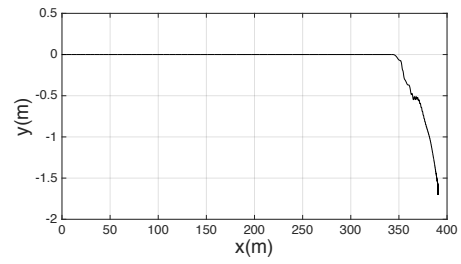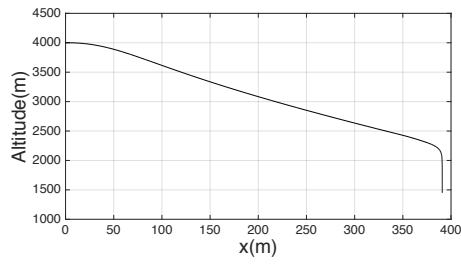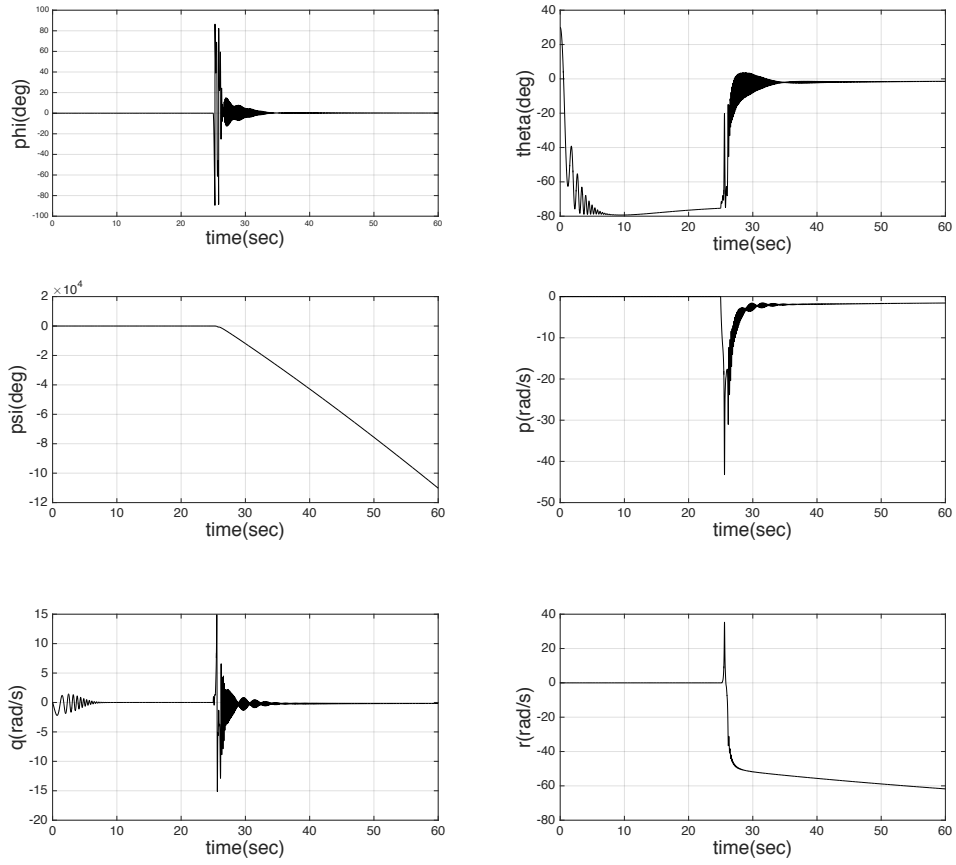
B.5 Right Turn Configuration

B.5-1 Initial Condition

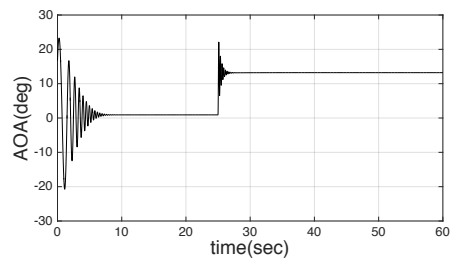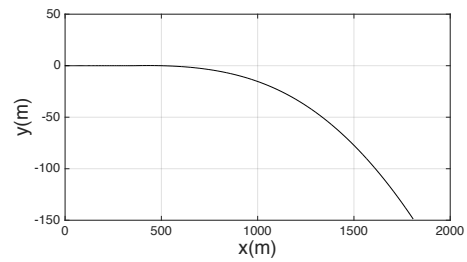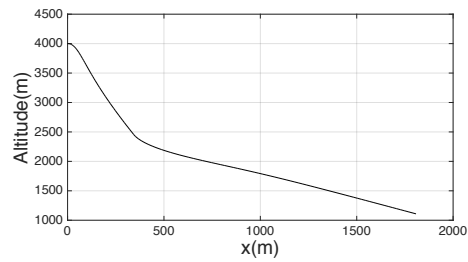| Elements of a state x	Units	Initial values x0 (time = 0)
u	m/s	10
v	m/s	0
w	m/s	3
X_e	m	0
Y_e	m	0
Z_e	m	-4000
p	rad/s	0
q	rad/s	0
r	rad/s	0
ϕ	$degree$	0
θ	$degree$	30
ψ	$degree$	0

B.5-2 Geometric Data and Moments of Inertia

I_{xx}	$kg * m^2$	3.7
I_{yy}	$kg * m^2$	12.4
I_{zz}	$kg * m^2$	15.7
I_{xz}	$kg * m^2$	0.1
I_{xy}	$kg * m^2$	0.4
I_{yz}	$kg * m^2$	0
Wing Area *(S)*	m^2	1.319
Wing Span *(b)*	m	1.228
Wing Chord (*c_bar)*	m	1.07

B. 5-3 Time History

Time interval	Configuration used in simulation
0 sec ~ 25 sec	Cruise
25 sec ~ 60 sec	Right Turn

B. 5-4 Flight Simulation
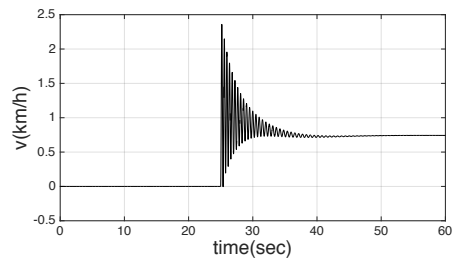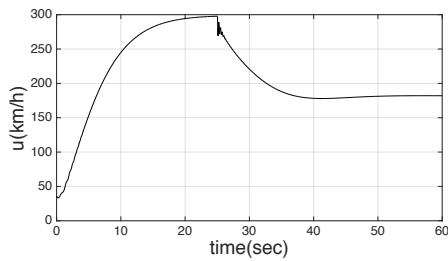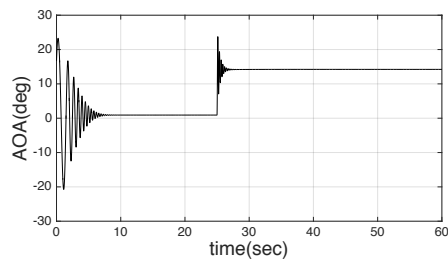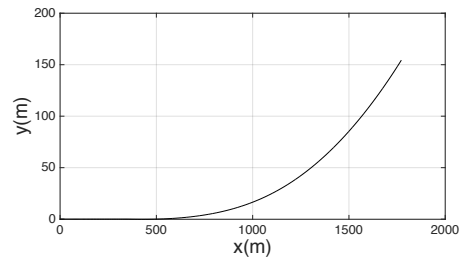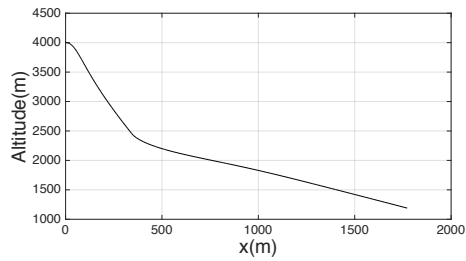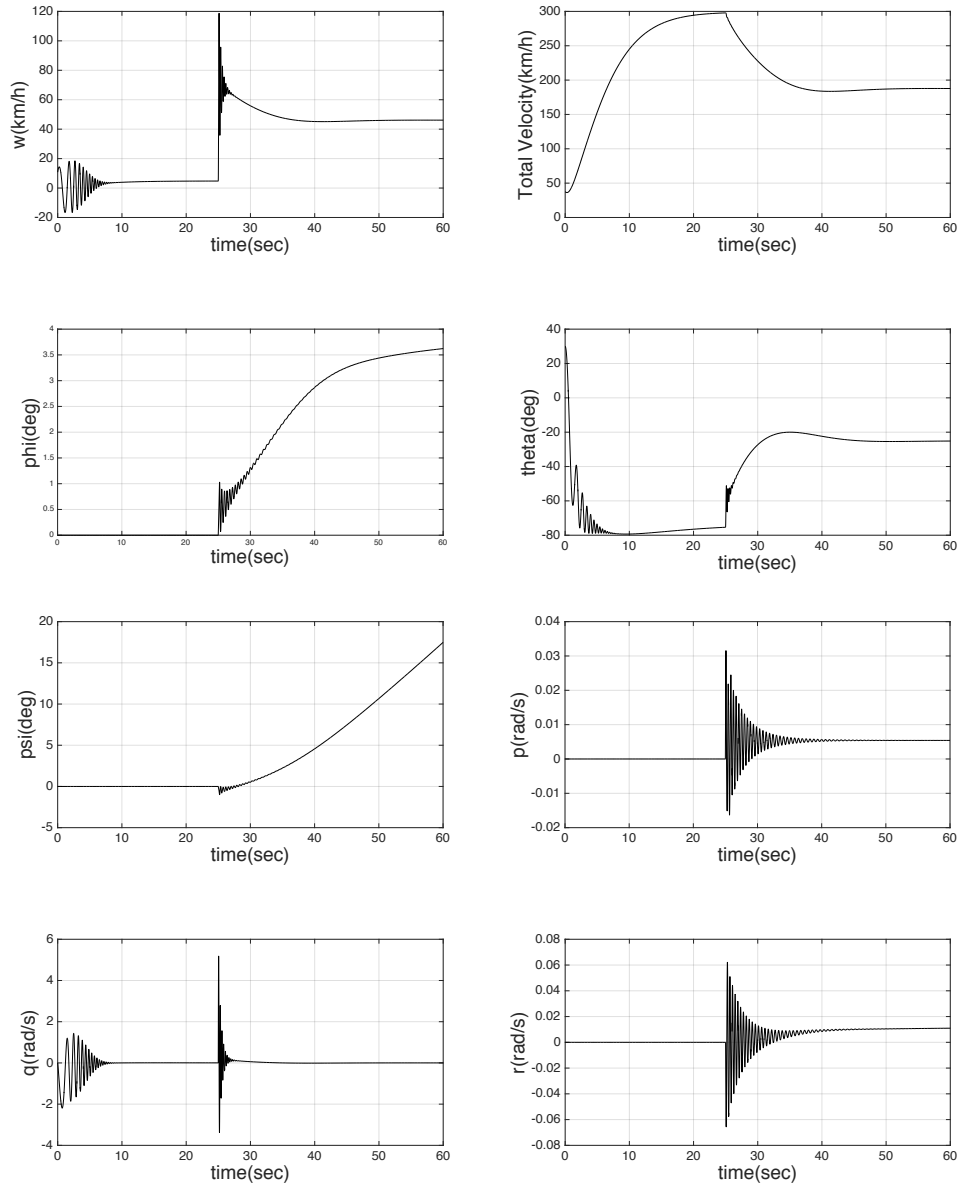
B.6 Left Turn Configuration

B.6-1 Initial Condition

Elements of a state x	Units	Initial values x0 (time = 0)
u	m/s	10
v	m/s	0
w	m/s	3
X_e	m	0
Y_e	m	0
Z_e	m	-4000
p	rad/s	0
q	rad/s	0
r	rad/s	0

ϕ	*degree*	0
θ	*degree*	30
ψ	*degree*	0

B.6-2 Geometric Data and Moments of Inertia

I_{xx}	$kg * m^2$	2.5
I_{yy}	$kg * m^2$	12
I_{zz}	$kg * m^2$	20
I_{xz}	$kg * m^2$	0
I_{xy}	$kg * m^2$	0
I_{yz}	$kg * m^2$	0
Wing Area *(S)*	m^2	1.319
Wing Span *(b)*	m	1.228
Wing Chord ($c\_bar)$	m	0.338

B. 6-3 Time History

Time interval	Configuration used in simulation
0 sec ~ 25 sec	Cruise
25 sec ~ 60 sec	Left Turn

B. 6-4 Flight Simulation
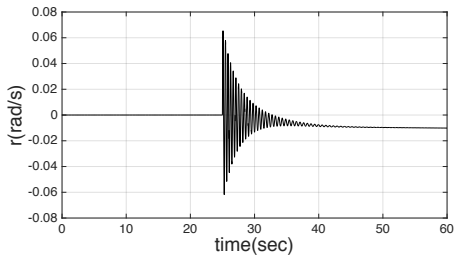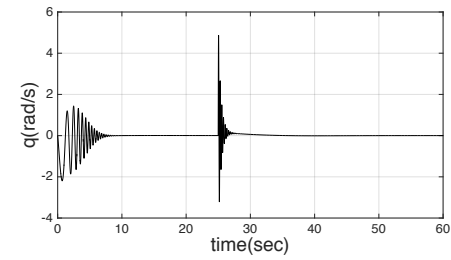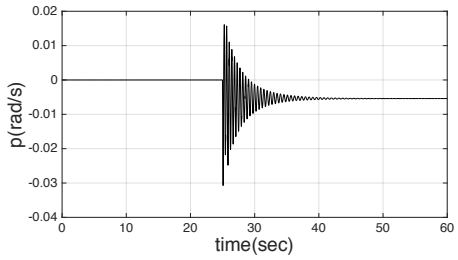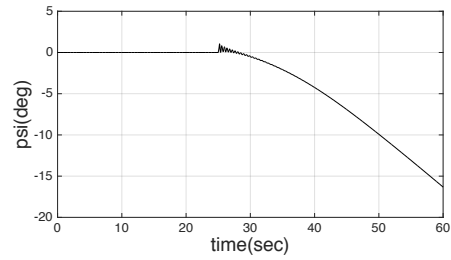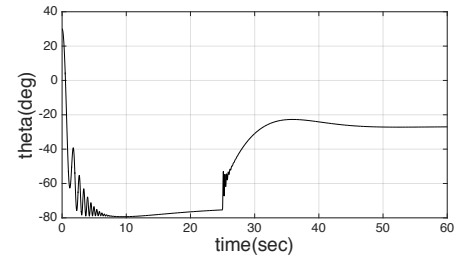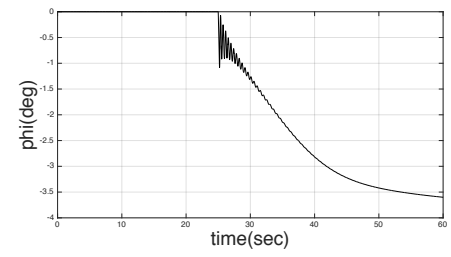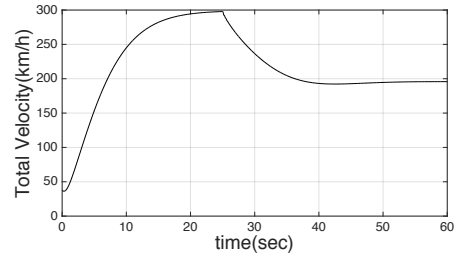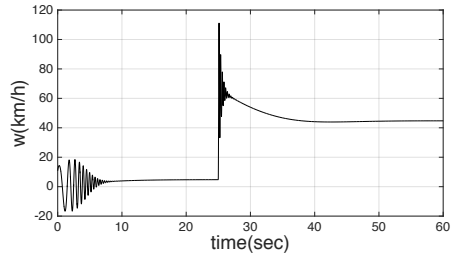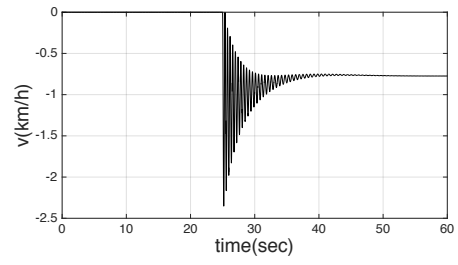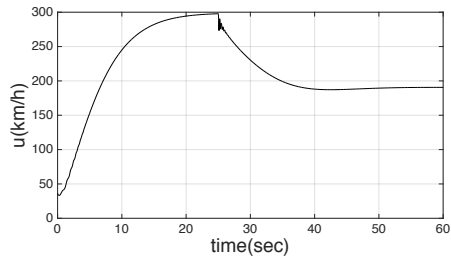
B.7 Rudder Configuration

B.7-1 Initial Condition

Elements of a state x	Units	Initial values x0 (time = 0)
u	m/s	10
v	m/s	0
w	m/s	3
X_e	m	0
Y_e	m	0
Z_e	m	-4000
p	rad/s	0
q	rad/s	0
r	rad/s	0
ϕ	$degree$	0
θ	$degree$	30
ψ	$degree$	0

B.7-2 Geometric Data and Moments of Inertia

I_{xx}	$kg * m^2$	4.4
I_{yy}	$kg * m^2$	12.4
I_{zz}	$kg * m^2$	16.2
I_{xz}	$kg * m^2$	0.8
I_{xy}	$kg * m^2$	0.2
I_{yz}	$kg * m^2$	0.4
Wing Area *(S)*	m^2	1.302
Wing Span *(b)*	m	1.857
Wing Chord (*c_bar)*	m	0.701

B. 7-3 Time History

Time interval	Configuration used in simulation
0 sec ~ 25 sec	Cruise
25 sec ~ 40 sec	Yaw and Roll

B. 7-4 Flight Simulation
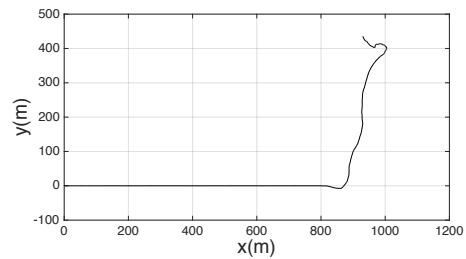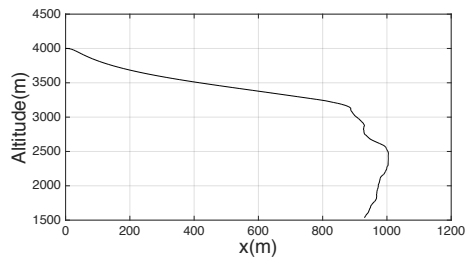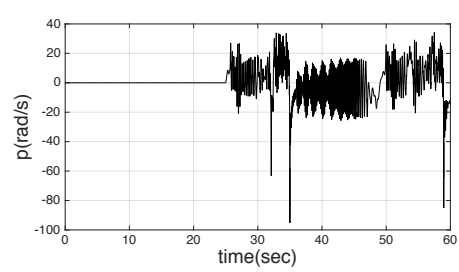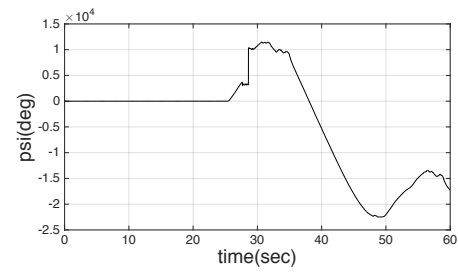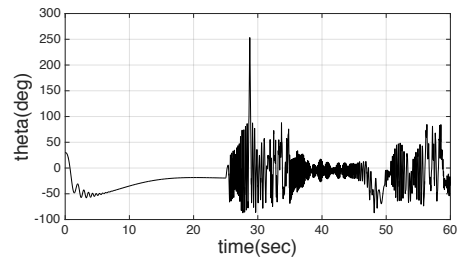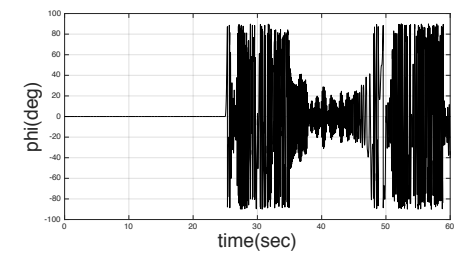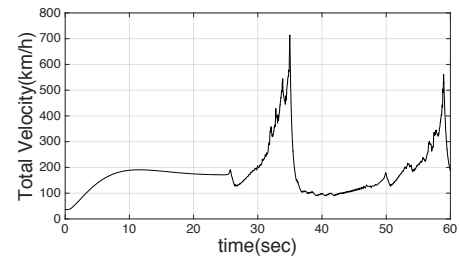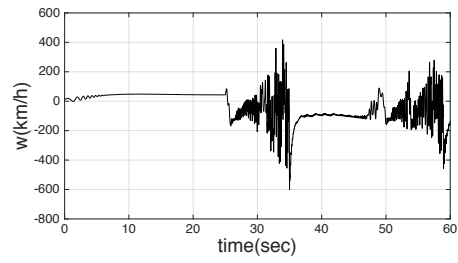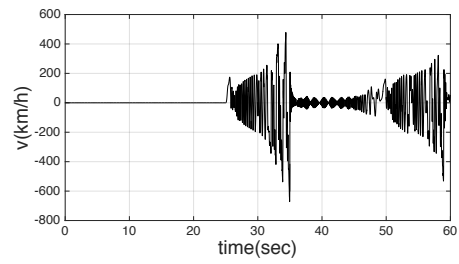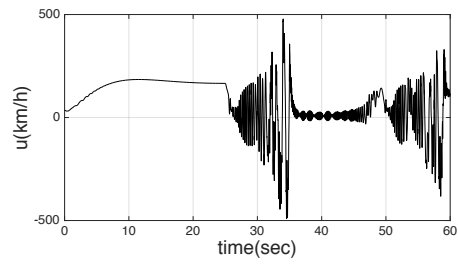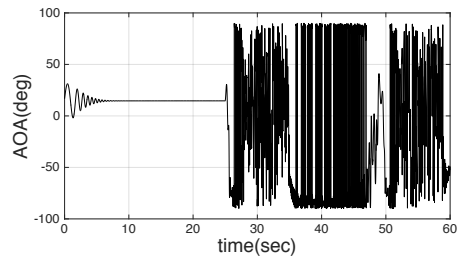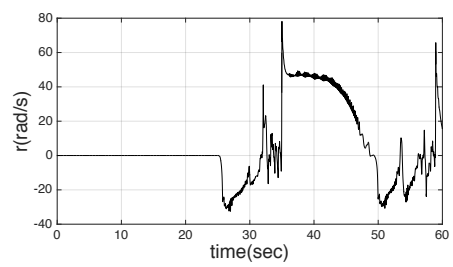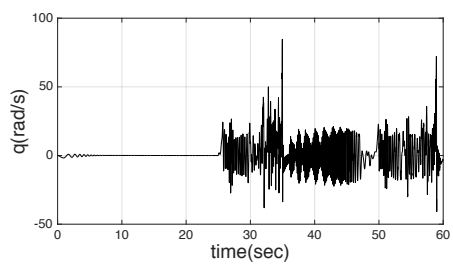
REFERENCES

1. Berry, M., Las Fargeas, J., & Blair, K. B. (2010). Wind tunnel testing of a novel wingsuit design. Procedia Engineering, 2(2), 2735-2740.

2. Robson, G., & D'Andrea, R. (2010). Longitudinal Stability Analysis of a Jet-Powered Wingsuit. In AIAA Atmospheric Flight Mechanics Conference (p. 7512).

3. Wingsuit Design and Basic Aerodynamics 2. (n.d.). Retrieved from http://mike.speedalbum.com/nl/files/Phoenix-Fly.pdf

4. Celeste, M. (n.d.). Flying Without Dying: The Future of Wingsuit Design. Retrieved June 4, 2015, from https://beholdtheinfinite.wordpress.com/2015/06/04/flying-without-dying-the-future-of-wingsuit-design/

5. Sestak, T. A. (2015). Developing a Robust Balance for Wingsuit Aerodynamic Research.

6. Stephanopoulos, K., Levy, B., & Rabadan Jr, I. (2015). Designing a High-Lift Performance Wingsuit.

7. Mei-Dan, O. (2013). Fatalities in Wingsuit BASE Jumping. *WILDERNESS AND ENVIRONMENTAL MEDICINE,* 321-327. Retrieved December, 2013.

8. Moment of inertia, http://wweb.uta.edu/faculty/ricard/Classes/KINE-3301/Notes/Lesson-11.html

9. Pillips, W. F. (n.d.). *Mechanics of Flight* (2nd ed.). John Wiley & Sons (P. 609 & P. 666)